

IONIC POLYMER METAL COMPOSITES (IPMCs) BASED ON RADIATION
GRAFTED POLYSTYRENESULFONIC ACID ONTO POLY(ETHYLENE- *ALT*-
TETRAFLUOROETHYLENE) (ETFE-*g*-PSSA)

BAHAR BURCU KARAHAN

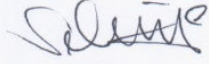
Submitted to the Graduate School of Engineering and Natural Sciences
in partial fulfillment of
the requirements for the degree of
Master of Science

SABANCI UNIVERSITY

Ionic Polymer Metal Composites (IPMCs) based on Radiation Grafted
Polystyrene sulfonic acid onto Poly(ethylene-alt-tetrafluoroethylene) (ETFE-g-
PSSA)

APPROVED BY :

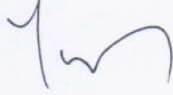
Assoc Prof. Selmiye Alkan Gürsel



Assoc Prof. Melih Papila



Prof. Yusuf Ziya Menceloğlu



Assoc Prof. Mehmet Ali Gülgün



Assoc Prof. Ali Koşar



DATE OF APPROVAL: 07/08/2012

© BAHAR BURCU KARAHAN 2012

ALL RIGHTS RESERVED

IONIC POLYMER METAL COMPOSITES (IPMCs) BASED ON RADIATION
GRAFTED POLYSTYRENESULFONIC ACID ONTO POLY(ETHYLENE- *ALT*-
TETRAFLUOROETHYLENE) (ETFE-*g*-PSSA)

Bahar Burcu Karahan

Material Science and Engineering, M.Sc. Thesis, 2012

Thesis Supervisor: Assoc. Prof. Selmiye Alkan Gürsel

Keywords: Ionic polymer metal composite (IPMC), radiation grafting, Poly(ethylene-*alt*-tetrafluoroethylene), polystyrenesulfonic acid, Nafion[®], actuation.

ABSTRACT

Ionic polymer-metal composites (IPMCs), one of the electroactive polymers, have revealed remarkable properties with its large bending behavior and force response under applied low voltages. Nafion[®] has been used for the manufacturing IPMCs due to its high ionic conductivity and mechanical strength. However, high cost and limited thickness availability of Nafion[®] diminishes its demand. As a promising alternative to the Nafion[®] based IPMCs, radiation grafted poly(ethylene-*alt*-tetrafluoroethylene)-*graft*-polystyrenesulfonic acid (ETFE-*g*-PSSA) membrane based IPMCs have been fabricated successfully in this study.

Poly(ethylene-*alt*-tetrafluoroethylene) (ETFE) is a hydrophobic polymer. In this study, hydrophilic properties were induced by radiation grafting followed by sulfonation. Radiation grafting, firstly creates active sites on the ETFE film by -irradiation with γ -rays. Secondly, polystyrenesulfonic acid side chains were grafted into ETFE film by grafting and with a subsequent sulfonation procedure. The introduction of sulfonic acid end groups supply hydrophilic properties to the hydrophobic base film. ETFE-*g*-PSSA membranes' properties were studied in terms of graft level, water uptake and ionic conductivity.

Ionic polymer metal composites (IPMCs) were produced by electroless plating of platinum (Pt) onto both surfaces of ETFE-*g*-PSSA membranes. ETFE-*g*-PSSA based

IPMCs strips showed an actuation performance under applied electric potentials. The superior actuation performance with higher displacement capabilities was achieved with respect to conventional Nafion[®] based IPMCs. The effect of grafting on actuation performance was investigated. In addition to these, different characteristics of ETFE-g-PSSA based IPMCs compared to the Nafion[®] based IPMCs were revealed. For ETFE-g-PSSA based IPMCs, an adaptation period to the applied electric field –prior to the first actuation of the tested sample- was observed such as the conditioning time in PEM (proton exchange membrane) fuel cells. Furthermore, the displacement capability was increased by the repeated actuation performances. Lastly, 5V and above applied potentials are affecting the displacement character of ETFE-g-PSSA based IPMCs widely. After application of 5V, in the next electromechanical tests, a reverse actuation character (actuation towards cathode and back-relaxation towards anode) was observed.

RADYASYONLA AŞILAMA YÖNTEMİ İLE ÜRETİLMİŞ POLİ(ETİLEN-*ALT*-
TETRAFLUROETİLEN)-POLİSTİRENSÜLFONİK ASİT ESASLI İYONİK
POLİMER METAL KOMPOZİTLER

Bahar Burcu Karahan

Malzeme Bilimi ve Mühendisliği, Yüksek Lisans Tezi, 2012

Tez Danışmanı: Doç. Dr. Selmiye Alkan Gürsel

Anahtar Kelimeler: İyonik polimer metal kompozit, radyasyon ile aşılama, poli(etilen-*alt*-tetrafluroetilen), polistirensülfonik asit, Nafion[®], eyleyici.

ÖZET

Elektroaktif polimerlerden olan iyonik polimer-metal kompozitler, yüksek bükülme ve kuvvet uygulama davranışlarıyla göze çarpan özellikler sunmuşlardır. Nafion[®], yüksek iyon iletkenliği ve mekanik dayanıklılığı gibi özelliklerinden dolayı iyonik polimer-metal kompozit üretiminde sıklıkla kullanılmaktadır. Fakat, pahalı oluşu ve kalınlık seçeneklerinin sınırlı oluşu Nafion[®] a olan talebi azaltmaktadır. Bu çalışmada Nafion[®] bazlı iyonik polimer- metal kompozitlere alternatif olabilecek bir malzeme olarak poli(etilen-*alt*-tetrafluroetilen)-*aşı*-polistirensülfonik asit membranı bazlı iyonik polimer metal kompozitler, başarılı bir şekilde sentezlendi.

Poli(etilen-*alt*-tetrafluroetilen), su sevmeyen bir polimerdir. Bu çalışmada, bu filme, radyasyon ile aşılama yöntemi ve onu takiben sülfonlama yapılarak su sevme özellikleri eklenmiştir. Radyasyon ile aşılama öncelikle film üzerinde γ - ışınları ile aktif kısımlar yaratılmıştır. Ardından ise polistiren yan zincirleri bu filme aşılama ve bunu takiben sülfonik asit grupları eklenmiştir. Sülfonik asit gruplarının eklenmesi, başlangıçta su sevmeyen filme, su sevme özellikleri katarak bir membran haline getirmiştir. Bu membranların özellikleri aşılama derecesi, su alım kapasitesi ve iyon iletkenlik açılarından incelenmiştir.

Poli(etilen-*alt*-tetrafluroetilen)-*aşı*-polistirensülfonik asit membranları, elektronsuz platin (Pt) kaplama yöntemiyle iyonik polimer metal kompozitler haline getirilmişlerdir. Bu kompozitler de Nafion[®] esaslı kompozitler gibi elektrik alanı altında bükülme

özelliđi göstermişlerdir. Bu yeni iyonik polimer metal kompozitler, Nafion® esaslı kompozitlerden daha üstün bükülme kapasitesi göstermişlerdir. Bunların yanı sıra, aşılamanın, bükülme performansına etkisi incelenmiştir. Ayrıca, poli(etilen-*alt*-tetrafluroetilen)-*aşı*-polistirensülfonik asit bazlı yeni iyonik polimer metal kompozitlerin, Nafion® bazlı kompozitlerden farklı olan karakteristik davranışları saptanmıştır. Yeni kompozitler, uygulanan elektrik alanında ilk defa bükülmeden önce PEM (proton deđişim membran) yakıt hücrelerinde olan ‘koşullandırma süreci’ne benzer bir adaptasyon periyoduna ihtiyaç duymuşlardır. İlk bükülme davranışını gösterdikten sonra ise, bükülme kapasiteleri tekrarlanan elektro-mekanik testlerle artmıştır. Bunların yanı sıra, 5V ve üstünde potansiyel alan oluşturulması, bu yeni kompozitlerin bükülme karakteristiklerini etkilemiştir. 5V uygulanan örnekler, sonraki testlerde, zıt-bükülme özellikleri (katoda doğru bükülme ve anoda doğru ters-gevşeme) göstermişlerdir.

ACKNOWLEDGEMENTS

I would like express my thanks to Selmiye Alkan Gürsel for her boundless academic and also non-academic helps and for her patience. She gave her support along with her sincerity always. It was a great pleasure to work with her in intimacy.

I would like to thank to Melih Papila for his guidance and advices. I am very glad to work with him since my freshman year. Discussions and meeting in his group were very delighted and phenomenal, all the time.

I wish to express my sense of gratitude to Yusuf Menceloğlu. He was always supportive and always a step behind of me in case if I need any advice since my freshman year. His door was always open for questions. I am also very thankful for his financial supports for my thesis project. It was a great pleasure to being met with him.

I would like to thank my thesis committee members Mehmet Ali Gülgün and Ali Koşar very much for their understanding and enthusiasm towards my study.

I am very thankful to Cleva Ow Yang and Mehmet Ali Gülgün for the intimate time that we spent together along the years.

I give the most cheerful thanks to my lab colleagues. My grad-life was very particular, interesting and marvelously funny. I would like to convey my thanks to Siegmar Roth's group, too; it was a very delightful scientific period of my life. I am thankful to Luleå-family for their super-fantastic friendship and support during all my academic studies. I am also very thankful to my AMS-friends for their love and patience.

Lastly, I would like to tell my gratefulness to my family. First of all to my grandparents; their love is always with me and to my parents... I am thankful to them for their geniality and leniency. I am thankful to my sisters' delicate generosity and care during all my education life.

TABLE OF CONTENTS

| | |
|---|------|
| ABSTRACT..... | iv |
| ÖZET | vi |
| ACKNOWLEDGEMENTS..... | viii |
| TABLE OF CONTENTS..... | ix |
| LIST OF FIGURES | xi |
| LIST OF TABLES..... | xv |
| 1 INTRODUCTION | 1 |
| 1.1 Smart Materials | 1 |
| 1.1.1 Electroactive Polymers | 3 |
| 1.2 Ionic Polymer Metal Composites..... | 4 |
| 1.2.1 Understanding the State of Ionic Polymer Metal Composites | 7 |
| 1.2.2 Electrode Layers | 14 |
| 1.2.3 Solvent..... | 15 |
| 1.2.4 Mobile Ions..... | 16 |
| 1.2.5 Characterization of IPMC- Actuation and Sensing Behavior | 17 |
| 1.2.6 Novel IPMCs | 18 |
| 1.2.7 Applications..... | 19 |
| 1.3 Nafion [®] and Poly(ethylene- <i>alt</i> -tetrafluoroethylene)..... | 21 |
| 1.3.1 Nafion [®] | 21 |
| 1.3.2 Poly(ethylene- <i>alt</i> -tetrafluoroethylene) | 26 |
| 1.4 Radiation Grafting..... | 27 |
| 1.4.1 Irradiation | 28 |
| 1.4.2 Graft Polymerization | 30 |
| 1.4.3 Conduction in Radiation Grafted Membranes..... | 34 |
| 1.5 ETFE BASED IONIC POLYMER METAL COMPOSITES | 35 |
| 1.6 OBJECTIVE | 35 |
| 2 EXPERIMENTAL..... | 36 |
| 2.1 Radiation Grafting..... | 36 |
| 2.1.1 Pre-irradiation..... | 36 |
| 2.1.2 Graft Polymerization | 36 |
| 2.2 Activation of Nafion [®] | 37 |
| 2.3 Sulfonation | 37 |
| 2.3.1 Water Uptake..... | 37 |
| 2.4 Ionic Conductivity..... | 38 |
| 2.5 Platinum (Pt) Plating..... | 39 |
| 2.5.1 Surface Roughening of the Membranes | 39 |
| 2.5.2 Ion-exchange (Adsorption)..... | 40 |
| 2.5.3 Primary Plating..... | 40 |
| 2.5.4 Secondary Plating..... | 40 |
| 2.6 Displacement Measurements | 41 |
| 2.7 Universal Testing Machine (UTM)..... | 41 |
| 2.8 Scanning Electron Microscopy (SEM) and Energy Dispersive X-ray Spectroscopy (EDX) | 42 |

| | | |
|-------|---|----|
| 3 | RESULTS AND DISCUSSION | 43 |
| 3.1 | Radiation Grafting..... | 43 |
| 3.1.1 | Improvements for Radiation Grafted Film Quality | 49 |
| 3.2 | Water Uptake | 52 |
| 3.3 | Ionic Conductivity..... | 54 |
| 3.4 | Mechanical Testing | 57 |
| 3.5 | Platinum (Pt) Deposition..... | 59 |
| 3.6 | Actuation and Displacement | 71 |
| 3.6.1 | Effect of Graft Level | 71 |
| 3.6.2 | Effect of Thickness | 72 |
| 3.6.3 | Effect of Voltage | 73 |
| 3.6.4 | Effect of Frequency | 74 |
| 3.6.5 | Effect of Ionic Conductivity and Water Uptake..... | 75 |
| 3.6.6 | Notes on Characteristics of ETFE-g-PSSA | 77 |
| 4 | CONCLUSION..... | 78 |
| 5 | FUTURE WORKS | 79 |
| | REFERENCES | 92 |

LIST OF FIGURES

| | |
|--|----|
| Figure 1. A primitive design for the self-swimming IPMC..... | 2 |
| Figure 2. Electric generation with the movements of water-waves..... | 2 |
| Figure 3. Movement of the IPMC in the water..... | 2 |
| Figure 4. An illustration of the bending behavior of an IPMC. The spaghetti-like structure imitates the polymeric membrane, where the red dots are the mobile cations. The two solid lines at the bottom and top of the membrane illustrate the metal electrode layers. The top drawing shows IPMC's initial state when there is not applied any electric field. The middle drawing shows the behavior when an electric field is applied. The bottom drawing represents the relaxation behavior when the electric field is removed [113]...... | 6 |
| Figure 5. The bending results in higher local surface resistance on the IPMC strip. Therefore, the voltage and current dynamics are changed on these regions [97]..... | 8 |
| Figure 6. (Color) Average light intensity and the corresponding tip displacement. Average fluorophore intensity was calculated from the selected cathode and anode area, respectively [90]. | 9 |
| Figure 7. Schematic diagrams of the IPMC actuation. (a) In initial state, hydrated cations and water molecules are distributed evenly in the membrane of IPMC. (b) State of the hydrated cation migration to cathode area and the resulting volume expansion of the region under the applied voltage and the concurrent exhausting of anode region's volume which leads to bending motion. (c) Relaxation of the IPMC [115]...... | 9 |
| Figure 8. Illustration of a possible microstructure for hydrated Nafion [®] /IPMC: (a) electrically neutral state with interconnected clusters, permeable to water and cation, and (b) in an electric field which redistributes the cations, leaving a net negative charge density near the anode and a net positive charge density near cathode [76]. | 10 |
| Figure 9. Uniaxial stiffness (Young's modulus) of bare Nafion [®] 117 and IPMC), where Li ⁺ is the migrated cation; vs. salivation; ethylene glycol (at the top left), glycerol (at the top right) and 12-Crown-2 (at the bottom) as the solvent. The same combination were also experimented for Na ⁺ and K ⁺ in the study [79]. | 11 |
| Figure 10. Comparison of the various approaches for the solution of the cation transport over time. Li ⁺ was used in the Nafion [®] based IPMC where the solvent was water. 1,25 V DC electric potential was applied [78]...... | 12 |
| Figure 11. Nafion [®] based IPMC's bending curvature response in 0,1 M Na ₂ SO ₄ (A) and 0,1 M Na ₂ SO ₄ + 30 mM H ₂ SO ₄ (B), driven by a step current [85]. | 13 |
| Figure 12. Streaming current in a channel [40]. | 14 |
| Figure 13. The compression device placement (left) and the Arrhythmia control of heart beats by IPMC strips (right) [112]...... | 20 |
| Figure 14. Nafion [®] | 22 |
| Figure 15. Cluster-network model for the hydrated morphology Nafion [®] [72]. | 23 |
| Figure 16. The platinized Nafion [®] proposed by Sadeghipour et al. [107]...... | 25 |
| Figure 17. Poly(ethylene- <i>alt</i> -tetrafluoroethylene) (ETFE). | 26 |
| Figure 18. A schematic and scriptural representation of radiation grafting. The red line on the schematic figure (left) represents a part of the polymer-backbone; the blue lines represent the grafted side chains. The former is represented with "A"s and the latter is represented with B _m and B _n on the scriptural figure (right)...... | 28 |
| Figure 19. Reactive active sites, the radicals, were illustrated with dots. | 29 |

| | |
|---|----|
| Figure 20. Irradiation and the grafting of the base polymer film. | 31 |
| Figure 21. Irradiation of polymer base under vacuum, simultaneously and in air. | 32 |
| Figure 22. Grafting front mechanism [17]. | 33 |
| Figure 23. Influence of poor solvent on the partitioning of monomer and solvent between solution and swollen polymer film [104]. | 33 |
| Figure 24. The transport of hydrogen ions (H^+) through water is accomplished by Grotthuss Mechanism, in which hydrogen bonds (dashed lines) and covalent bonds (solid lines) between water molecules are broken and re-formed. | 34 |
| Figure 25. Model of proton conduction. Grotthuss Mechanism (top); the protons are passed along the hydrogen bonds. Vehicle Mechanism (bottom): the movement takes place with aid of a moving “vehicle”, e.g. H_2O or NH_3 as complex ion (H_3O^+ or NH_4^+) [102]. | 35 |
| Figure 26. Styrene (left) and isopropanol (right). | 36 |
| Figure 27. In-plane ionic conductivity configuration [39]. | 38 |
| Figure 28. Ion conductivity cell [39]. | 39 |
| Figure 29. Pairs of grafted films are represented in ‘Graft Level <i>versus</i> Grafting Time’ graph. | 43 |
| Figure 30. Comparison of surface grafting yield and volume grafting yield determined by FTIR-ATR for 30 μ m (left) and FTIR in transmission for 100 μ m ETFE film (right) (irradiated with 100 kGy; grafted at 50 °C; ethanol used as a solvent with crosslinker and inhibitor addition) [43]. | 45 |
| Figure 31. ‘Graft Level <i>versus</i> Grafting Time’ representations for 100 μ m films with overall grafting results. | 45 |
| Figure 32. ‘Graft Level <i>versus</i> Grafting Time’ representations for 150 μ m films with overall grafting results. | 46 |
| Figure 33. ‘Graft Level <i>versus</i> Grafting Time’ representations for 200 μ m films with overall grafting results. | 46 |
| Figure 34. ‘Graft Level <i>versus</i> Grafting Time’ representations for 250 μ m films with overall grafting results. | 47 |
| Figure 35. Deviations in graft levels at higher grafting time periods. | 47 |
| Figure 36. Grafting reactor (left) and sulfonation reactor (right) | 49 |
| Figure 37. Expansion of grafted films. 150 μ m ETFE film in pristine (left), GL: 14% (middle) and GL: 95% (right) states | 50 |
| Figure 38. Homogenously grafted ETFE films: 100 μ m (top-left), 150 μ m (top-right), 200 μ m (bottom-left), 250 μ m (bottom-right) | 50 |
| Figure 39. Non-homogenously grafted and formless 250 μ m ETFE films. | 51 |
| Figure 40. New steel grafting reactor for 14 x 16 [cm^2] films (left). New sulfonation reactor (right). | 51 |
| Figure 41. Sulfonation reaction of polystyrene grafted ETFE films. | 52 |
| Figure 42. Water Uptake <i>versus</i> Graft Level values. | 53 |
| Figure 43. ‘Ionic Conductivity <i>versus</i> Graft Level’ results. | 55 |
| Figure 44. ‘Ionic Conductivity <i>versus</i> Water Uptake’ results. | 55 |
| Figure 45. Changes in Water Uptake and Ionic Conductivity with respect to Graft Level in 100 μ m wet membranes. | 56 |
| Figure 46. UTM results of different thicknesses of raw ETFE films and wet ETFE membranes. Nafion [®] 115 is in pristine state (non-activated). | 57 |

| | |
|---|----|
| Figure 47. UTM results for 100 μm raw ETFE and grafted 100 μm ETFE films, under tension..... | 58 |
| Figure 48. The linear elastic part of Nafion [®] 115 and the 100 μm wet ETFE-g-PSSA membranes..... | 59 |
| Figure 49. Non- displaced 100 μm _GL: 80% ETFE-g-PSSA/IPMC surface (bottom). Surface of pristine, non-Pt deposited ETFE film, 250 μm ; scale bar: 10 μm (top, left). Surface of 17% grafted, non-Pt deposited 100 μm _ETFE film; scale bar is 20 μm (top, right). For larger non-Pt deposited images, please see Appendix C..... | 60 |
| Figure 50. Cross-section of non-displaced 100 μm _GL: 80% ETFE based IPMC..... | 61 |
| Figure 51. The EDX surface spectrum of the non-displaced 100 μm _GL: 80% ETFE-g-PSSA based IPMC surface. | 61 |
| Figure 52. Cross-section of 200 μm _GL: 55% ETFE based IPMC. | 62 |
| Figure 53. Surface of displaced 200 μm _GL: 55% ETFE based IPMC. Applied maximum voltage is 3V; both in DC and in AC form..... | 62 |
| Figure 54. Surface of displaced 100 μm _GL: 80% ETFE based IPMC both under AC and DC. The applied maximum voltage is 5V to 10 V in DC..... | 63 |
| Figure 55. Tip of repetitively displaced 100 μm _GL: 80% ETFE based IPMC (cross-section)..... | 64 |
| Figure 56. Tip of the repetitively displaced 100 μm _GL: 80% ETFE based IPMC (Cross-section). | 64 |
| Figure 57. EDX spectrum of the repetitively displaced tip, 100 μm _GL: 80% ETFE based IPMC (cross-section). Point analysis (red cross) was made at the center. | 65 |
| Figure 58. EDX spectrum of the non-displaced 100 μm _GL: 80% ETFE based IPMC (cross-section). Point analysis (red cross) was made at the center. | 66 |
| Figure 59. The non-displaced 100 μm _GL: 80% ETFE based IPMC (cross-section). Red cross indicates that point analysis was made between the center and the edge..... | 67 |
| Figure 60. The non-displaced 100 μm _GL: 80% ETFE based IPMC (cross-section). Red cross indicates that point analysis was made close to the edge. | 67 |
| Figure 61. The non-displaced 100 μm _GL: 80% ETFE based IPMC (cross-section). Red cross indicates that point analysis was made at the edge..... | 68 |
| Figure 62. The repetitively-displaced 100 μm _GL: 80% ETFE based IPMC (cross-section). Red cross indicates that point analysis was made at the center. | 68 |
| Figure 63 The repetitively-displaced 100 μm _GL: 80% ETFE based IPMC (cross-section). Red cross indicates that point analysis was made between the center and edge. | 69 |
| Figure 64. The repetitively-displaced 100 μm _GL: 80% ETFE based IPMC (cross-section). Red cross indicates that point analysis was made at the edge..... | 69 |
| Figure 65. The EDX surface spectrum of the displaced 100 μm _GL: 80% ETFE-g-PSSA based IPMC. Point analysis made on the membrane, where a part of Pt plate was broke off..... | 70 |
| Figure 66. The EDX surface spectrum of the displaced 100 μm _GL: 80% ETFE-g-PSSA based IPMC. Point analysis made on the Pt surface..... | 70 |
| Figure 67. Bending of 150 μm _GL: 77% under 3V DC (left). Relaxation appeared when electric field was removed (right). Back-relaxation was not observed..... | 71 |
| Figure 68. Tip Displacement <i>versus</i> Graft Level in different thicknesses under 1V and 0,5 Hz..... | 71 |

| | |
|---|----|
| Figure 69. ‘Tip displacement <i>versus</i> DC Voltage’ with ETFE-g-PSSA in different thicknesses and similar graft levels | 72 |
| Figure 70. ‘Tip Displacement <i>versus</i> Voltage under AC Potential’ for 100 μm _GL: 70% and GL: 80% ETFE-g-PSSA based IPMC at various frequencies. | 73 |
| Figure 71. ‘Tip Displacement <i>versus</i> Frequency’ for 100 μm _GL: 70% ETFE-g-PSSA based IPMC..... | 74 |
| Figure 72. ‘Tip Displacement <i>versus</i> Frequency’ for 100 μm _GL: 80% ETFE-g- PSSA based IPMC..... | 74 |
| Figure 73. Tip Displacement <i>versus</i> Graft Level under 1 V and 0,5 Hz. | 75 |
| Figure 74. Tip Displacement <i>versus</i> ionic conductivity under 1 V and 0,5 Hz..... | 76 |
| Figure 75. Tip Displacement <i>versus</i> Water Uptake under 1 V and 0,5 Hz. | 76 |

LIST OF TABLES

| | |
|--|----|
| Table 1. Modulus of Elasticity of 100 μm wet ETFE-g-PSSA membranes..... | 58 |
|--|----|

1 INTRODUCTION

1.1 Smart Materials

Smart materials are synthetic materials which have natural properties in an applied specific field. External stimuli such as stress, temperature, electricity or magnetism, which create fields, can initiate the specific function of the smart material; or the specific functions, when activated, can lead back to the initial stimuli, as a consequence- in other words, materials' function can be controlled by these external stimuli and *vice versa*. Some of these functions are the voltage generation under an applied mechanical stress, and *vice versa*, in *piezoelectrics*; the large strains which are produced in *dielectric elastomers* when an external electric field is applied; the deformation recovery in *shape memory materials* by remembering the original state when the material is heated; the color change in response to change in temperature in *thermochromic materials* and the color change in response to light in *photochromics* [96]. The intrinsic structure of these materials endows them with peculiar functions; hence consequences of the applied external stimuli indicate these functions as natural properties.

'Smart materials behave like transformers of an energy form'. *Piezoelectrics* and *ferroelectrics* convert the electric charge, field and current – electric form of the energy- to and from the mechanical energy. *Magnetostrictives* convert the magnetic form of the energy to mechanical forms. In electrorheological and magnetorheological fluids, the electric and magnetic forms of energy are transformed into physical state (potential) energies; the materials use electric and magnetic forms of energy to convert the liquid to the solid state; and *vice versa*. Electroactive materials change its shape (a mechanical form of energy) under an applied field (i.e. the electrical energy) [38] such as *ionic polymer metal composites*.

Smart materials mostly simplify the device structure, reduce the weight and can increase the life time of the application. On the other hand, smart *systems* can also be developed in order to respond to an external change. The importance of the smart materials, in this manner, is the fact that the response is given only by a single material [96]. This unique character opens up a route to specific designs for materials; where a response can be the initiator of another motion that creates a

cycle in which the material satisfies its own needs to act. In this case, only one material acts as a whole system. From this point of view, we can derive a specific

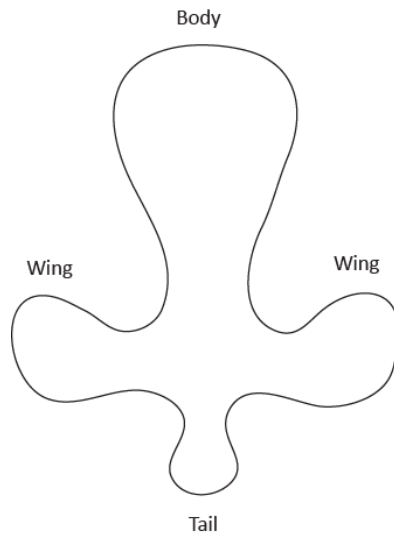


Figure 1. A primitive design for the self-swimming IPMC.

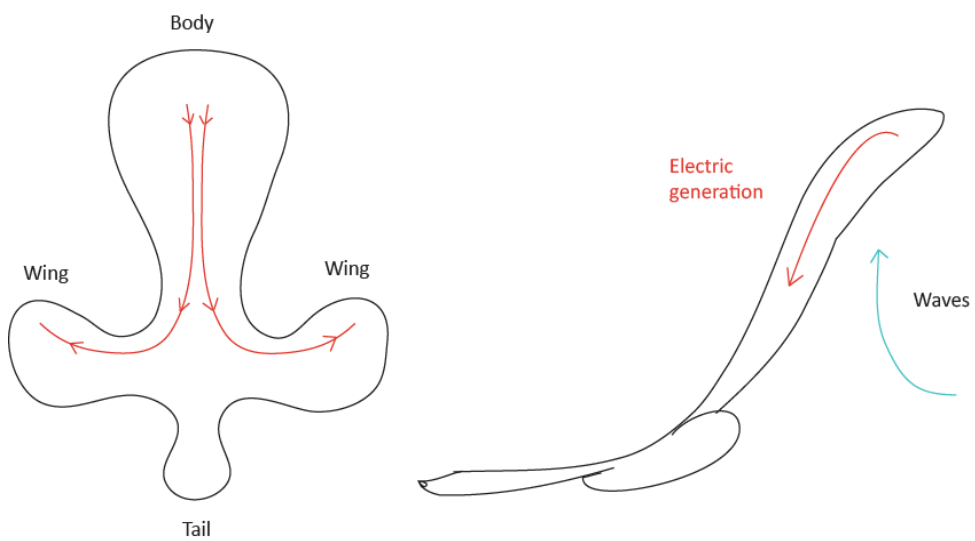


Figure 2. Electric generation with the movements of water-waves.

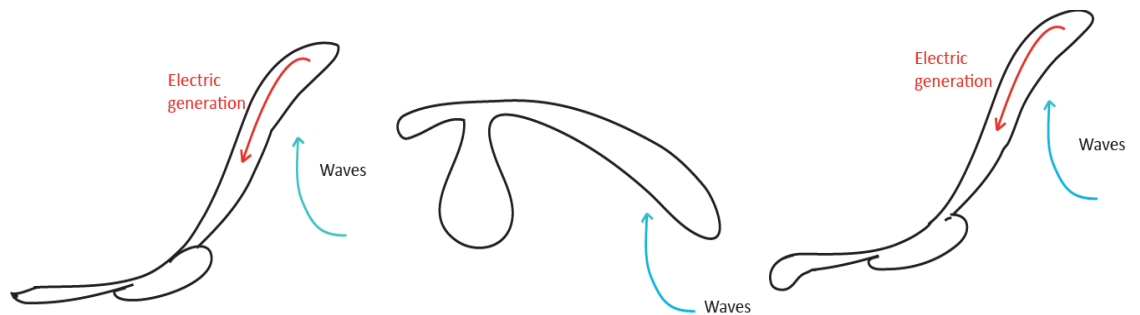


Figure 3. Movement of the IPMC in the water.

design of an ionic polymer composite, as illustrated in Figure 1. In this design, electricity is generated when the material mechanically bends and bending occurs as a response to the external stimuli of the electric field. More specifically, the movements of the waves can lead to bending of material which results in electric generation. The generated electric potential can be used to bend the composite material (Figure 2) (The mastery of the mechanical engineering might be also working in the manner of communication of the continuously created responses that are the initiator of the next movement.). Therefore, the ionic polymer metal composite can move in the water (Figure 3). Flatau and Chong [38] resemble the occurrence to a living body system: “smart structures/materials basically possess their own sensors (nervous system), processor (brain system), and actuators (muscular systems); thus mimicking biological systems”, like an independent living organism.

1.1.1 Electroactive Polymers

Electroactive polymers (EAP) are a subgroup of smart materials. Electroactive polymers convert the energy form by using a polymeric medium. In general, it is assumed that the intermolecular interactions are energy form transformers: the repulsive forces expand the polymer and attractive forces shrink the polymer, which are initiated by an electric field. The changes in these counteracting forces are controllable by the solvent, gel composition, temperature, pH and light (etc.) parameters [13].

The history of EAP dates back to 1880s, where Roentgen experimented with the charge and discharge of a rubber band. In 1899, Sacerdote, following up this subject observed the rubber’s strain response with respect to the applied electric field. In 1925, finally a breakthrough was achieved when the electret was found, which is a piezoelectric polymer material (During the solidification of carnauba wax, rosin and beeswax by cooling, the mixture was subjected to a DC potential field and piezo activity has been observed) [13].

The electroactive polymers are divided into two groups: electronic electroactive polymers and ionic electroactive polymers. The electronic EAPs are dielectric electroactive polymers, electrostrictive graft elastomers, electrostrictive paper, electrovisco-elastic elastomers, ferroelectric polymers and liquid crystal elastomers. The required activation field is larger than 100 V/ μm . Electronic type of EAPs is described

as they are squeezed by attraction force between the charged electrodes [9]. On the other hand, ionic EAPs consist of a polymer electrolyte and two electrodes where the electroactivation takes place through the thickness of polymer. It is said that electroactivation occurs due to the diffusion of ions. Ionic EAPs are the carbon nanotubes, conductive polymers, electrorheological fluids, ionic polymer gels and ionic polymer metal composites. For the ionic EAPs, 1-2 V is sufficient to activate the material. Another attractive property of ionic EAPs are their operation capability in wet environments with a significant displacement output. However, the low force or torque has been pointed out as a limiting disadvantage [9] for actuation performance; but this disadvantage can be turned into a profit in another application area. For instance, an IPMC-brush or an IPMC-spatula can be produce for use in archeological discoveries in order to decently clean finding.

The electroactive materials have light weight, noiseless actuation, simple mechanics and large displacement capabilities [98]. EAPs are fracture tolerant and pliable; they can be configured into desired shapes; hence the properties can be tailored for a broad range of applications. Furthermore, the resemblance of EAPs with artificial muscles is striking; where both of them are resilient, damage tolerant and have large actuation strains (stretching, contraction, bending). Visco-elastic EAPs are able to expose more life-like aesthetics (like the android head [9], vibration and shock dampening, and more flexible actuator configurations. In a different approach, it can be seen that gears, bearings, and other parts that complicate the construction of expensive, heavy and sensitive robots might be eliminated by using EAPs [9]. To my mind, the most important property of EAPs is that the ease in shape giving that allows creating various designs which can satisfy the standing necessity.

1.2 Ionic Polymer Metal Composites

Ionic polymer metal composites (IPMC) are one of the electro-active polymers. The *smart* behavior of IPMC was explored by Sadeghipor [107] and Oguro [86] during 1990s. The discovery of smart behavior of IPMC is directly related to Nafion[®]'s nature, one of the most used base membranes for IPMCs. Nafion[®] is a perflourinated sulfonic acid membrane, essentially a cation-exchange resin. Its *smartness* was revealed when Nafion[®] was used in a hydrogen pressure cell. This cell is an electrochemical cell, a protonic conducting medium bordered on two sides by electrocatalytic electrodes. The

cell produces voltage when there is a difference in hydrogen gas pressure across the protonic conducting medium. Originating from this resemblance, Sadeghipor et al. [107] noticed that electroded Nafion[®] senses the pressure difference across its thickness and as a consequence it responds with a voltage generation. The primitive hydrogen pressure cell system was the inspiration for the smart behavior of platinized Nafion[®], as the up-to-date name of IPMC (ionic polymer metal composite) [107].

The improvements in IPMCs brought a conceptual description for these electroactive materials: Ionic polymer metal composites are a sandwich of an ion conducting membrane in between of two metal electrode layers (Figure 4). The literature states that the ion mobility is the principle of the working mechanism. The ions move in the ion exchange membrane across the thickness with an electrical field that is applied through the metal electrodes. As a result, IPMC strip bends. Consequently a certain amount of displacement and force is generated. Moreover, when IPMC is bent a certain amount of voltage is generated due to the imbalance in the internal ion pressure across the membrane.

The ionic polymer metal composites became renowned with an arm wrestling contest between robotic arms and a human arm in 2005. The contest, proposed by Yoseph Bar-Cohen, was seen as an incentive for engineers and scientists worldwide to advance the improvements in electroactive polymers. Three parties joined to the contest against a 17 years old, female opponent. Although the winner was the human opponent, the ERI arm, comprising of 8 IPMC strip and dielectric elastomeric resilient EAP, showed a success of withstanding/enduring/ 26 seconds against its competitors (The competitors were EMPA, an dielectric elastomer EAP; and VT, PAN gel fibers) [12].

After this glorious fame, IPMC attracted significant attention due to its large bending strains and ability to respond to low applied voltages (< 3 V) [113; 11; 63; 120]. Owing to the large strain response, IPMCs have earned the sobriquet: “the artificial muscles”. Additionally, exhibiting an electric field as a result of a mechanical bending acquired the *smart* reputation to the IPMCs and the sensing property. It has been reported that as sensors, IPMCs are one magnitude order more sensitive than traditional piezoelectric materials [40]. Furthermore, its fast response to the change in applied electric field, the flexibility, compactness, quiet operation, durability and the ease in shaping created a covetable research area [55]. Beside of these, IPMC are reliable for over 1 million cycles [119] (estimated) and 250,000 cycles experimentally

reported [89]. By all these properties IPMCs have taken its place in actuation and sensing applications.

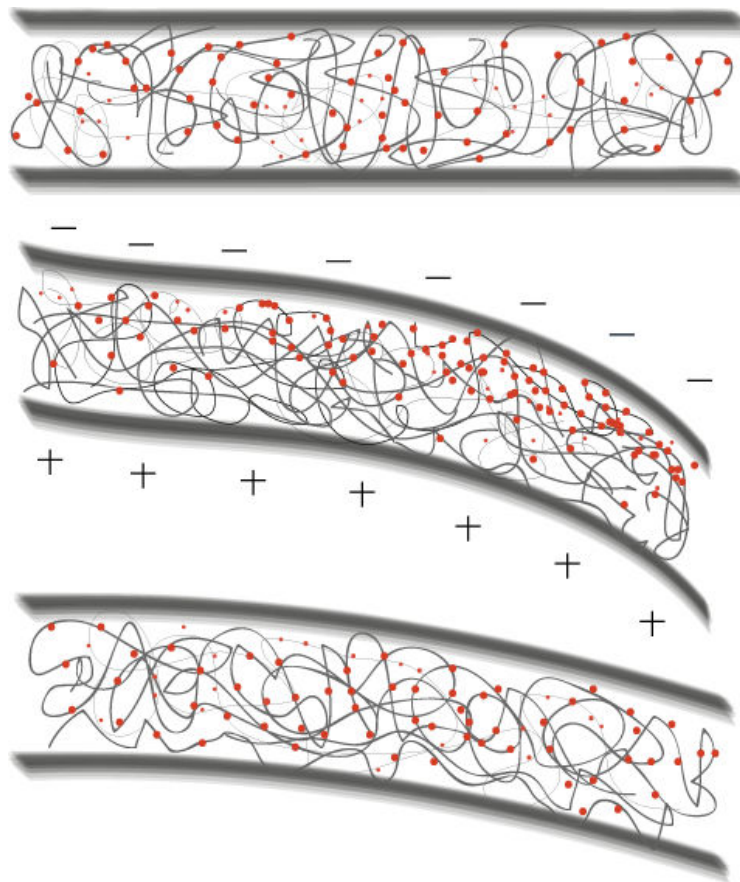


Figure 4. An illustration of the bending behavior of an IPMC. The spaghetti-like structure imitates the polymeric membrane, where the red dots are the mobile cations. The two solid lines at the bottom and top of the membrane illustrate the metal electrode layers. The top drawing shows IPMC's initial state when there is not applied any electric field. The middle drawing shows the behavior when an electric field is applied. The bottom drawing represents the relaxation behavior when the electric field is removed [113].

Ionic polymer metal composites' researches have been focusing on two different areas: one of them is that the fundamental understanding of the working principle of the IPMC and the one other is that the development of the novel IPMCs and enhancing their actuation and sensing performance [89]. The former has been oriented around a few base-ideas that are the charge dominating [115; 90; 15; 95] and solvent dominating transport [78; 76; 91; 1]; and additionally many models have been presented to explain the coupled behavior of mechanical and electrical response in the IPMC constitution [6; 64; 110; 83; 37; 8; 88]. The latter have been oriented along investigation and development of metal electrode layers [22; 99; 4; 100], ion conducting medium [73; 81;

80; 87; 79] and the –mobile- ions [73] in order to improve the actuation and sensing properties.

1.2.1 Understanding the State of Ionic Polymer Metal Composites

The working mechanism of ionic polymer metal composites is, yet to be exactly, not understood. However, various modeling researches have been published in order to understand the state of IPMC's actuation and sensing principles. Even though, a common and complete result has not been achieved to date, the intention to approach to the most realistic explanation revealed some important details of IPMC properties. Furthermore, the effort that has been spent over the understanding the state has brought out some smartly characterization methods [90; 62; 85] as well as developments in the performance [79; 115; 89].

The modeling investigations mostly centered over the charge dynamics (on the electrodes, in the electrode-membrane interface and in the membrane) [119; 97; 90] and over the solvent effect [78; 76; 91; 1].

Some of the most recognized models are introduced below:

Wallmersperger et al. [119] proposed a chemo-electrical model which focuses on the charge accumulation at the polymer-metal interface in order to determine the strain (which occurs due to the bending behavior) and strain rate that are generated during the actuation of IPMC. The model is based on the one-dimensional Nernst-Planck equations for charge conduction; where the effects of charge gradients and electric potential gradients in space and time were considered. The model computes the charge density as a function of applied electric field and the electrochemical boundary conditions in IPMC. The IPMC was based on the Nafion[®] 117 membrane and various electrodes were used: copper, silver and gold.

Kim et al. [97] have focused on the electrode-membrane interface as Wallmersperger et al. [119]. Kim et al. have used the Poisson-Nernst-Planck system of equations in order to simulate the charge dynamics and the resulting displacement of IPMC. The model couples the current in the polymer membrane to the electric current in the continuous electrode layer. It is mentioned that the calculated data based on this model can be used to optimize the values of the membrane thickness, stiffness, thickness of the electrodes and the applied voltage in order to achieve the desired

actuation. Furthermore, the authors mentioned that this model can be a base for more sophisticated works such as for 3D calculations: as the twisting actuation of IPMC, where multiple electrodes are used in design in order to give or enhance the twisting. Additionally, the study showed some details in IPMC bending properties as the bending causes an increase in the –local- electrical resistance on the convex side of the electrode (Figure 5) and also it is showed that an amount of charge remained in the IPMC – structure- after the removal of the electric field and relaxation; hence it was discharged prior to the experimental measurements in the study. In this study Nafion[®] 117 is also the base membrane and metal electrodes deposited with electroless plating method.

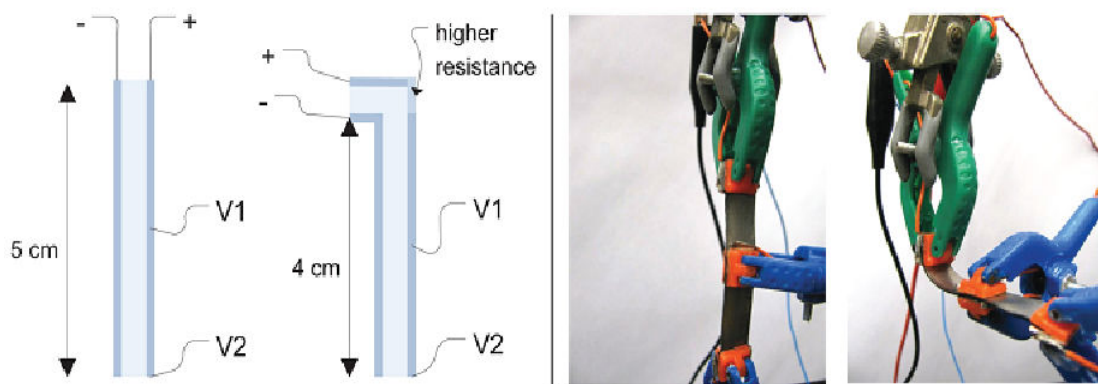


Figure 5. The bending results in higher local surface resistance on the IPMC strip. Therefore, the voltage and current dynamics are changed on these regions [97]

On the other hand, another experimental study based on charge dynamics –more explicitly based on the ion transport- has been experimented with fluorescent spectroscopy [90]. Fluorescent spectroscopy was used to understand the ion transport in a Nafion[®] based IPMC under an applied DC voltage. The intensity of the light, created due to the cation migration, on the photograph was correlated with the IPMC’s displacement, where ethidium bromide (EtBr) was used as the fluorescent molecular probe (Figure 6). An initial increase in cation concentration in cathode side was observed when the electric field was applied. Subsequently, an eventual decrease in cation concentration in the cathode side in the still-presence of the applied electric field was reported (Figure 6). The removal of the electric field resulted in recovery of the initial charge distribution. The study concluded that the cations and the hydrated cations migrate toward the cathode as depicted in Figure 7; therefore the volume expansion results in the bending of the IPMC [90].

A similar approach has been proposed by Shahinpoor and Kim [115]. The working principle has been described as an ion-induced, electrophoresis-like, hydrated cations create a pressure gradient which results in bending of IPMC, likewise in Figure 7. In this study, the appearance and disappearance of water was observed during the expansion and contraction of the surface -during the bending and relaxation-; hence the study conducted the working mechanism of IPMC to the ion induced water transport.

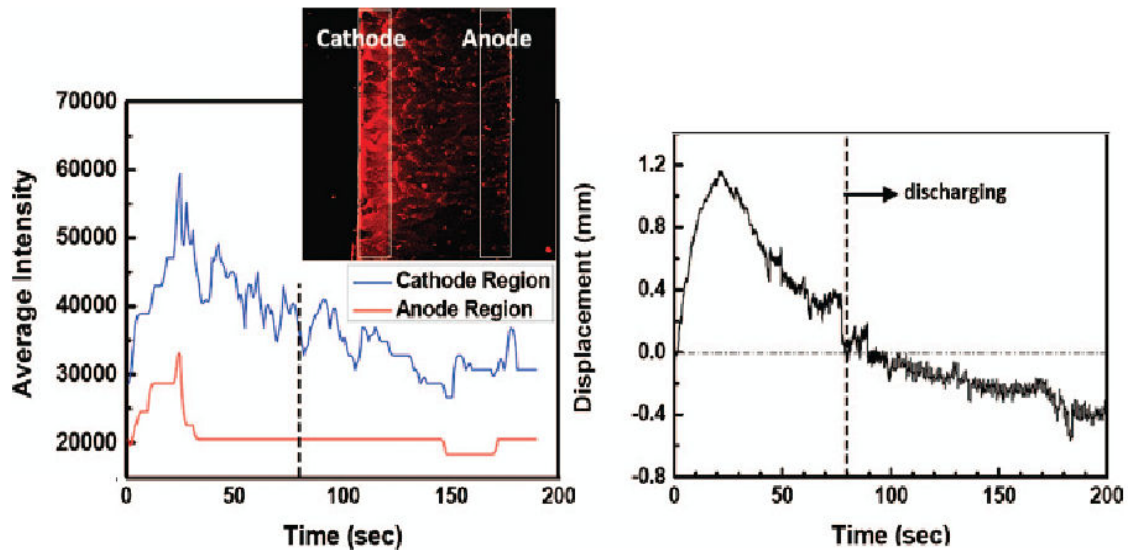


Figure 6. (Color) Average light intensity and the corresponding tip displacement. Average fluorophore intensity was calculated from the selected cathode and anode area, respectively [90].

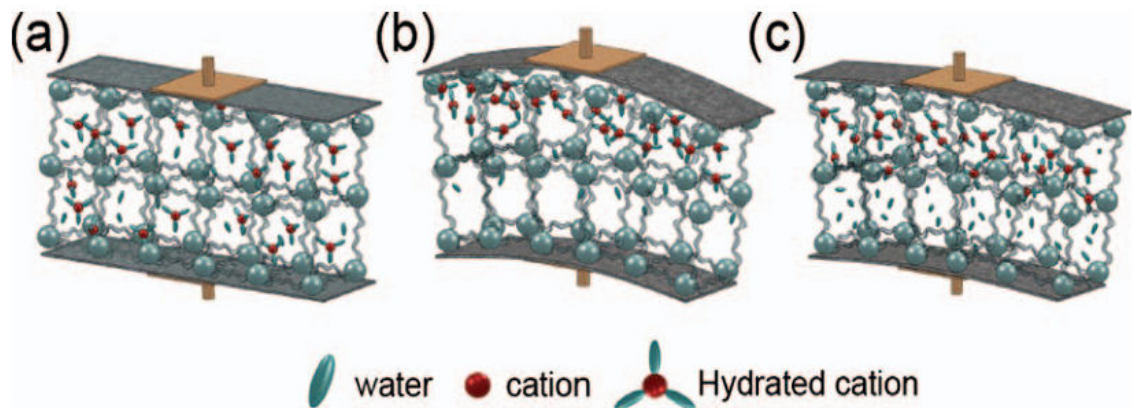


Figure 7. Schematic diagrams of the IPMC actuation. (a) In initial state, hydrated cations and water molecules are distributed evenly in the membrane of IPMC. (b) State of the hydrated cation migration to cathode area and the resulting volume expansion of the region under the applied voltage and the concurrent exhausting of anode region's volume which leads to bending motion. (c) Relaxation of the IPMC [115].

In addition to these, Costa Branco and Dente [25] presented a continuum model of IPMC actuation that assumes the driving mechanism is electrostatic forces and IPMC actuation is arising from the local charge imbalances across the polymer membrane.

Nemat-Nasser and Zamani [78] have approached to the bending phenomena in a different manner than the widely used cation transport phenomenon, as aforementioned. Nemat-Nasser and Zamani have completed a modeling investigation which is based on the solvent transport. Their study assumes the existence of clusters in the membrane structure and asserts that application of an electric field produces two thin boundary layers close to the electrodes (Figure 8). When an electric field is applied, the cations in anode boundary are depleted, while the cathode boundary layer intakes the excess of the cations. Hence an imbalance within the clusters (but not in the IPMC) occurs (Figure 8). This creates a change in osmotic, electrostatic and elastic forces. These forces tend to expand or contract the corresponding clusters and forces the solvent out of or into the clusters. As a result, IPMC bends.

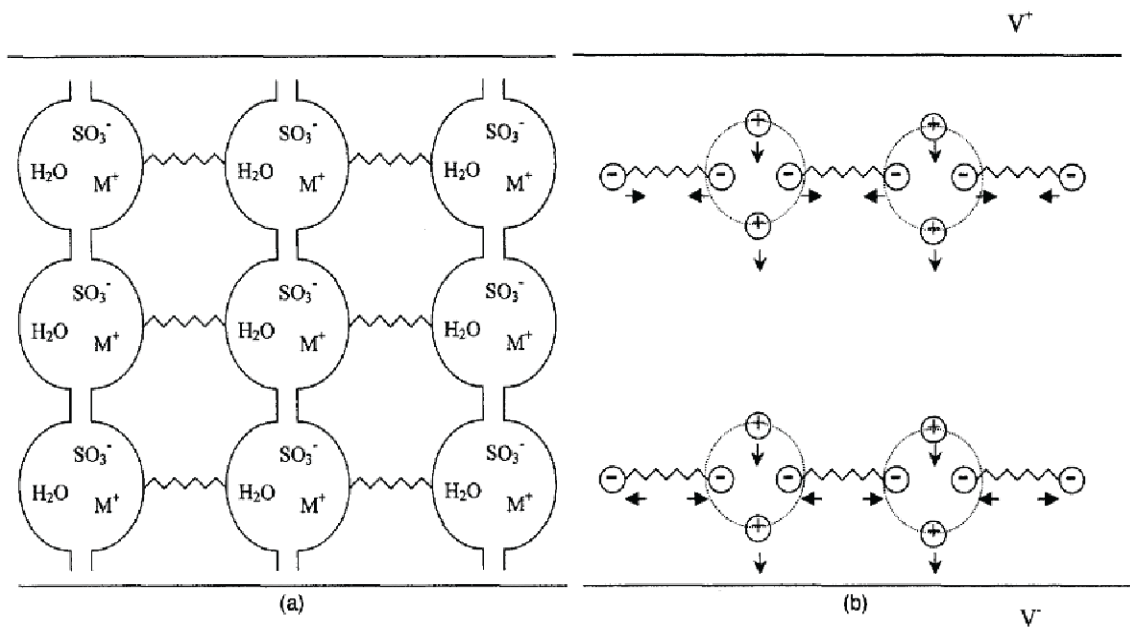


Figure 8. Illustration of a possible microstructure for hydrated Nafion®/IPMC: (a) electrically neutral state with interconnected clusters, permeable to water and cation, and (b) in an electric field which redistributes the cations, leaving a net negative charge density near the anode and a net positive charge density near cathode [76].

Therein, the model takes the volume fraction of solvent within each boundary layer as a base and assumes that the layers are controlled by the effective pressure, where the effective pressure is created by the osmotic, electrostatic and elastic forces in the corresponding clusters. Hence, stiffness and solvation were modeled by measuring the

solvent uptake of the dry bare polymer or the IPMC. It is assumed that the membrane or IPMC absorbs the solvent until the pressure within the clusters is balanced with the elastic stresses that are consequently developed in the backbone of the polymer. Therewith, the stiffness of the membrane was calculated as a function of volume fraction of the solvent uptake. Afterwards, the results of this calculation were used to calculate the stiffness of IPMC by addition of the effect of the metal electrodes. The experimental data, the measured stiffness versus solvent uptake, presented showed a successful correlation with the created model (Figure 9).

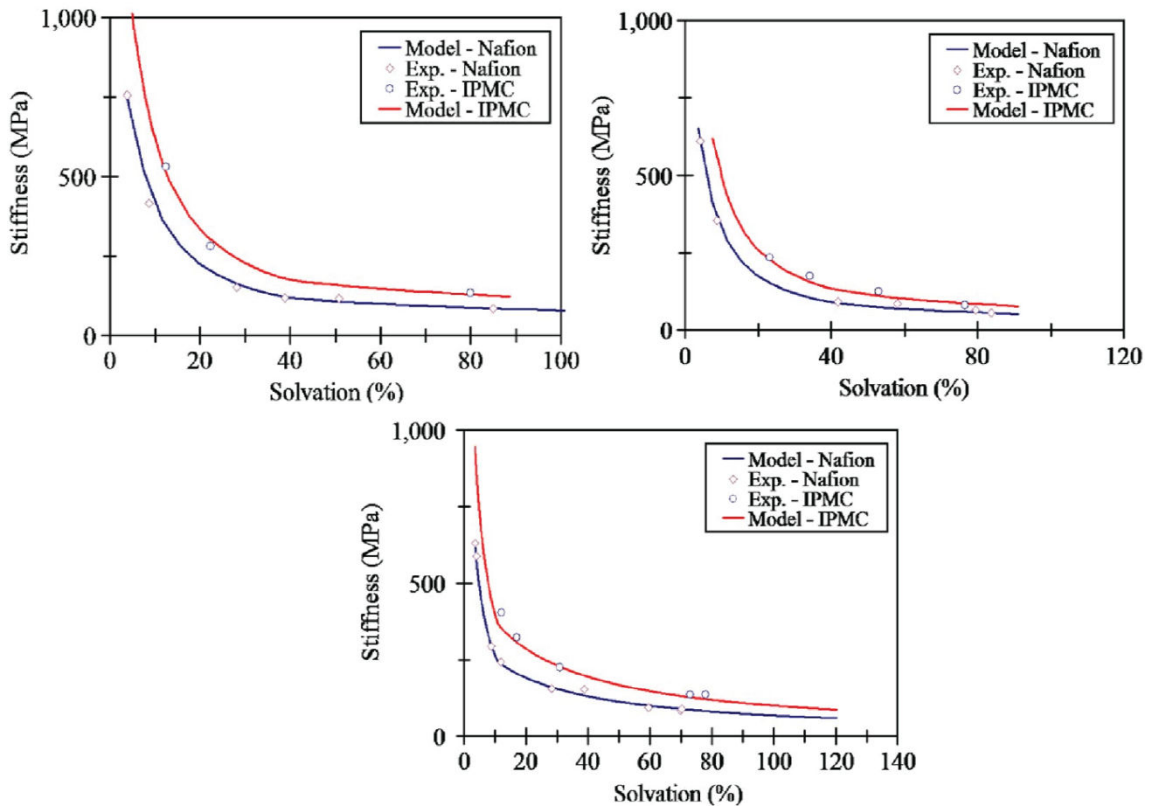


Figure 9. Uniaxial stiffness (Young’s modulus) of bare Nafion[®] 117 and IPMC), where Li^+ is the migrated cation; vs. solvation; ethylene glycol (at the top left), glycerol (at the top right) and 12-Crown-2 (at the bottom) as the solvent. The same combination were also experimented for Na^+ and K^+ in the study [79].

On the other hand, the redistribution of the cations under the applied voltage was modeled via the coupled electrochemical equations. The coupled electrochemical equations include the net flux of the species which exist due to the electrochemical potentials (the chemical concentration and the electric field gradient). It is assumed that the cation migration occurs at first, subsequently the diffusion-controlled solvent transport takes place. Therefore, the resulting total flux consist of the cation migration

and solvent transport. The system has been resolved both numerically and analytically with the approximations, the details can be found elsewhere [78]. The results of the calculations are shown in Figure 10, which is consistent with the designed model.

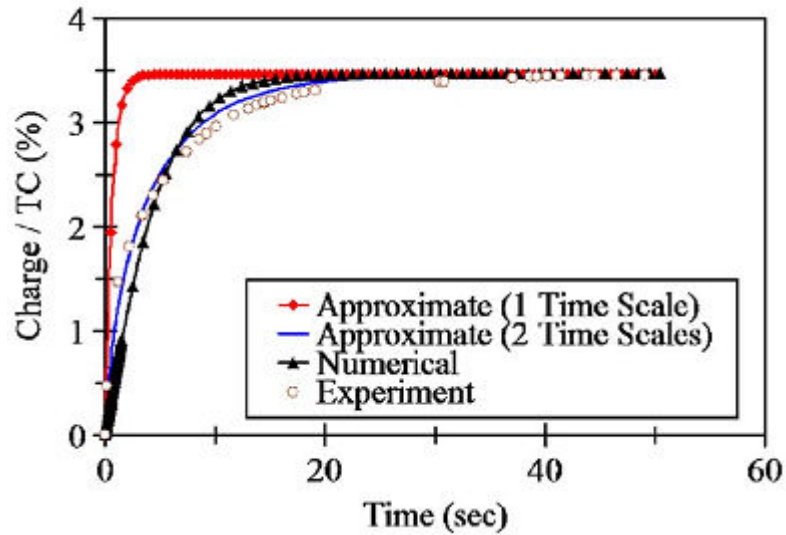


Figure 10. Comparison of the various approaches for the solution of the cation transport over time. Li^+ was used in the Nafion[®] based IPMC where the solvent was water. 1,25 V DC electric potential was applied [78].

As a last step of the proposed mechanism, the boundary layers were studied. In the analysis of anode layer, the depletion of the cations from anode side results in a pressure difference and also since the cations were depleted electrostatic interaction forces develop among the remaining fixed anions, where the dipole-dipole interaction diminishes. On the other hand, on the cathode boundary layer the osmotic pressure and the electrostatic interaction forces were taken into account. In the electrostatic interaction forces, two forms were identified: the attraction due to the cation-anion pseudodipoles – that were already present in the cluster- and the repulsion due to the extra cations that were migrated into the cluster –which interacts with the existing pseudodipoles-. It is said that, the latter produces additional stress and this leads to expansion or contraction of the clusters. Therein, the expansion and contraction behavior depends on the cations distributed over the fixed anions.

Finally, this model [78] explains the behavior when the applied electric field is removed. The experimental observations have led to the statement: some of the cations were rapidly removed to the anode boundary layer and some of the cations were transported back into the interior of the membrane. The relaxation model of the IPMC due to the discharging was proposed similar to the charging phenomena.

Likewise the Nemat-Nasser and Zamani's wide work [78], mechanical actuation of IPMC is explained by a mixture framework theory. One of the solid species was used to model the polymeric ion exchange matrix; another species was used to model the ionic medium and the uncharged solvent; lastly one more species was used for modeling the gaseous charged ions [31]. This model uses the osmotic pressure, electrostatic forces, polymer swelling and analytically derived boundary layer formation. The same mixture based model is published as a two-dimensional plate like model (similar to general models for piezoelectric bimorph plates) in order to show that the electric capacitance of IPMC which is proposed as depending only on IPMC's dielectric constant and the depth of the oppositely charged ion boundary layers for sensing and actuation property [94].

Asaka and Oguro [85] have reported a work based on an electro-kinetical study. This study presented IPMC's electro-mechanical response kinetics while indicating some important properties of the working principle. It is indicated that IPMC actuates towards the anode side; however after a characteristic time, the pH of the polymer membrane affects the further bending (or relaxation) direction. This phenomena was shown experimentally: The Nafion[®]-IPMCs (Nafion[®]-112, 115 and 117) bent towards the anode side firstly and then bend back to the cathode side (back-relaxation) after characteristic time in the acid solution (Figure 11.B); however in the salt solution after the characteristic time, even though the bending time has changed the direction of bending did not change (continued towards anode), where initially IPMC bent toward anode side (Figure 11. A).

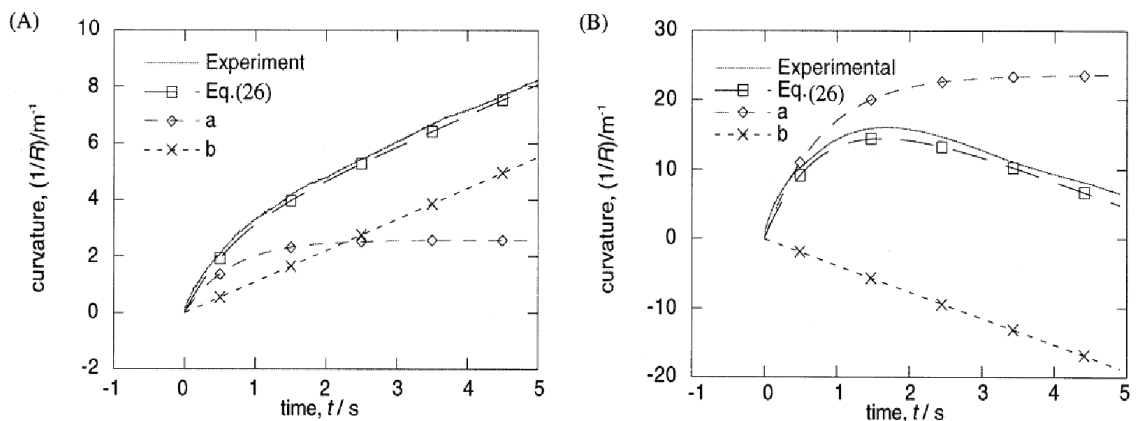


Figure 11. Nafion[®] based IPMC's bending curvature response in 0,1 M Na₂SO₄ (A) and 0,1 M Na₂SO₄ + 30 mM H₂SO₄ (B), driven by a step current [85].

All above mentioned models are based on the actuation performance of the IPMC. In terms of sensing, Gao and Weiland [40] built a model which is based on the

morphology of Nafion®. The sensing mechanism was explained in terms of the streaming potential. Streaming potential is the ion transport from the high chemical energy metal phase to the lower chemical energy electrolyte (the ion conductive polymer membrane) phase when an electric double layer has been formed due to the submerging the electrode in an electrolyte. In addition to this, an application of a pressure gradient along the surface electrode and concurrently shearing the base polymer membrane against the electrode resulted in disruption of electric current in the electrode. Conclusively, a potential and a current in the electrode is generated which are known as the streaming potentials and streaming current (Figure 12) [40].

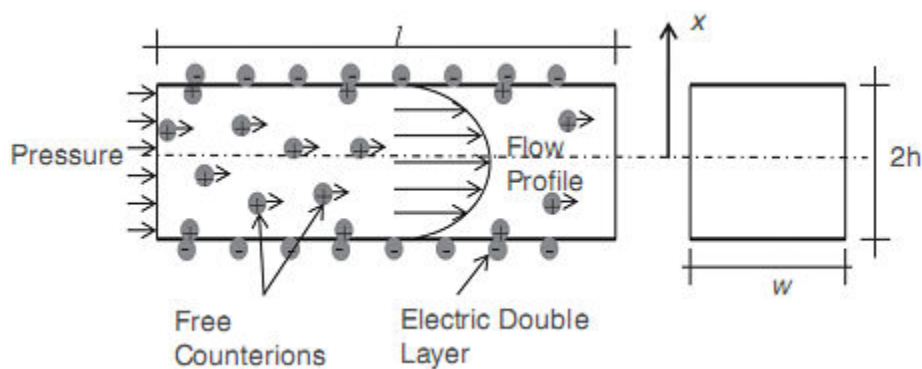


Figure 12. Streaming current in a channel [40].

1.2.2 Electrode Layers

The electrode layers have been produced generally by two different methods: the initial compositing process and the surface electroding process. The initial compositing process forms a rough surface while surface electroding process forms more uniform, less-rough well-deposited Pt-layers, generally. The latter is denser and deeper than the former.

Type of the electrode metal, surface morphology and metal particles' diffusion range into the membrane are important factors for IPMC actuation performance [89].

Type of the electrode material affects the displacement behavior of IPMC because of the fact that electrode material influences the thermal and mechanical behavior of IPMC strongly. Various metals such as Pt, Pd, Au, Ag and some transition metals like Fe and Ni and also the carbon nanotubes have been used for electrode layers in IPMC [89; 23]. Additionally, metal composites such as Pt/Ag¹⁴ or Pt/Au¹⁵ were used for IPMC electrodes. Beside of precious metal composites, (Pt)/nonprecious (like (Pt)/Cu) metal

composites have been preferred in order to reduce the manufacturing cost while improving the electrical conductivity [89].

In the enhancement of electrical conductivity of the electrode layers, Au has been widely investigated among the above-mentioned electrodes. It was reported that the Au showed the highest tensile strength and modulus in both dry and fully hydrated operating conditions; with a favorable thermal behavior, glass-transition temperature and melting point [89]. In addition to these, in comparison with Pt since it is one of the most used electrode materials for IPMC, Au electrodes are softer, more stable in acid, more conductive and less electro-chemically active [117]. Furthermore, Au showed smaller particle morphology, good particle penetration and more clearly formed surface compared to the other electrode layers [89].

Likewise the electrode material, surface morphology also affects the bending properties of IPMC. For instance, it was reported that anisotropic surface roughness enhances the bending response [117]. On the other hand, several methods were developed in order to control and increase the displacement output. Dry film photoresists were used to pattern the electrode layers. The resulting IPMC was able to dispose complex motions like peristaltic movements [54]. In another investigation, it was observed that the chemically plated metal electrodes, which creates porosity on the surface, exhibit appearance and disappearance of water on the surface during the contraction and expansion of the IPMC. This decreases the effective output force. In order to dissipate loss of outcome, another study used dispersing agents to create more uniform electrode plates, where the Pt particles were distributed in smaller diameters [115]. The poly(vinyl pyrrolidone) was also used as a dispersing agent which increased the penetration depth of metal particles. This study noted that the use of dispersing agent produces uniform electrode layers that increases the electrical conductivity and the actuation performance of the IPMC [89]. Beside of all these improvements, coatings have been used for longer-life performance of IPMC [62].

1.2.3 Solvent

Water (deionized) is the one of the most used solvents in IPMC. In the water swollen IPMCs, the initial actuation occurs in a fraction of second [79]. This is known as one of the characteristic of the IPMCs. However, this fast response disables to observe the IPMCs actuation behavior and also the applied voltage is hold below the

1,3V at room temperature in order to avoid water electrolysis. Furthermore, in air operation conditions water evaporates in a short period of time [40]. Therewith, ethylene glycol, glycerol and also crown ethers have been brought out to use in IPMC to swell the IPMC membrane [79; 78]. 2V-3V potentials are suitable to be applied with these solvents. These solvents were used to retard the actuation for inspection of the IPMC behaviors since it has been proposed that solvent affects speed of the actuation [79]. The above mentioned polar solvents have a higher viscosity than water. Therefore, the actuation speed can be directly correlated with solvent viscosity. Additionally, ionic liquids have been used in polymer electrolyte membranes in order to enhance the actuation performance and also ionic liquids enable the superior orientation in the IPMC membrane structure [119].

It was also reported that the harmony of the cation and solvent used in membrane affects the actuation performance. For example, in Nafion[®]-based IPMCs, Li⁺ exposes a small back-relaxation towards cathode in water-swollen state; however when ethylene glycol, glycerol or 12-Crown-4 is used as solvent, an extensive back relaxation towards cathode was observed with an initial small actuation towards anode side. Furthermore, K⁺ shows extensive back relaxation in water, ethylene glycol, glycerol; however any back-relaxation towards cathode was not seen in 18-Crown-6; but a relaxation or a further actuation towards anode side was observed in Nafion[®]-based IPMCs when 18-Crown-6 as a solvent. Likewise, back-relaxation phenomena was observed with Na⁺ as the base cation in water, ethylene glycol, glycerol and 18-Crown-6 solvents; but not in 15-Crown-5 solvent in the Nafion[®] membrane based IPMCs [78].

1.2.4 Mobile Ions

Li⁺, Na⁺, K⁺ [79] and H⁺ in the water hydrated form are the mostly used forms of the cations (the counter ions) in the IPMCs. In addition to these, Rb⁺, Cs⁺ and also alkyl-ammonium cations, tetramethylammonium (TMA⁺) and tetrabutylammonium (TBA⁺) have been experimented in actuation performance [77].

Nafion[®]-based IPMCs actuate towards anode, a volume expansion is observed on cathode side, in the case of swelling the membrane with cation as mobile ions. This phenomenon has been accepted as the IPMCs' bending property; however the use of various cations (with different backbones) revealed that the actuation direction and

speed can vary with respect to the cation type, and also the solvent and the backbone as stated before.

Nemat-Nasser and Wu [77] were published a general trend of actuation behavior of Nafion[®]-based IPMCs with different cation forms. It was observed that, in a water saturated Nafion[®]-based IPMC in an alkali-metal cation form bends towards anode firstly; subsequently followed by a slow relaxation towards cathode in an applied (1 V) DC electrical field.

In TMA⁺ form, Nafion[®]-based IPMC's actuation was about twice larger than that in the alkali-metal cation forms; however with a lower speed. Nafion[®]-based IPMC's in TMA⁺ form, reached its maximum displacement in 1,3 seconds, where in alkali-metal cation forms the maximum displacement was reached in a fraction of 1 second). On the other hand, the behavior in TBA⁺ form was reported that a very slow actuation and a low displacement have seen towards anode without any back-relaxation [77]. Furthermore, it is reported that actuation displacement of TMA⁺ and Li⁺ were recovered partially under an applied DC voltage, where as the back-relaxation in Na⁺, K⁺, Rb⁺ and Cs⁺ was greater than the displacement achieved during the actuation (IPMCs bent back beyond their initial positions) [77]. The higher back-relaxation maybe attributed to the visco-elastic behavior of the polymeric membrane. The displaced cations may be stretching the polymer chains which may add extra energy to the polymer chains; therefore during the back-relaxation, when the polymer chain removes the tension a spring effect may led to higher back-relaxation in Nafion[®]-based IPMCs.

1.2.5 Characterization of IPMC- Actuation and Sensing Behavior

The standard characterization of IPMC actuation has been characterized by a laser system which detects the motion of the tip displacement or a camera that records the displacement movement [55]. Owing to the fact that the bending shape of IPMC differs a lot, the tip displacement has been intended to be measured, while models have been proposed to anticipate the shape of the initiated bending [64; 7]. Fluorescent spectroscopy was used to taking photographs of a displacing Nafion[®]- based IPMC and for observations of the cation migration in the membrane. The intensity of the light that is created due to the cation migration depicted on the photograph (Figure 6). The intensity has been correlated with the IPMC's displacement that was observed with a laser optical displacement sensor [90]. Electromyography (EMG) was also used to detect

the IPMC actuation, where the initiating field was created by a contracted muscle of a human. The displacement of IPMC was measured by the EMG signals [62]. Moreover, in displacement measurements, changes in surface electrode resistance were observed with respect to the compression or in the extension of an IPMC. This relation was used in relating capacitance, the surface resistance and the applied voltage as well as with the potential created across the IPMC strip [36]. On the other hand, micro-balance load cells have been used to measure the output force [16].

1.2.6 Novel IPMCs

Novel IPMCs have been produced with many different production methods as well as with many different constituents. An Ionic Polymer-Metal- ZnO Composite was synthesized. Photoluminescence (PL)-quenching was observed both on mechanical bending and under applied electric field [58]. Electrospinning was used to built Nafion[®] nanofibrous mats as an IPMC ion conductive membrane [20]. The ionic conductivity have not showed any difference with the conventional Nafion[®]- based IPMCs in water-hydrated conditions. However, in ionic liquid saturated condition the ionic conductivity was increased about to three folds and higher strain speed was observed. Perfluoroalkylacrylate-acryl acid copolymers with different types of counter cations were synthesized via radical copolymerization of fluoroalkylacrylate and acrylic acid in order to produce IPMC [49]. Fullerene-reinforced Nafion[®] were used for IPMC applications as well, where a significant increase in tensile strength and Young's modulus were observed; the harmonic and low frequency responses at low voltages were improved and also the straightening-back of IPMC considerably decreased by the cooperation of the fullerenes [51]. Likewise, partially cross-linked and sulfonated poly(vinyl-alcohol) (PVA) membranes were prepared for IPMC [61]. In addition to this, poly 2-acrylamido-2-methyl-1-propanesulfonic acid (PAMPS), were used to synthesize IPMC's polymeric ion exchange membranes [48; 28; 101]; for example, a blend PVA, which is water soluble, and (PAMPS), which is highly ionic conductive, were synthesized and very high bending (> 100°) IPMC synthesized while reducing the back-straightening [28]. On the other hand, Nafion[®]'s surface was treated with O₂ plasma in order to change the surface morphology. In this study, the surface resistance was decreased and electrical capacitance was increased while these improvements were resulted in enhancement in actuation, force and operational life time [108].

1.2.7 Applications

Artificial muscle analogy for IPMCs was one of the starting points for the wide-open vision for applications. IPMC has been a good opportunity in the biorobotics, biomedical devices and medical usage due to its soft but fast actuation property [85; 97]. And also the actuation performance of IPMC that is initiated by the electromyography (EMG) signals was an intention to show the potential applications of IPMCs in biomimetics [62] and artificial muscles, or in prosthesis [9]. Furthermore, IPMCs have been adapted as robotic actuators such as underwater fish like microrobot [44] and electrical sensors like micro pumps, diaphragms for micropump devices and active vibration control systems [89; 111; 109; 7]. On the other hand, underwater propulsion device have been designed due to the ability of IPMC to operate in wet conditions as a unique characteristic [97; 57; 111].

The large capacitance behavior of IPMC was used in energy storage areas [58] like energy harvesters for battery charging systems. By benefiting from the electrical power generation due to the mechanical flexing (bending), smart paper-like thin sheet batteries were made [111]. Herein, smart behavior reveals in thin-sheets property of being rechargeable with moisture. The advantageous part is that, this thin sheets can be bonded, glued or attached to any flexible (or rigid) substrate and also be laminated in order to sense the mechanical motion.

Shahinpoor and Kim [112] were designed a device consists of IPMC actuators in order to compress and assist heart and control the arrhythmia of heart (Figure 13). It is proposed that this device can be externally implanted to the heart and partly sutured without a contact by internal blood circulation. Therefore, this implementation prevents the blood clots, thrombosis and similar complications which are currently a problem of the present artificial hearts and heart assist devices. However, the implement is not contacted with blood, it is in contact with the cells, tissues and human body fluids (Figure 13). Hence, it is noted that the study must be extended to plasma proteins adsorption, macrophage adhesion, tissue damage fibroblast deposition and capsulation [112]. On the other hand, toxicity investigations on IPMC are a topic which is needed to be studied in terms of bio-medical applications.

Moreover, a low cost fabrication method has been proposed in the scope of creating an active cardiac catheter. The bending motion of IPMC was offered to be controlled by

a conventional PID controller by Bo-Kai Fang et al. [35]. Therewith, the utilization design expanded to use of IPMC as a head of active guide-wire system without a bulky sensor or a conventional controller from cardiac operations [36]. Furthermore, a biomimetic micro-collector was proposed in order to treat chronic total occlusion [21]. The micro-collector was designed as a jellyfish to environ and collect the clots by an inverse jelly movement. The innovation in this study is a photosensitive and biocompatible polymer surface coating that prevents the bubble occurrence on the platinum surface which might be either due to the electrolysis of water or the solvent leakage. The photosensitive coating resulted in decrease in displacement capacity with respect to a non-coated IPMC strip. Besides of these, a gripper [47; 32] and a robotic arm lifter has been produced [9].

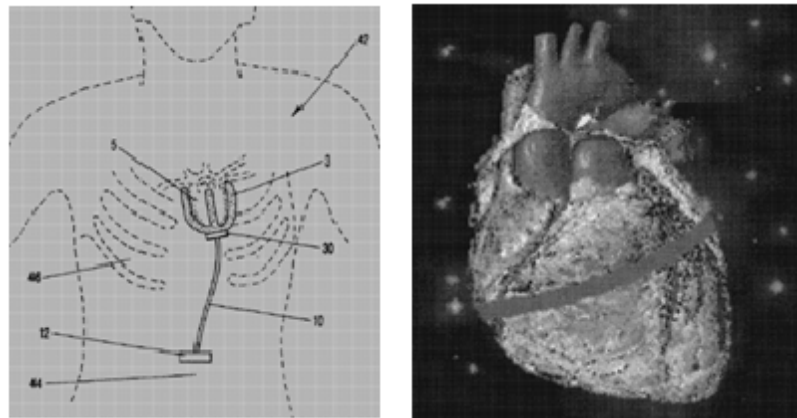


Figure 13. The compression device placement (left) and the Arrhythmia control of heat beats by IPMC strips (right) [112].

On the other hand, IPMC is one of the favorite topics in space applications as robotic arms, end effectors, actuators and controllers. In the explorations of neighbor planets, in order to improve the research capacity and human safety, it is stated precise vibration and pointing control is crucial (estimations made by NASA in 1990s on ‘human mission to Mars’ (around mid 2030s)); where IPMC materials can play significant role. IPMC based artificial muscles can be embedded to spacesuits that assist exercising of the astronauts’ muscles by nature of IPMC actuation. The launch and on-orbit vibrations can also be measured through the incorporation of IPMC into spacecraft due to the IPMC’s sensing nature. In addition to these, one of the most intriguing designs of IPMC is the robotic insects/worm-like designs in exploring the planetary surfaces. It was proposed that the planet can be navigated by a Mars turtle,

worm or a Mars fly over, on and below the surface. Hence astrobiological, chemical, spectral and geologic data can be collected by the IPMC micro-sensors placed on the robots or directly by IPMC robot. The high maneuverability and flexibility of IPMC enriches the space investigation devices/robots [60].

Loss of bone mass, reduction in muscle volume and strength in human were observed during the astronauts' mission (For instance, 'Human mission to Mars' foresees that the mission cover 850-900 days (550-560 days on Mars)). In order to keep the astronauts healthy, fabrication of a tight suit is suggested that is designed with IPMC actuators/muscles in touch with human muscles. A combination of selective electric pulse sequences on IPMC artificial muscles provides external exercising of the astronauts' body. The same approach can be used in physiotherapy. And also astronaut's physical performance and response time can be enhanced with a similar IPMC incorporated suit in space environments, especially during extravehicular activities [60].

IPMCs can be employed for satellites, too. Vibrations on satellites are inconvenient for the microgravity researches and experiments that require vibration-free environments; as well as for the crew. In this case, the vibrations can be recorded by placing IPMC to the structural vibration points on the satellites. These records lead to new satellite models and designs. On the other hand, IPMC can be placed to the strategic points to create a reverse vibration owing to reduce the satellite vibrations. The power consumption, minimal volume and weight, and fast response properties of IPMC redounds its preference [60].

It is expected that in the future, IPMCs is going to be able to broadly spread in many areas from small-sized biomedical devices to large-scale aerospace actuators as well as in many other industrial applications [89].

1.3 Nafion[®] and Poly(ethylene-*alt*-tetrafluoroethylene)

1.3.1 Nafion[®]

Nafion[®] is synthesized via the copolymerization of a perfluorinated vinyl ether comonomer with tetrafluoroethylene (TFE) (Figure 14). The Nafion[®] films, which are used in this study, can be achieved from the thermoplastic -SO₂F form of ionomer by extruding into sheets in desired thickness. Since strong interactions between ionic

groups difficulty in melting process, the $-\text{SO}_2\text{F}$ form is the preferred structure. This precursor does not induce the clustered morphology, but it does induce Teflon[®]-like crystallinity. Teflon[®]-like crystallinity is tenacious in conversion of sulfonyl fluoride form, for example, into K^+ form with reaction of KOH in water and DMSO (dimethyl sulfoxide, an important polar aprotic solvent). Hence, the $-\text{SO}_3\text{H}$ form is derived with soaking the film into a sufficiently concentrated aqueous acid solution. This step is called as activation of Nafion[®] films [72] for exhibiting its ion conductive character.

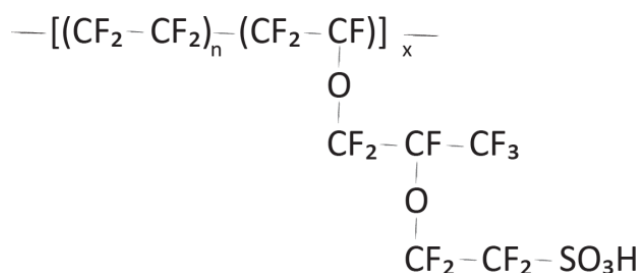


Figure 14. Nafion[®]

Ion conductive character and ionic aggregation in Nafion[®] have been attracted attentions towards modeling ionomeric structure in the polymer. The structural investigations of hydrated Nafion[®], hence investigations on the working mechanism of ionic conduction, have been started during 1970s. By the late 1970s, an experimental evidence for consistency of ionic aggregates in Nafion[®]'s structure emerged from the small-angle X-ray scatterings (SAXS). Hence, the ionic domain morphology had an importance in Nafion[®] structure. Gierke and co-workers [72], analyzed, a range of equivalent weights, in the unhydrolyzed sulfonic acid form and the neutralized metal sulfonate form (“For the unhydrolyzed precursor, a low angle SAXS maximum near $0.5^\circ 2\theta$ and a diffraction peak at $18^\circ 2\theta$ (superimposed on a broad amorphous halo from 10° to $20^\circ 2\theta$) were observed for samples having equivalent weights (equivalent weight, EW, the grams of polymer per equivalent of sulfonate groups) ranging from 1100 to 1800 g/equiv.”). The increasing intensity of the scattering and diffraction peaks with the equivalent weight (with an increase in between the statistical length of crystallizable PTFE chain segments and the side chains) were observed and it was examined that these peaks disappear at the temperatures close to the melting point of the PTFE.

Therefore, these results were attributed to the crystalline organization within the fluorocarbon matrix of Nafion[®].

On the other hand, the hydrolyzed Nafion[®] showed another scattering peak at $1.6^\circ 2\theta$, which corresponds to a Bragg spacing of 3-5 nm. These features were attributed to characteristics of a system that consists of *ionic clusters* in a semicrystalline matrix. The ionic clusters, generally, in perfluorosulfonate ionomer literature, are defined as the ionic aggregates separated with a nano-phase (It is important to note that, this terminology differs from the currently used definition for the other dry ionomers, such as sulfonated polystyrene) [72].

Unlikely, the crystalline features' SAXS and WAXD results, the ionomer peak showed an increase in intensity and shift to lower angles with the decrease in equivalent weight. And also, the ionomer peak shifted to lower angles and showed an increase in intensity with increasing water content of the polymer matrix. Originating from these findings, and based on the most prevalent three models –at that time–: a spherical cluster model on a paracrystalline lattice, a core-shell model, and a lamellar model; Gierke and co-workers [72] proposed that water-swollen structure of Nafion[®] consists of approximately spherical shaped ionic crystals forming an inverted micellar structure, shown in Figure 15. In addition to these, the ion transport pathway was presented with interconnecting narrow channels between the clusters –by with the considerations of the ion permselectivity of Nafion[®] and a percolation way for the ions in the structure–. Hence the model was named as the cluster-network model, also referred as cluster-channel model. The cluster-network model has been received the most significant acceptance in the Nafion[®]'s literature until today [72].

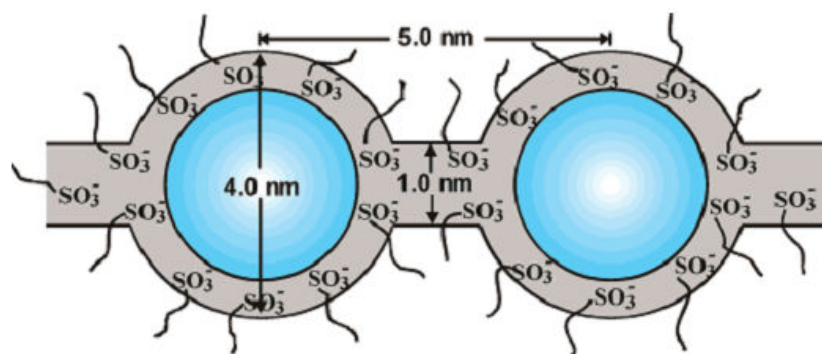


Figure 15. Cluster-network model for the hydrated morphology Nafion[®] [72].

Many developments has been proposed over the cluster-network channel; as the interconnections were bridged by single ionic sites rather than the organized ionic channels; or a connected networks of rods opposing to the locally ordered spherical clusters; while the cluster-network was proposing a nonrecoverable plastic flow, a reversible swelling-deswelling behavior is observed. The later studies showed that the d spacings are propotional to the volume of absorbed water by using the SAXS data of the Gierke's work. Arising from this observation, the ionic domains were defined as hydrophilic "micelle" layers separated by the PTFE like crystal thin lamellars. When water is absorbed from in between the lamellas; the lamellas are separated and the d spacing is increased. That is to say, the d spacing between the ionic domains are propotional to the volume fraction of water in the polymer matrix and it is proposed that the swelling behavior should be completely reversible in order to eliminate the morphological reorganization of the structure. A synchrotron SAXS study led to development in more lamellar models. The most fundamental result was the 4 nm Bragg spacing, d, which had been already coherent with the all other SAXS measurements. In this study, the morphological structure was resembled to a sandwich, where the outer portion –the shell- composed of the side chains, sulfonic acid groups, and the inner liquid portion –the core- consisted of water/methanol molecules and the channels as the proton conduction pathways, the former structural elements were described as being juxtaposed linearly so that the liquid-core regions are contiguous –resembles a sandwich-. In addition to these, many other models have been proposed, in which some of them appeared in the scale of developments while some of them lost its effectiveness [72].

The earliest motivation of Nafion[®] research, in terms of applications, was concentrated on permselective membrane separator in electrochemical cells, in industrial scale production of NaOH, KOH and Cl₂. In the frame of this focus, the Nafion[®] membrane has been used to keep Cl₂ and H₂ gases separated and preclude the unfavorable back migration of hydrated OH⁻ ions from concentrated NaOH_(aq) or KOH_(aq) catholyte chamber while allowing transport of the hydrated Na⁺ ions from the NaCl_(aq) anolyte chamber [72]. The latest interest in Nafion[®]'s research towards fuel cells due to its proton conducting property [5; 50; 124; 67; 126; 72]. In this sense, another addressable topic is the degradation of Nafion[®] -in fuel cell environment-. It is mentioned that peroxide radicals attack the H-ending terminal groups of the polymer. The H₂O₂ is formed -during the fuel cell operation- due to the reactions between oxygen

and hydrogen and then decomposes to $\cdot\text{OH}$ and $\cdot\text{OOH}$ radicals. Hence, these radicals start the chemical decomposition of the polymer [72]. In addition to these, Nafion[®] has been a starting point for ionic polymer metal composites [107; 86]

Sadeghipour et al. [107] discovered Nafion[®] -based hydrogen pressure cells were potential micro-systems for efficient vibration damping. The viscoelastic property, an intermediate behavior of the elasticity of a crystalline solid and the viscosity of a liquid, of Nafion[®] was the main motivation to rely on an inherent internal damping in Nafion[®] -based hydrogen pressure cells. The research presented that the Nafion[®] was deficient in terms of satisfying the expectations in vibration damping; however this investigation brought the contribution of a new, Nafion[®] -based, *smart material*.

Initially, Nafion[®] was used as a proton conducting medium inside hydrogen pressure cells, as the cell built up by sandwiching the Nafion[®] membrane with conductive adhesives to two metal electrodes on both sites, but afterwards it was platinized on both sides as metal electrodes and today's IPMC has emerged. (Figure 16). Concurrently, Oguru et al. [86] have presented an investigation of bending behavior of an ion conducting polymer film-electrode composite under applied low voltage. Hereafter, ionic polymer composites developed in manner of actuation and sensing at applied low voltages.

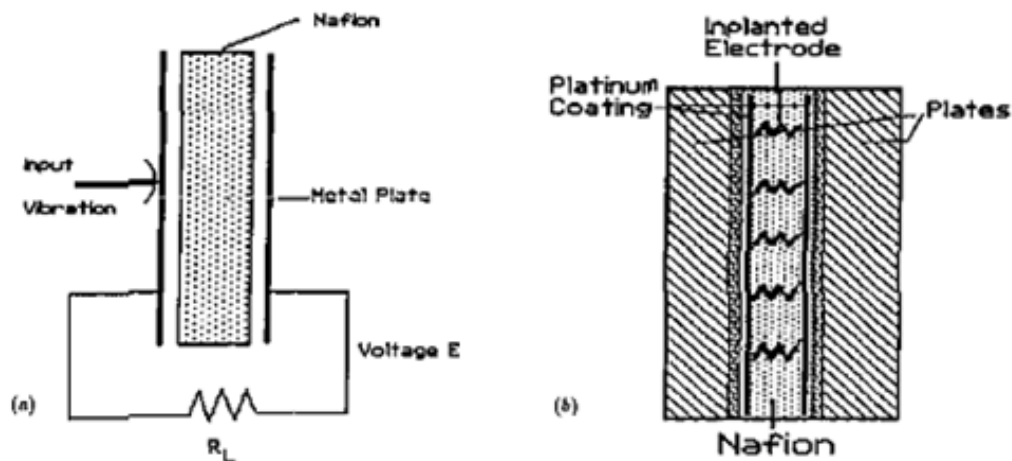


Figure 16. The platinized Nafion[®] proposed by Sadeghipour et al. [107].

1.3.2 Poly(ethylene-*alt*-tetrafluoroethylene)

Poly(ethylene-*alt*-tetrafluoroethylene) (ETFE) is one of the fluoropolymers. Fluoropolymers are chemically inert materials with good high temperature resistance. These properties arise from the strong carbon-fluorine bond. Indeed it is the strongest bond among the carbon bonds with all known elements, yet. Fluoropolymers are mostly preferred for the harsh chemical environments. Hence, chemical modifications of fluoropolymers are arduous. Although its high chemical stability, fluoropolymers are one of the most sensitive polymers to radiation. Therefore, high energy radiation (X-rays, γ -rays, vacuum ultraviolet, excimer or Ar^+ lasers, electron and ion beams) bestows an opportunity to create active sites on the fluoropolymer structure that opens a route to modify the fluoropolymers chemically. Furthermore, radiation induced processes supply an advantage to modify both surface and bulk properties of the fluoropolymers [29].

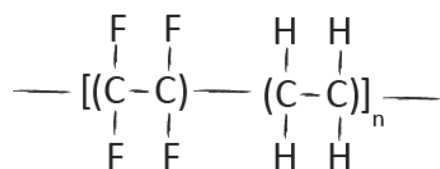


Figure 17. Poly(ethylene-*alt*-tetrafluoroethylene) (ETFE).

Poly(ethylene-*alt*-tetrafluoroethylene) (ETFE) is a 1:1 alternating copolymer of ethylene and tetrafluoroethylene (Figure 17). Ethylene-tetrafluoroethylene, as an alternation of polyethylene and poly(tetrafluoroethylene), combines the properties of both fluorocarbon and hydrocarbon polymers [75]. ETFE is a semi-crystalline, melt processable perfluorinated polymer. It is non-reactive with acids or alkalis and has a low surface energy by being highly pure as a fluoropolymer [121; 123; 93]. ETFE has better radiation stability and has relatively higher electrical and thermal resistance than its perfluorinated cooperators. ETFE is less dense, tougher, stiffer and has a high tensile strength, flexural modulus and creep resistance than the fully fluorinated poly(tetrafluoroethylene) (PTFE) and poly(tetrafluoroethylene-co-perfluorovinyl ether). It also presents very high resistance to be solved in common solvents, like PTFE, and a high resistance to radiation as well as fatigue [75]. Hence, perfluorinated polymers are convenient base materials for ion exchange membranes. On the other hand, these properties, which reflect its substantial chemical and physical stability, are a difficulty for the chemical modifications by conventional oxidizing agents. Therefore, ionizing

radiation is a convenient route for creation of reactive species on the surface as well as in the bulk of the fluorinated polymers [123; 29].

Although, ETFE, is an enduring material to exposure of radiation, the radiation causes degradation of its molecular structure [29]. Cross-linking has been observed during the irradiation process [106]. Tetrafluoroethylene, contained in ETFE, has an initial bond breaking in the side chains (C-F) rather than in the main chains (C-C); hence the chain scission occurs. The scission of C-F bond yields highly reactive fluorine atom which immediately attacks a C-C bond in the main chain. As a result, two chain fragments are produced [123]. On the other hand, with a similar approach as the ethylene a part of ETFE, it has been observed that degradation resulted from radiation in polyethylene can be a concern for crosslinking (The lower the molecular weight, the more the radiation degradation) [71]. (The covalent bond energies of ETFE are: H-F bond is 5.82 eV; C-F bond is 4.42 eV; C-H bond is 4.28 eV; C-C bond is 3.44 eV [123].

As, it induces crosslinking and also chain scission in the base fluoropolymer film [106], irradiation creates pores and roughness on the film (surface), too. 300 to 500 nm hollows and bulges have been observed on the film surface. On the upper side of the film, where the films were irradiated through the thickness during the manufacturing process and only the upper side of the film underwent direct contact with the radiation, 300-400 nm roughness was observed; while the roughness has been in 400-500 nm size on the opposite side. This difference has been attributed to back-scattering phenomena from the metal surface of the irradiation apparatus [106].

Beside of all its properties that are important scientifically, in economical terms ETFE-sulfonic acid membranes are much cheaper (30-100 \$/m²) than the other poly(perfluoro sulfonic acid) based membranes (500-2000 \$/m²) [106].

1.4 Radiation Grafting

Radiation initiated polymer modification has been of interest since the 1950s [17; 74]. Radiation grafting refers a grafting method where the active sites on the polymer backbone are created by radiation randomly and grafting of side chains to the backbone on these active sites by covalent interactions, more specifically by free radical polymerization [29; 3; 74].

In this thesis, radiation grafting is in interest in the manner of grafting of polymer films and producing utilizable membranes in ionic polymer metal composites.



Figure 18. A schematic and scriptural representation of radiation grafting. The red line on the schematic figure (left) represents a part of the polymer-backbone; the blue lines represent the grafted side chains. The former is represented with “A”s and the latter is represented with B_m and B_n on the scriptural figure (right).

Synthetic membranes are the heterogeneous solid-phases. They are usually used as barriers between two –other- phases where the transport of molecular or ionic species of liquids; or gases in contact with their surfaces are allowed under a driving force. The membranes supplies selective transport of distinct species over the others and regulate the transport of species at different controlled rates. The former is called as selectivity and the latter is called as permeability or flux. The selective transport of species occurs owing to the differences in size, shape, chemical properties or electrical charge of the component in the mixture [74]; the permeability is also affected by the same properties.

In polymeric membrane preparation, many techniques have been developed like dip-coating, interfacial polymerization, in-situ polymerization and graft copolymerization as well as radiation-induced graft polymerization. Radiation-induced graft polymerization is known as a technique where different forms of the polymers like films, resins and fibers can be used [74]. Therefore, radiation-induced grafting is a particular interest in our research since our preliminary materials is poly(ethylene-tetrafluoroethylene) films.

1.4.1 Irradiation

The preeminence of radiation activation is arising from the sovereignty of non-initiator and catalyst used performance; hence the ability to polymerize in a wide range of temperatures, including the low temperatures, in various states of monomers like in bulk, in solution, in emulsion and also at solid state [74], where conventional methods fail. The initiation step is a ready variation of active sites -for example a primarily carbon-based radical creation or hydroperoxy based-. Radiation-induced grafting is able to create active sites either only on the surface or also in the bulk of the film. The total

irradiation dose and the irradiation rate can be varied. The readily fabricated form of the material can be modified directly in irradiation [17] and also the polymerization is able to start and end on the polymer film –without the necessity of additional processing like recasting-. Furthermore, two highly incompatible polymers can be combined in order to create a –grafted- polymer with new properties uniquely [74].

Radiation exposure onto polymers can create active sites, as radicals, on the polymer (Figure 19) as well as results in structural changes like chain scissions and crosslinks in the base film [29]. The radiation exposure can be applied either with electromagnetic waves, i.e. X-rays and gamma rays, or with charged particles, such as beta particles and electrons [3]. Electrons (and other charged particles) lose energy during the travel across the film mainly because of inelastic scatterings. Hence penetration depth decreases and the direction of travel changes. Thereby electromagnetic radiation, such as gamma rays, is the preferred radiation type. A portion of photons can transmit by losing intensity but keeping their original state of energies and directions (exponential attenuation law). The conserved energy and the unchanged direction of photons supply control over rate of irradiation dose with an attenuator without influencing the photon energy [3].

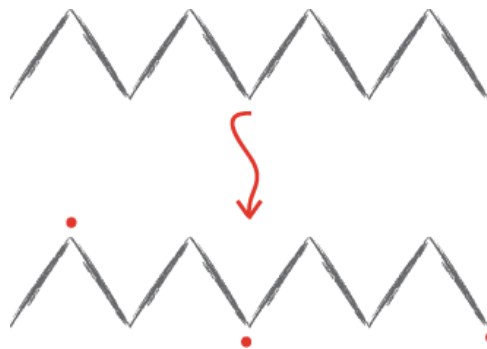


Figure 19. Reactive active sites, the radicals, were illustrated with dots.

The ^{60}Co is one of the versatile gamma radiation source, currently. The half-life of the ^{60}Co is 5.3 years and the emitted radiation is 1.17 MeV and 1.33 MeV (mean value of 1.25 MeV). The cavity-type unit and the cave-type unit of ^{60}Co are available for irradiation. The latter type is used in industrial scale productions [3; 116].

Absorbed dose is the expression of the polymer under exposure to the radiation. The amount of energy transferred to the matter is the absorbed radiation dose by the material; which is described by the unit in Gray (Gy), up-to-date [3].

$$1 \text{ Gy} = 1 \frac{\text{J}}{\text{kg}} = 1 \text{ m}^2 \cdot \text{s}^{-2}$$

The irradiation dose has a great importance in terms of change in physical structure of the polymer. In this study, poly(ethylene-*alt*-tetrafluoroethylene), a fluoropolymer, is used as the base polymer. Fluoropolymers have outstanding structural properties by having a high chemical resistance, mechanical strength, high temperature stability and good weathering behavior, especially in oxidizing environments. However, high energy radiation interactions may alter these physical and chemical properties. The irradiation causes ionization of the polymer matrix which results in formation of ions, radicals and excited species. Hence, the chain scission and crosslinking are the consequences, and also volatile species are formed, which lead to significant change in the molecular weight. The magnitude of these changes is also dependent on nature of radiation, irradiation temperature, and the irradiation dose besides of the chemical and physical nature of the polymer matrix [3; 29].

1.4.2 Graft Polymerization

A graft polymer indicates, generally, a main polymer chain is branched with one or more type of molecules, in which these side chains are constitutionally or configurationally distinct from the main chain. This structural difference of the grafted side chains opens up a route to modificate the polymeric material with desirable physical and chemical properties.

In radiation-induced graft polymerization, active sites, i.e. radicals, are created by the radiation overall the polymeric base material thereof the polymer chains have been resembled to a macro-radical [3]. The polymerization of monomer instantaneously starts on the chain (Figure 20). The extent of the polymerization of the monomer (illustrated with B in Figure 18) on the base polymer film (represented with A in Figure 18) is the yielded grafting amount and expressed as degree of grafting or graft level [29].

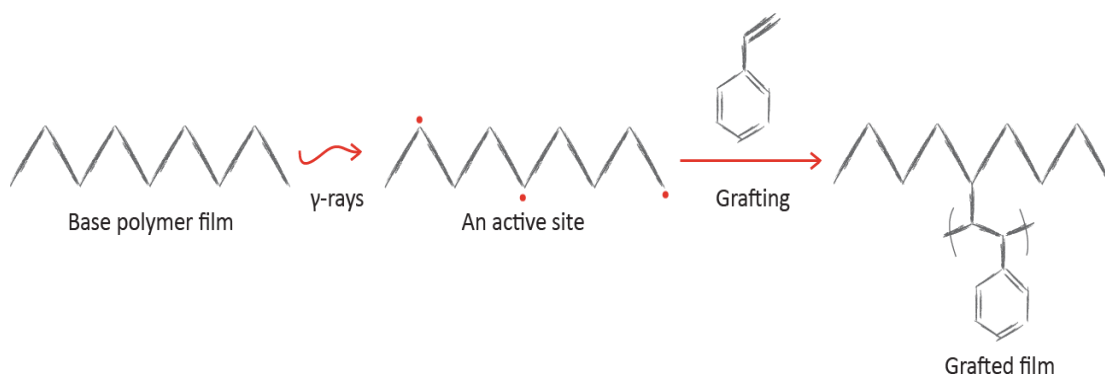


Figure 20. Irradiation and the grafting of the base polymer film.

Advantageous side of the active-polymer macromolecule might be the fact that conventionally difficult polymerizations, can be proceeded without initiator residues and/or catalysts. Furthermore, the polymerization can operate even at low temperatures; unlikely with initiators and catalysts containing polymerizations [3].

Radiation grafting can be carried out in three different ways as simultaneously, under vacuum and in air. The different methods of irradiation of polymers play an important role in designation of the physical characteristics of the radiation grafted membranes, i.e. level of grafting [3].

In simultaneous radiation grafting, both the base polymer and the monomer are exposed to the radiation (Figure 21). The monomers are polymerized on the base polymer via the in situ free radical sites [3] and the polymer is pre-swollen with the monomer [17]. Owing to the fact that monomer is also under the radiation exposure continuously, the plausible extensive homopolymerization; thereof the monomer wastage and a low efficiency of the grafting is a possible consequence [3].

In hydroperoxide method, the operation environment is air. The radicals occur on the polymer backbone and subsequently, interaction of these radicals with oxygen creates peroxides (Figure 21). The radiation grafting is initiated by the decomposition of peroxides decomposes at elevated temperatures. The disadvantages of this method is that significant high doses of irradiation is needed to create sufficient amount of hydroperoxides in order to achieve reasonable graft levels; and the oxidative degradation, which might present even before the initiation of grafting [3].

In the trapped radical method, the radiation exposure applied under vacuum or in inert atmosphere. Hence, the formed radicals remain being trapped within the polymer matrix (Figure 21) [3]. The irradiated films are kept at low temperatures to guard the trapped radicals.

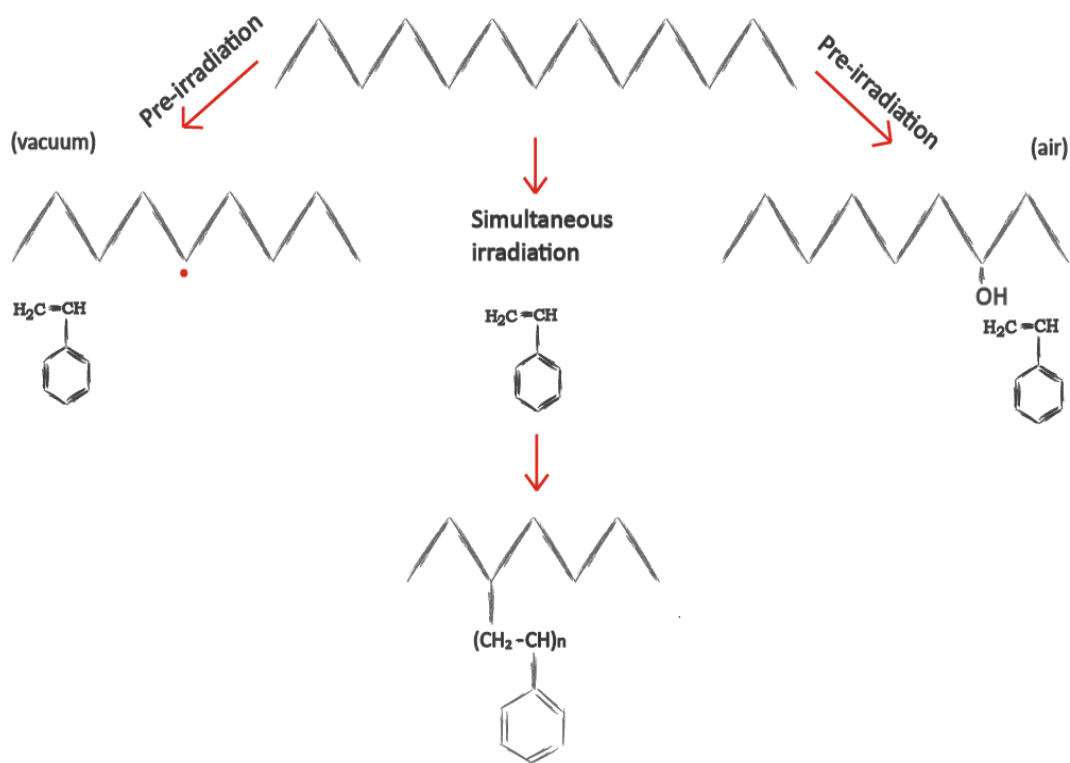


Figure 21. Irradiation of polymer base under vacuum, simultaneously and in air.

The monomer transport, in bulk polymerization, into the radiated films is said to be often a rate-limiting step [19]. It is shown in simultaneous radiation grafting of styrene monomer into polyethylene film (PE). Furthermore, the PE base film, even pre-swollen with the monomer, indicated the polymerization is often the diffusion limited [84]. When the base polymer film cannot be pre-swollen in the monomer solution, the pre-irradiation method can be used and the grafting has been proposed to proceed with grafting front mechanism (Figure 22) [17; 19; 29].

Grafting front mechanism proposes that the grafting initially starts only at the surface since the surface is the immediate contact with the monomer solution (Figure 22-a). When the regions of the grafted surface swell in monomer solution; monomer can diffuse deeper into the interiors of the film and polymerizes (Figure 22-b). Swelling of polymer film by solvent helps monomer diffusion [3; 104]. This process repeats step by step until the two grafting-fronts meet (Figure 22-d). It is found from the cross-sectional analysis that non-uniform grafting occurs due to the grafting by a front mechanism. The grafting on the surface is inevitably higher than the grafting in the interior of the polymer film, which is a handicap in ion transport applications [66].

On the other hand, grafting-front mechanism is a challenging statement due to the very short lifetimes of the radicals. However, it has been reported that radical decay can

be controlled by choice of the grafting solvent [103]. A solvent that is incompatible with the polymer increases radical life time by guarantying slow radical recombination [103; 104]. Owing to the incompatibility of the non-solvents with the grafted polymers, the non-solvents adjust the monomer concentration within the base polymer film without penetrating into the polymer phase (Figure 23) [103]. This effect has been explained by *Trommsdorf-Norrish* effect [104; 29; 118], which is caused by insolubilization of grafted polymer chains in the base polymer film. *Trommsdorf-Norrish* effect (autoacceleration effect) is that when polymerization proceeds, there is an increase in the viscosity in the entourage. The increase in viscosity reduces the mobility of reacting species. This affects the mobility of growing polymer's molecules more than the mobility of monomers or the fragments, arising from the decomposition of the initiator. Therefore, termination by combination with other growing polymer chains is hindered; but monomer diffusion is still allowed (initiation and propagation reactions still continue). Hence, such a decrease in the termination step leads to an increase in the overall rate of polymerization [82; 29].

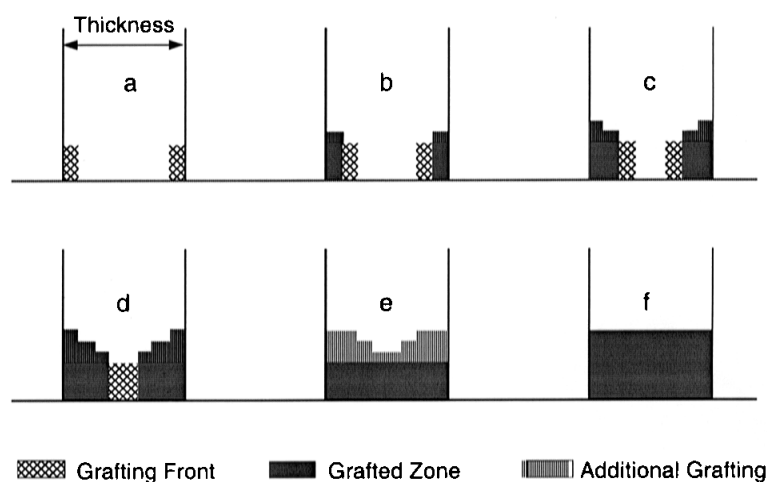


Figure 22. Grafting front mechanism [17].

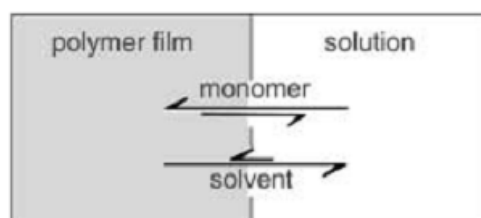


Figure 23. Influence of poor solvent on the partitioning of monomer and solvent between solution and swollen polymer film [104].

1.4.3 Conduction in Radiation Grafted Membranes

Protons are known as the main source of conduction in fluorinated acidic polymers, such as polystyrenesulfonic acid grafted ETFE, in the water swollen state [3] as well as in the polymer electrolyte membrane (PEM) fuel cells [41; 3; 29; 59; 92]. The proton conduction mainly attributed to two mechanisms: the Grotthuss Mechanism and the Vehicle Mechanism [45; 26; 27; 34; 69; 102].

Grotthuss Mechanism, also called as “flip-flop” or “hop-and-turn” mechanism, is the transfer (hop) of hydrogen nuclei between the hydrogen-bonded water molecules which are arranged in a single line and subsequent rearrangement of the hydrogen-bonded network (Figure 24). The former occurs by the transfer of a proton from an oxonium ion to a water molecule by tunneling in a hydrogen bond and the latter is the reorientation (rotation) of the water molecule in order to be able to receive the next proton [2;102]. This flow transports the hydrogen nuclei to the end of the water line.

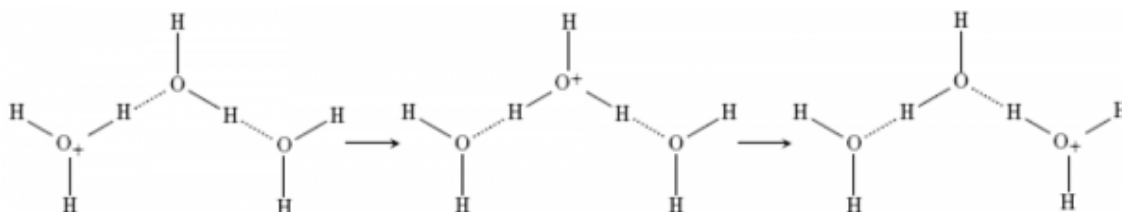


Figure 24. The transport of hydrogen ions (H^+) through water is accomplished by Grotthuss Mechanism, in which hydrogen bonds (dashed lines) and covalent bonds (solid lines) between water molecules are broken and re-formed.

Vehicle Mechanism states that the protons migrate as OH_3^+ or NH_4^+ by being bonded to a vehicle such as H_2O or NH_3 , while the “unladen” vehicles move in the opposite direction (In Grotthuss Mechanism H^+ migrates) (Figure 25) . The vehicle shows a diffusion coefficient which corresponds to the proton conduction and shows the behavior of a Bronsted base (proton acceptor) towards its crystallographic environment (Figure 25) [102].

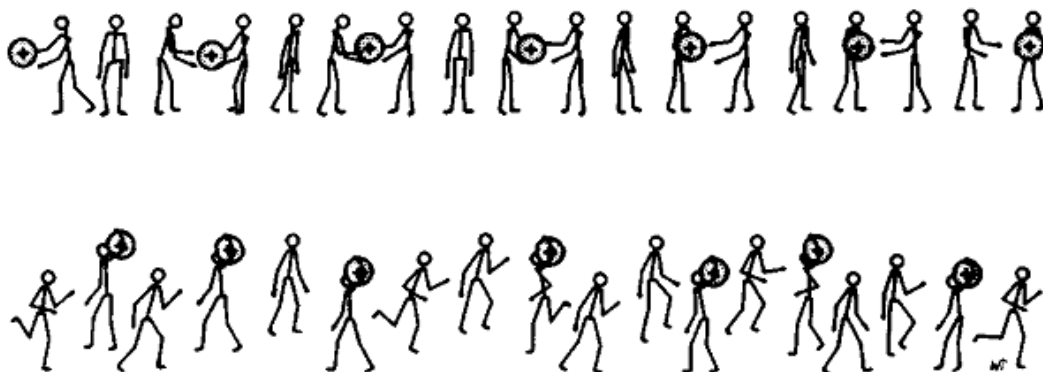


Figure 25. Model of proton conduction. Grotthuss Mechanism (top); the protons are passed along the hydrogen bonds. Vehicle Mechanism (bottom): the movement takes place with aid of a moving “vehicle”, e.g. H₂O or NH₃ as complex ion (H₃O or NH₄⁺) [102].

1.5 ETFE BASED IONIC POLYMER METAL COMPOSITES

Nafion[®] has been used for the manufacturing IPMCs due to its high ionic conductivity and mechanical strength. However, high cost and limited thickness availability diminish Nafion[®]'s demand. Poly(ethylene-*alt*-tetrafluoroethylene) (ETFE) is a fluoropolymer as Nafion[®]'s polymer backbone. The similar backbone structures of these polymers were an inspiration to produce an alternative base film for IPMCs.

On the other hand, many radiation-grafted fluoropolymers as proton conducting medium have been already produced for fuel cells applications in order to replace Nafion[®] with a promising new material [3; 42; 41; 29]. Therefore, modification of ETFE films with polystyrenesulfonic acid by radiation induced grafting was aimed in order to mimic the Nafion[®]'s structure and in order to produce an alternative IPMC material.

1.6 OBJECTIVE

The objective of this study is to produce a novel ionic polymer composite (IPMC) based on radiation grafted poly(ethylene-*alt*-tetrafluoroethylene)-*g*-polystyrenesulfonic acid (ETFE-*g*-PSSA) membranes and reveal its actuation performance.

2 EXPERIMENTAL

The ETFE films (100 μm , 150 μm , 200 μm and 250 μm) were purchased from Nowofol GmbH (Siegsdorf, Germany), Nowoflon ET 6235 Z.

Chemicals:

Nafion[®]- 0,05 mm thick (Alfa Aesar) Isopropanol (Sigma-Aldrich, 99%); styrene (Sigma-Aldrich, 99%); hydrogen peroxide (Riedel-de Haen, 35 %); chlorosulfonic acid (Fluka); dichloromethane (Merck); tetraammineplatinum(II) chloride monohydrate (Pt(NH₃)₄Cl₂ · H₂O (Alfa Aesar)); sodium borohydride (NaBH₄) (Merck); hydrazine hydrate (Merck); hydroxylamine hydrochloride (NH₂OH-HCl) (Alfa Aesar, 99%); ammonium hydroxide solution (Riedel-de Haen); hydrochloric acid (Sigma-Aldrich, 99%).

2.1 Radiation Grafting

2.1.1 Pre-irradiation

100 μm , 150 μm , 200 μm and 250 μm thick ETFE films, in 8x8 [cm²] and 8x1 [cm²] dimensions, were irradiated in air with γ -rays (⁶⁰Co γ -source) at 50 kGy doses in Gamma Pak, Tekirdağ, Turkey.

The irradiated films kept at -40 °C in order to prevent radical decay and used for approximately 4-6 months long.

2.1.2 Graft Polymerization

Grafting solution is prepared as a mixture of 120 mL styrene in 330 mL isopropanol and 150 mL deionized water. The irradiated ETFE films were placed into reactors purged with nitrogen for 30 min in order to prevent the degradation of radicals. The

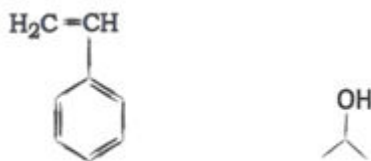


Figure 26. Styrene (left) and isopropanol (right).

reaction was carried out at 60 °C in a thermostated water bath for different time intervals. After grafting, the grafted films were washed with toluene to remove unreacted monomer and other impurities and dried at 80 °C.

The extent of polymerization in the side chains is called as the degree of grafting (DOG) or graft level (GL). The GL determined gravimetrically by calculating the percentage of mass increase [74; 29]. Graft levels are analyzed gravimetrically; since it has been reported that grafting is a bulk property and it is averaged over film thickness and area [18].

$$\text{Graft Level [w\%]} = \frac{m(g) - m(o)}{m(o)} 100[\%]$$

; where $m(g)$ is the weight of the grafted film and $m(o)$ is the weight of the base film.

2.2 Activation of Nafion[®]

The Nafion[®] 115 (Fuel Cell Earth, LLC) has pretreated by boiling in 3 % v/v H₂O₂ for 1 hour to remove impurities; subsequently boiled in 1M H₂SO₄ for 1 hour to activate the membrane. Finally, the Nafion[®] 115 membrane has boiled in deionized water twice in order to remove the H₂SO₄ residues completely. After, the purification and activation procedure has completed, Nafion[®] 115 has been stored in deionized water at room temperature as ready-to-use [24].

2.3 Sulfonation

Sulfonation was performed with chlorosulfonic acid in dichloromethane (2% (v/v)) for 5 hours at room temperature. The radiation grafted membranes were hydrolyzed and ion-exchanged with using sodium hydroxide. Hydrochloric acid used to regenerate the acid form of the membrane. Finally, the membranes immersed into deionized water for 5 hours at 80 °C for water swelling [41].

2.3.1 Water Uptake

Nafion[®] 115 and all the ETFE-g-PSSA membranes were cut into 2x2 [cm²] dimensions. The cut pieces were dried at 65 °C in vacuum oven for 9 hours. The dried membranes were weighted and then these membranes kept in deionized water for 24

hours. After 24 hours, the wet state was weighted and gravimetric water uptake analysis has been done according to:

$$\text{Water Uptake [w\%]} = \frac{m(w) - m(d)}{m(d)} 100[\%]$$

; where $m(w)$ is the weight of the wet membrane and $m(o)$ is the weight of the dry membrane.

2.4 Ionic Conductivity

The ionic conductivity of the all samples was measured by BekkTech Conductivity Cell (BekkTech LLC Fuel Cell Testing & Diagnostic Services). In plane, four electrode conductivity testing was made on the PTFE (Teflon) body of the cell with the Pt wires (Figure 28). Samples were cut in the 2 x 2 [cm²] dimensions. All ionic conductivity measurements were made in deionized water.

$$R = \frac{\Delta V}{\Delta I}$$

$$\sigma = \frac{L}{R * A} = \frac{L}{R * W * T}$$

; where L is the length between the inner-electrodes, W is the width of the sample and T is the thickness of sample (Figure 27) and R is the resistivity of the sample.

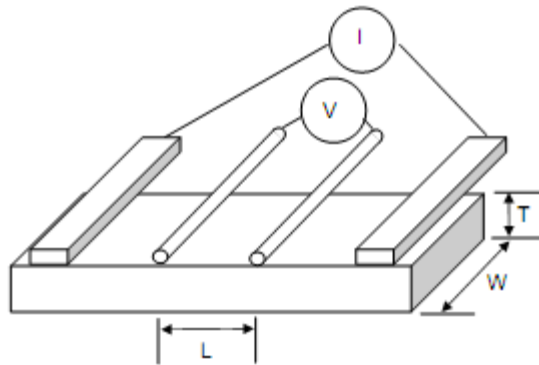


Figure 27. In-plane ionic conductivity configuration [39].



Figure 28. Ion conductivity cell [39].

2.5 Platinum (Pt) Plating

Pt was deposited onto ETFE-g-PSSA membranes with electroless plating as it is described in the literature [56]. The Pt deposition takes place in four steps:

2.5.1 Surface Roughening of the Membranes

- a. Mild Sandblast: The surface area of the membranes was increased for Pt deposition by sandblasting. Abrasive papers (400C, Egeli Abrasives, Silicon Carbide Water Proof Abrasive Paper-Electro coated) were used for roughening. The Nafion[®] and ETFE membranes were placed in between two emery papers and a metal cylinder were rolled on them.
- b. Ultrasonic Washing: The residues were removed by ultrasonic washing in water approximately for 15 minutes.
- c. HCl Treatment: The impurities and ions were removed by boiling the membranes in dilute hydrochloric acid (HCl aq, 2 N solution) for 30 minutes. Subsequently, membranes were rinsed with deionized water.
- d. Water Treatment: Membranes were boiled in deionized water for 30 minutes to remove acid and to swell the membrane.

The roughened membranes were stored in deionized water.

2.5.2 Ion-exchange (Adsorption)

- a. A solution of 2 mg Pt/ml platinum complex (Tetraammineplatinum (II) chloride monohydrate ($\text{Pt}(\text{NH}_3)_4\text{Cl}_2 \cdot \text{H}_2\text{O}$) were prepared. The Nafion[®] and ETFE membranes were immersed into the solution, containing more than 3 mg of Pt per cm^2 surface area.
- b. After immersing the membrane, 1 ml of ammonium hydroxide solution (5 %) was added for neutralization (It is assumed as 1 ml of ammonium hydroxide is proportioned according to the 30 cm^2 membrane area.)
- c. The membrane were kept in the solution at room temperature for more than 3 hours (one night usually).

2.5.3 Primary Plating

- a. 5 wt% aqueous solution of sodium borohydride was prepared. After rinsing the membrane with water, the membranes (total surface area of the membranes is 30 cm^2) were placed into 180 ml water bath and stirred at 40°C .
- b. 2 ml of the sodium borohydride solution was added (5 wt% NaBH_4 aq) every 30 min for 7 times (total surface area of the membranes is 30 cm^2).
- c. In the sequence of addition (4 hours long), temperature was raised up to 60°C gradually.
- d. 20 ml of the reducing agent (sodium borohydride solution) was added and the solution was stirred for 1.5 hr at 60°C . Black layer of fine Pt particles were deposited onto the surface of the membrane.
- e. The membranes were rinsed with water and immersed into the dilute hydrochloric acid (0.1 N) for an hour.

2.5.4 Secondary Plating

The amount of platinum deposited with the primary plating (reduction process) is only less than 0.9 mg/cm^2 , which depends on the ion exchange capacity, thickness of the membrane and the structure of the Pt complex. Additional amount of platinum is plated by developing process on the deposited Pt layer.

- a. 240 ml aqueous solution of the complex ($\text{Pt}(\text{NH}_3)_4\text{Cl}_2 \cdot \text{H}_2\text{O}$) was prepared, containing 120 mg of Pt and 5 ml of the 5% ammonium hydroxide solution was added.

- b. 5% aqueous solution of hydroxylamine hydrochloride ($\text{NH}_2\text{OH}\cdot\text{HCl}$) and 20% solution of hydrazine (NH_2NH_2) were prepared.
- c. The membranes were placed into the Pt solution at 40°C and stirred.
- d. In every 30 minutes, 6 ml of the hydroxylamine hydrochloride solution and 3 ml of the hydrazine solution were added to the Pt solution.
- e. In the sequence of addition, temperature was raised up to 60°C gradually for 4 hours, and gray metallic layers of the growth process were observed.
- f. At the end of this process, a small amount of the solution was boiled with the strong reducing agent (NaBH_4) in order to check the end point. (It is dangerous to add NaBH_4 powder in a hot solution, because of the gas explosion. So add NaBH_4 solution to a cold solution, then, warm the solution in a water bath)
- g. If any Pt ion remains in the plating solution, the color of the solution turns to black. In such cases, Pt development should be continued with addition of the $\text{NH}_2\text{OH}\cdot\text{HCl}$ and NH_2NH_2 solutions.
- h. When there is not any Pt remained in the sampled solution, the membranes were rinsed with water, and boiled in dilute hydrochloric acid (0.1 N) to remove the ammonium cation in the membrane. After washing with water, H^+ in the composite can be exchanged for any cation by immersing in a solution of the chloride salt of the cation.

2.6 Displacement Measurements

The Pt deposited IPMC were cut into 5 mm x 35 mm in rectangle form. One side of the rectangular sample was sharpened by cutting the edge like a triangle in order to observe the tip displacement accurately (the free end). The other side of the sample kept same (the fixed end). Displacement measurements were made by an IDS camera (UI-1480LE-C) with Pentax lens (1/2", 16.0mm, F1,4). Agilent 33120A 15MHz Function/Arbitrary Waveform Generator was used to supply electric potential. The movement of the IPMC strip was recorded on a milimetric grid and the tip displacement was calculated vectorially according to Pythagorean Theorem.

2.7 Universal Testing Machine (UTM)

Mechanical properties of radiation grafted wet membranes were investigated by using Zwick/Roell Z100 Universal Testing Machine (UTM) 200N Pneumatic tensile

grips. Samples were cut into 8 cm x 2 cm with a snap-off blade utility knife; and were tested at constant displacement rate of 100mm/min.

2.8 Scanning Electron Microscopy (SEM) and Energy Dispersive X-ray Spectroscopy (EDX)

For morphological and structural analysis SEM (Leo Gemini) and EDX (Röntec) was used. SEM images were taken by secondary electron beam. The samples coated with carbon prior to characterization.

3 RESULTS AND DISCUSSION

3.1 Radiation Grafting

The ETFE films were grafted as two replicates in order to crosscheck the accuracy of the resulted graft levels. For two separate grafting processes, same conditions were supplied (two different films with same thicknesses were grafted separately under same conditions in the same experimental run). Among the pairs, the ones resulted in similar graft levels (the difference in graft levels of the pairs that are lower than 8%) with homogenous film appearance were chosen to be depicted in Figure 29. The overall grafting results are presented in Appendix A/1.

The graft levels were increased by increasing grafting time (Figure 29). The more the ETFE-base film is hold in the grafting solution (at 60°C), either the more the growth of polystyrene chains is allowed –mostly around the surface- or the more styrene monomer diffuses into the membrane and polymerization proceeds more in the interior of the film in the extent of the grafting-front mechanism [17]. The former may lead to less but longer polystyrene chains and the latter may lead to more but shorter polystyrene chains for a grafting procedure in a given period of time.

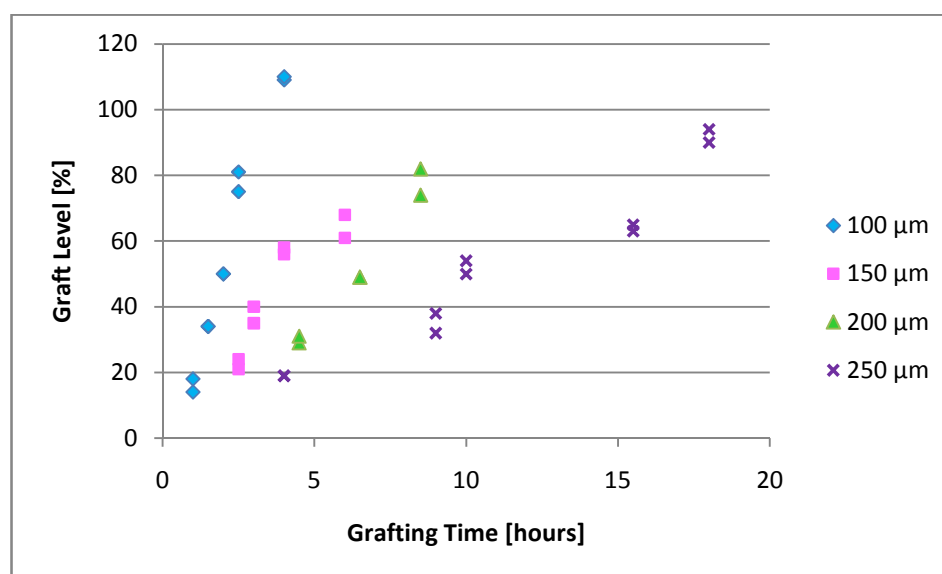


Figure 29. Pairs of grafted films are represented in ‘Graft Level *versus* Grafting Time’ graph.

Grafting of thicker films required more time to reach to the similar graft levels with thinner films (The onset of the similar graft levels shifts to right by increasing thickness) and the slope of the trends decreased by increasing thickness (Figure 29).

The former indicates that grafting does not occur only on surface; but diffusion –of either monomers or polymer chains or both- also exists [43]. The solely surface grafting would give the same onset for all different thicknesses. Because the parameters which can affect the surface graft level such as the type of the base film, size of the base film, pre-irradiation conditions, grafting solution, N₂ purging, grafting temperature are kept the same; where thickness is the only varying parameter. Additionally, all the films with different thickness were purchased from the same company (Nowoflon ET- 6235 Z). Therefore, shifts in the graft level onsets on the grafting time axis indicate that the grafting is diffusion induced and interior regions of the ETFE film is also grafted with polystyrene. On the other hand, these onset shifts may also support the “grafting-front-mechanism” [17] due to diffusion and step by step increase in the graft levels by increasing time. The same trend has been reported for grafting of styrene/divinylbenzene into poly(tetrafluoroethylene-*co*-hexafluoropropylene) in isopropanol solution and the behavior was attributed to the progress of the grafting front [103].

The latter also supports the grafting front mechanism. The monomer diffusion even may get harder due to the *Trommsdorf-Norrish* effect [104; 118]. The more the polymer growth, the more increase in viscosity. Therefore, the monomer diffusion takes more time to reach to the reactive sites both on the growing chain and in the interior of the film. Hence, the slope of the ‘Grafting Level vs. Grafting Time’ decreases. It has been also reported that the monomer diffusion to the next reactive sites through the base film is the determining factor for the time delay [103]. This time delay (t_0) is caused by the slow propagation of the grafting front towards the center of the polymer film (in the initial polymerization rate). This leads to grafting mostly on the surface; since the monomer diffusion is restricted while the polymerization conditions still proceeds. Therefore, in thicker films, the surface grafts are seen dominantly. This claim is supported by the work of Guilmeau et al. [43] (Figure 30).

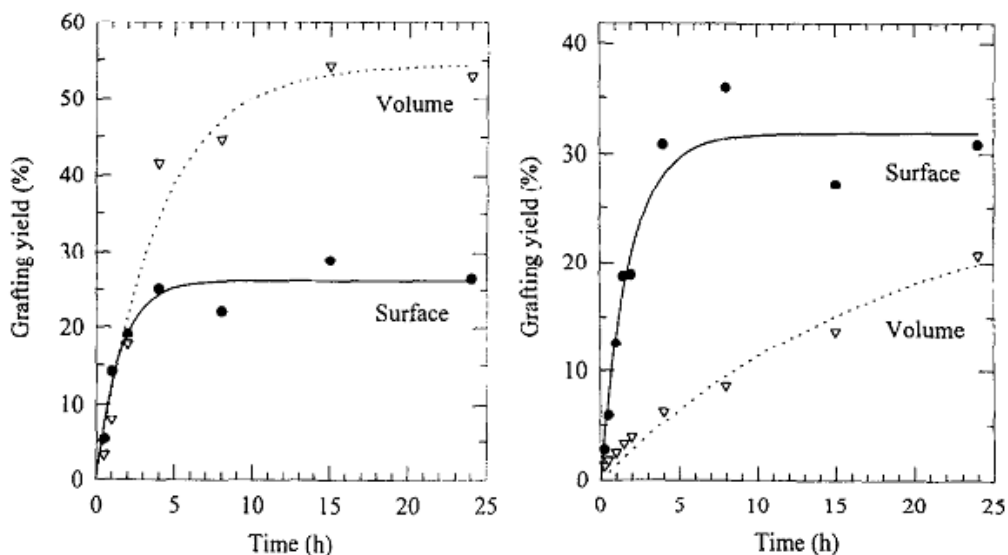


Figure 30. Comparison of surface grafting yield and volume grafting yield determined by FTIR-ATR for 30µm (left) and FTIR in transmission for 100µm ETFE film (right) (irradiated with 100 kGy; grafted at 50°C; ethanol used as a solvent with crosslinker and inhibitor addition) [43].

On the other hand, deviations are apparent when the data is expanded with the inconsistent grafting pairs in the graphical representations as well (Figure 31-34). The deviations increase when the grafting time increases. Please note that for the consistent grafting pairs, the markers on the graphs seems like a single marker or very close to each other; for the inconsistent pairs (orange markers) a space appears.

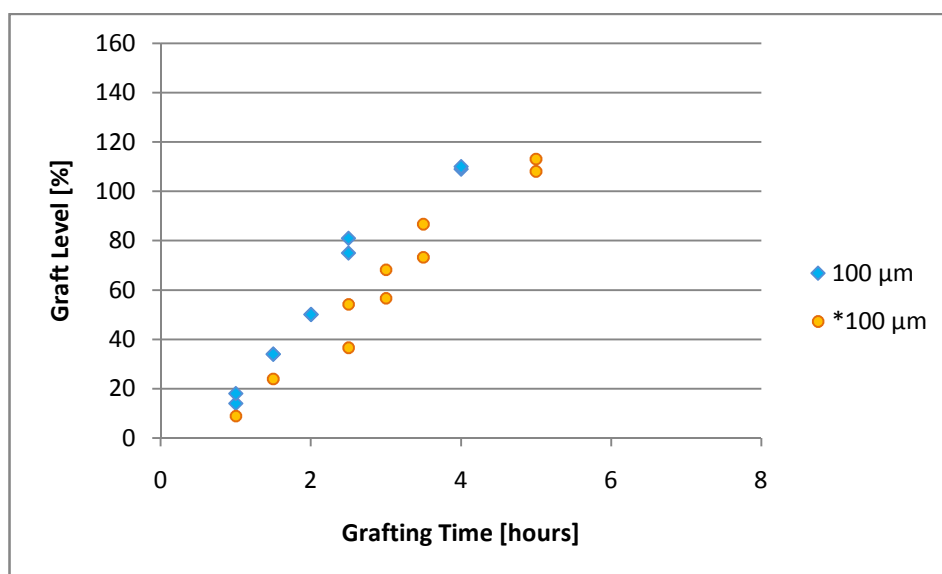


Figure 31. ‘Graft Level *versus* Grafting Time’ representations for 100µm films with overall grafting results.

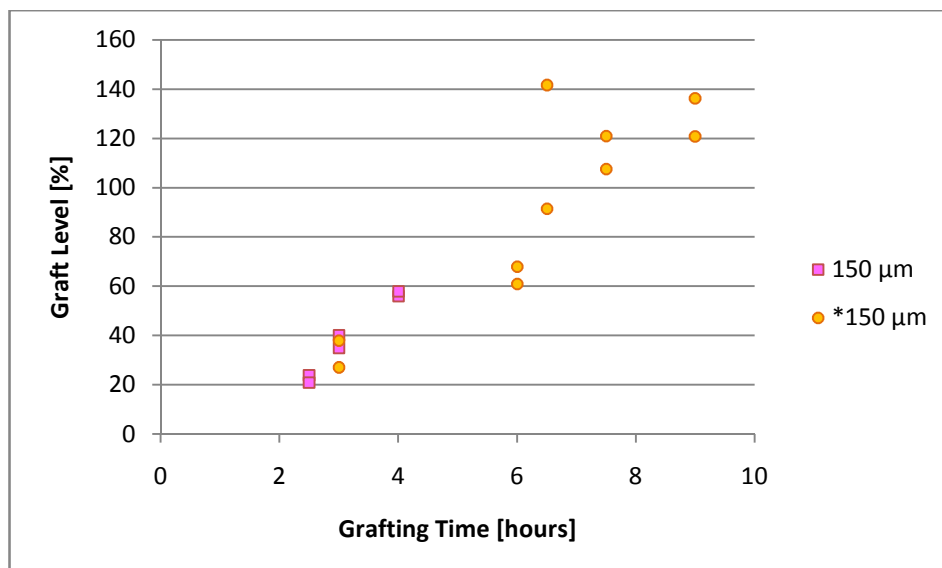


Figure 32. ‘Graft Level *versus* Grafting Time’ representations for 150μm films with overall grafting results.

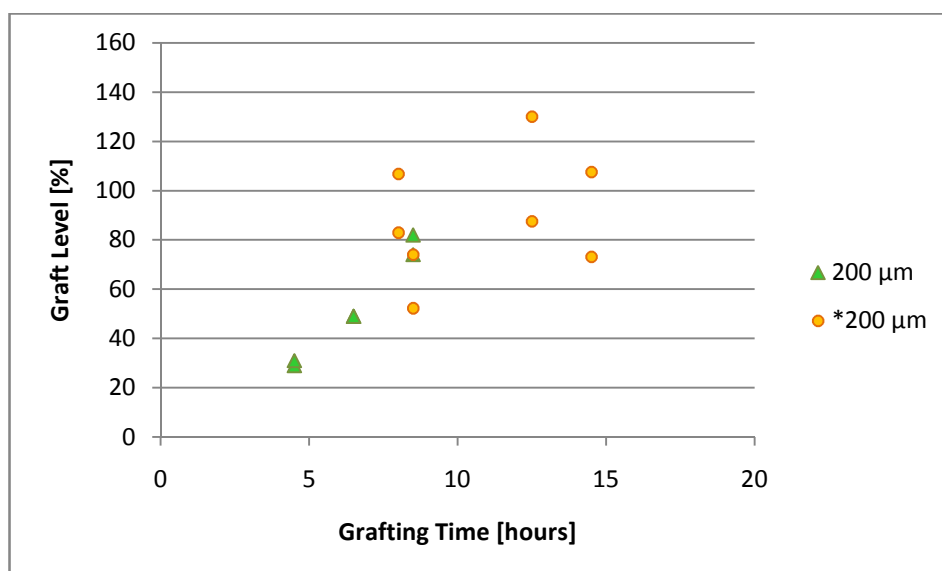


Figure 33. ‘Graft Level *versus* Grafting Time’ representations for 200μm films with overall grafting results.

The deviations in the grafting might be arising from radical-radical recombination. Since 50 kGy is moderately high radiation dose, a large amount of radical presence is expected. Due to the high radical concentration, radical-radical recombination is an expected consequence [3]. Furthermore, radical termination due to impurities might be also a reason. The experimental errors may have taken part into the deviated results. For instance, the non-precise degassing system may cause to decay of radicals. Therefore the active radical sites might be terminated before the polymerization. Moreover, it

might be arising from the washing and drying steps due to the fact that the grafting residues may not be precipitated totally and a part of the solvent may not be evaporated completely.

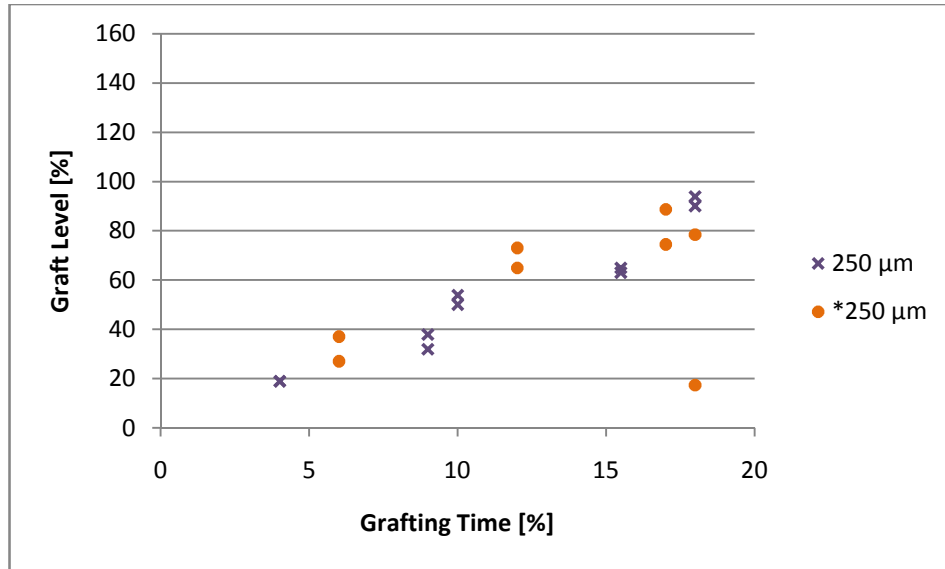


Figure 34. ‘Graft Level *versus* Grafting Time’ representations for 250µm films with overall grafting results.

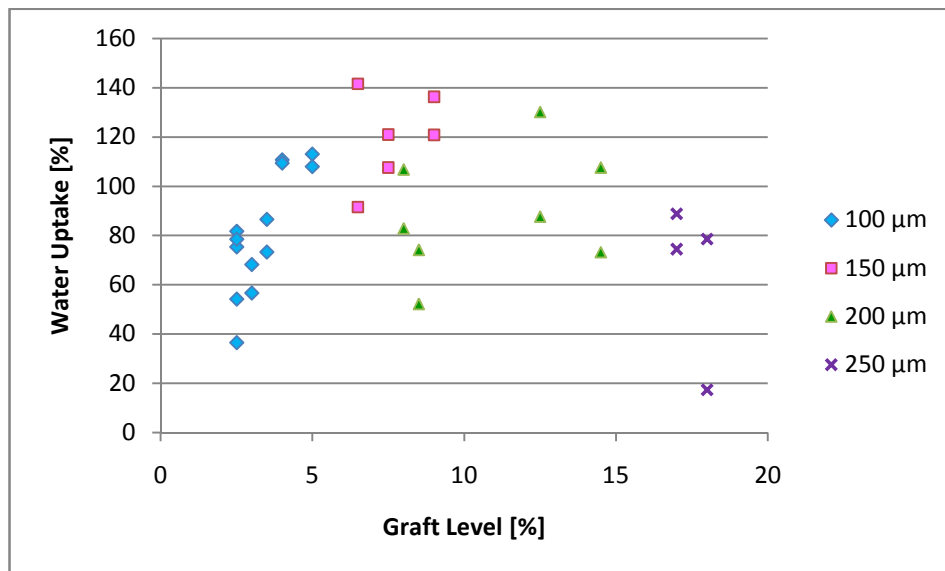


Figure 35. Deviations in graft levels at higher grafting time periods.

The inconsistency in the grafting pairs, thus the graft levels, might also be arising from the experimental processing system. Narrow cylindrical glass reactors were used in grafting of ETFE films (Figure 36). 8x8 [cm²] ETFE films were rolled and placed into the glass reactor. The rolled form of the films may cause to difficulty in intake of

monomer to the films. Therefore, the diffusion of the monomer into the film may become harder; which may capsize the front growth of the polymer chains: monomers may not be able to reach to the active sites or to the growing front of the polymer chains. In this case, monomer can prefer to form a homopolymer rather than grafting into the film. Moreover, if the homopolymer concentration increases in the entourage, these homopolymers may behave as impurity and even complicates the further grafting [41]. Moreover, the narrow reactors obstruct the film expansion (Figure 37). Hence, limited expansion of the films in the rolled form in the narrow cylindrical reactors might reduce the monomer intake and/or homogeneous polymer growth.

Likewise, access to the available polymerization space –in the interior of the membrane- might be blocked by the long grafted side chains around the surface region, especially at higher grafting time periods (Figure 35). Therefore further polymerization is disabled in the extent of grafting front mechanism. Oppositely, the growing chains can widen the interior of the ETFE film; hence the more space might be created for new polymer growths and very high graft levels may be achieved.

Additionally, a saturation degree in graft levels has been reported elsewhere [3]; after a certain graft level, further grafting cannot occur while grafting time increases. A saturation level has not been observed in this study; however, Figure 29 shows a moderately linear increase in relatively shorter grafting time periods. After this linear regime saturation level may be achieved. But, the saturation level may be hidden under the deviations. For instance, since the films are saturated for further grafting; homopolymerization on the surface is triggered. Homopolymerizations on the surface may also cause the deviation of the results at longer time period grafting [29] by increasing the grafting level abruptly. In addition to these, it has been reported that homopolymer occurs much more in the grafting that are made for longer time periods [104]. Therefore the much larger deviations in Figure 35 can be explained by the high amount of homopolymer formation.

Figure 29 depicts that graft level can be controlled by the grafting time. The increasing grafting time periods results in increasing graft levels until a certain level, where deviations start. Figure 29 and 35 show that thinner films have a narrower time range of controllable grafting. This can be an indication of that grafting fronts meet in shorter time periods in thinner films or saturates earlier than thicker films, as expected.

It is necessary to mention that determining and following the trend in ‘Grafting Level vs. Grafting Time’ was not an aim of this study. A kinetics based approach has

not been applied for the experiments. Nevertheless, the resultant data were interpreted accordingly to the present literature. The aim has been that manipulation of graft levels with grafting time in order to reach to the desired graft levels. The desired graft levels were intended to use in the observations of the affect of graft level in IPMC actuation.

3.1.1 Improvements for Radiation Grafted Film Quality

The influence of the shape of grafting reactors on grafting yield was mentioned in the first part of the section. In addition to this, physically formless films were produced in some cases due to the reactor shape (Figure 36, Figure 39).

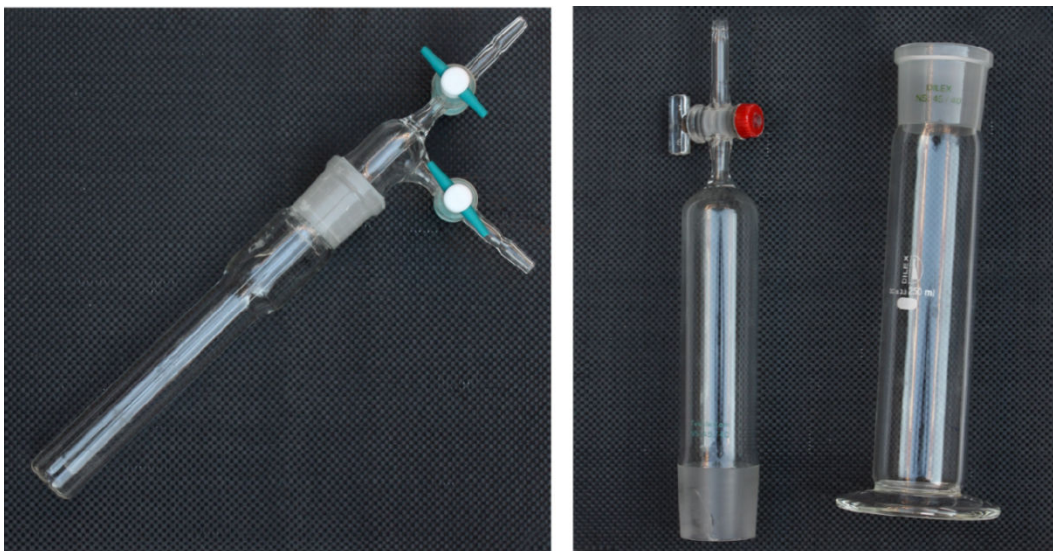


Figure 36. Grafting reactor (left) and sulfonation reactor (right)

First of all, the explicit film expansion caused by the grafting was observed qualitatively. In order to observe the expansion of the films in the narrow glass reactors, 8×1 [cm^2] films were used instead of 8×8 [cm^2] since 8×1 [cm^2] dimensions can fit into the glass reactor completely. A very distinct expansion, approximately 25% and more enlargement in film size at high graft levels, was qualitatively observed in 8×1 [cm^2] films (Figure 37). The higher the graft level, the larger the expansion was obtained (Figure 37). The large expansion in high graft levels indicates that the grafting expands the pristine ETFE films due to the penetrated polystyrene chains. That is to say, these narrow cylindrical reactors reduce the expansion capability of the films in 8×8 [cm^2] dimensions during grafting.



Figure 37. Expansion of grafted films. 150 μm ETFE film in pristine (left), GL: 14% (middle) and GL: 95% (right) states



Figure 38. Homogeneously grafted ETFE films: 100 μm (top-left), 150 μm (top-right), 200 μm (bottom-left), 250 μm (bottom-right)

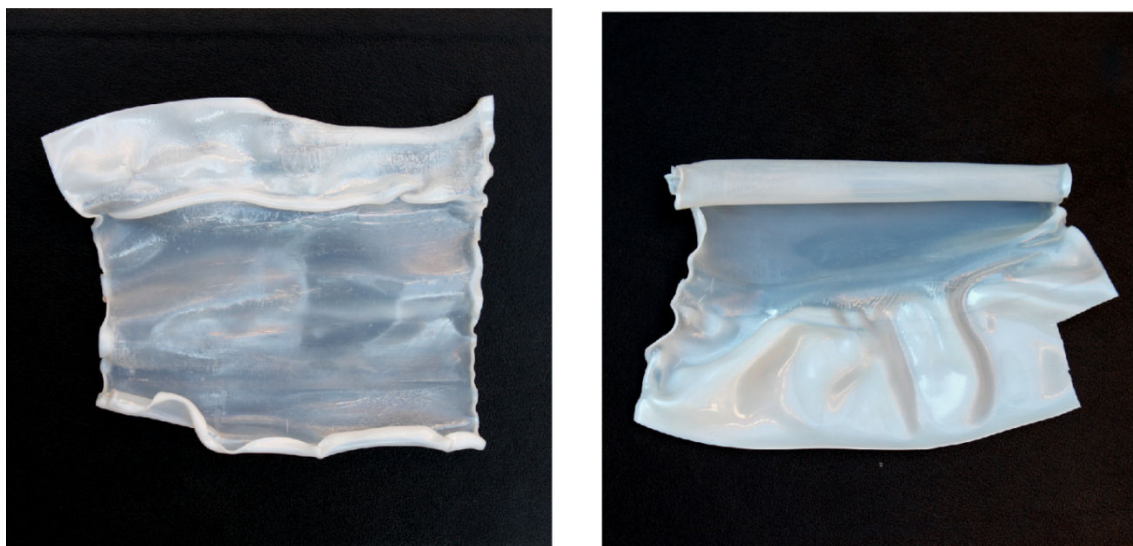


Figure 39. Non-homogenously grafted and formless 250µm ETFE films.

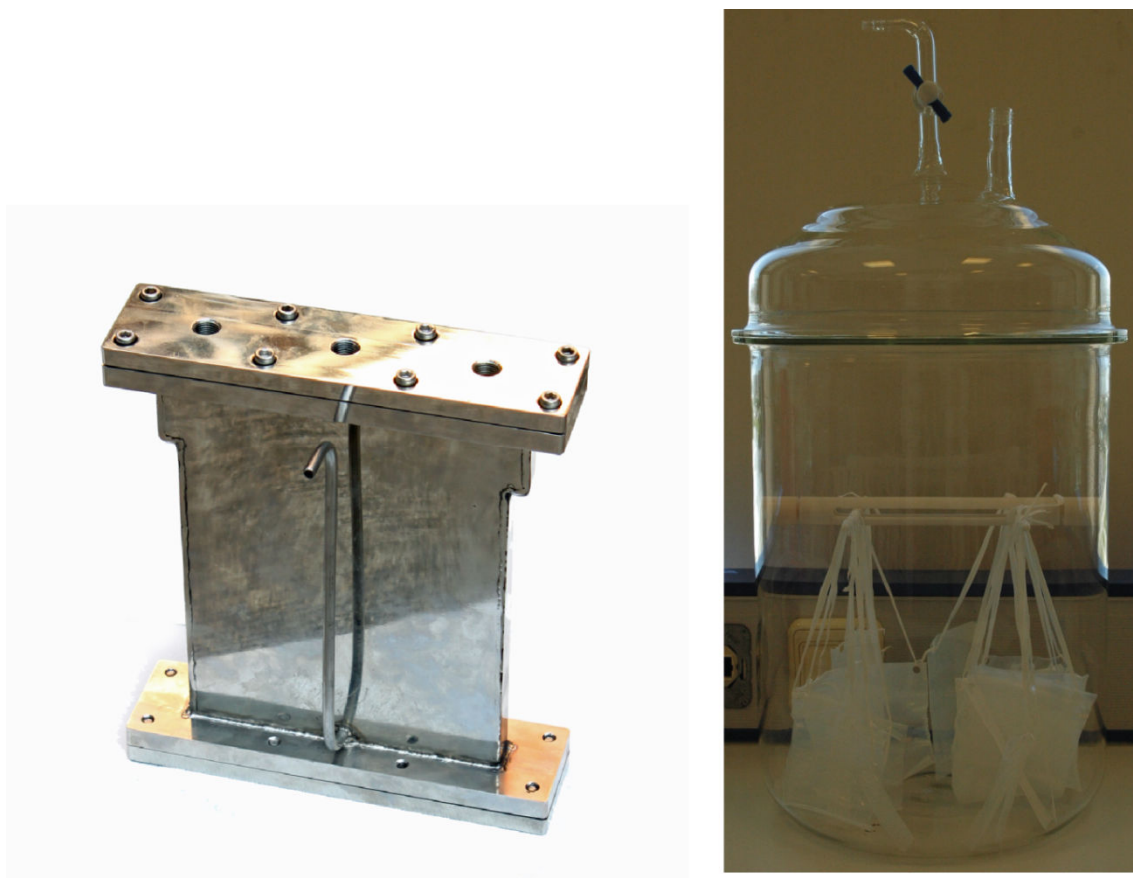


Figure 40. New steel grafting reactor for 14 x 16 [cm²] films (left). New sulfonation reactor (right).

These narrow reactors have been properly used in the grafting of 25µm ETFE and FEP films in our group at Sabanci University; however in the 100µm to 250µm thick

films, monomer diffusion, polymer growth and the physical film quality were affected by the limited film expansion, and *vice versa*. Hence alterations were observed in the graft levels and film quality. In order to overcome this situation, new grafting and sulfonation reactors were designed and manufactured (Figure 40). The new reactors allow the usage of larger film dimensions (up to 14x16 [cm²]). The larger films allow to use the same membrane for different characterization methods widely and improvement in both grafting yield and film quality is expected.

3.2 Water Uptake

The proton conduction in the films mainly originates from the water content as literature states [2; 102]. However, both ETFE films and graft copolymers cannot swell with water due to its hydrophobic nature. Therefore, hydrophilic properties are needed to be introduced into ETFE films.

Hydrophilic properties were introduced by addition of the sulfonic acid groups into the graft copolymer film. ETFE films were grafted with polystyrene in order to create suitable sites, aromatic rings, for the addition of sulfonic acids, firstly. Secondly, sulfonic acids were bind to these aromatic rings of polystyrene by electrophilic substitution (Figure 41) [3]. Hence, the polystyrene grafted ETFE films became able to uptake water by conversion of the film into a membrane by addition of sulfonic acid groups.

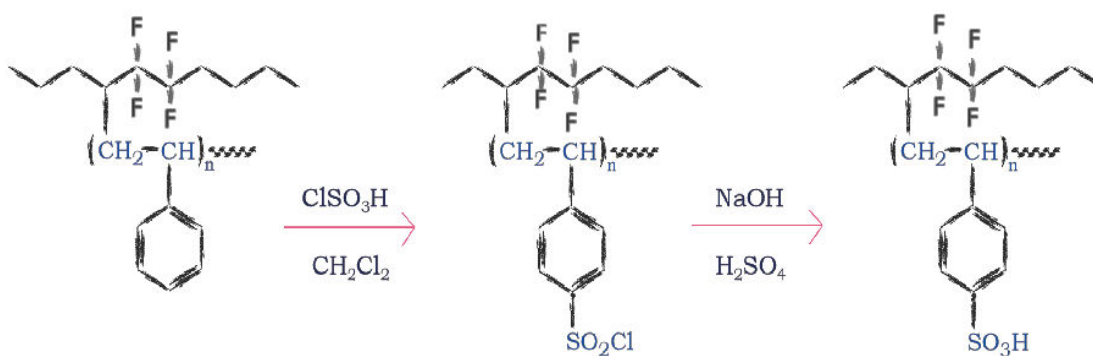


Figure 41. Sulfonation reaction of polystyrene grafted ETFE films.

The increasing graft level induces the increasing water uptake values, (Figure 42). Because of the fact that increasing amount of grafted polystyrene chains increases the graft level, which means that number of aromatic rings increase. The more the aromatic

rings is the more available site for sulfonic acid groups [3]. It has been reported that sulfonation also proceeds with a front mechanism as well as grafting [3]. The regions close to surface are sulfonated firstly and then sulfonation proceeds through the interior of the grafted film.

A strict linear increase was not observed in any thicknesses; neither has been observed in the literature [41]. This may be attributed to the microstructure of the grafted films [41]. The grafted polystyrene chains may have not been formed homogeneously all over the film. The random dispersion of grafting may cause differences in morphology, connectivity and geometry of the hydrophilic/hydrophobic domains [41]. Therefore, different graft levels may yield random water uptake values. Nevertheless, an increasing regime in water uptake values has been observed with the increasing graft level.

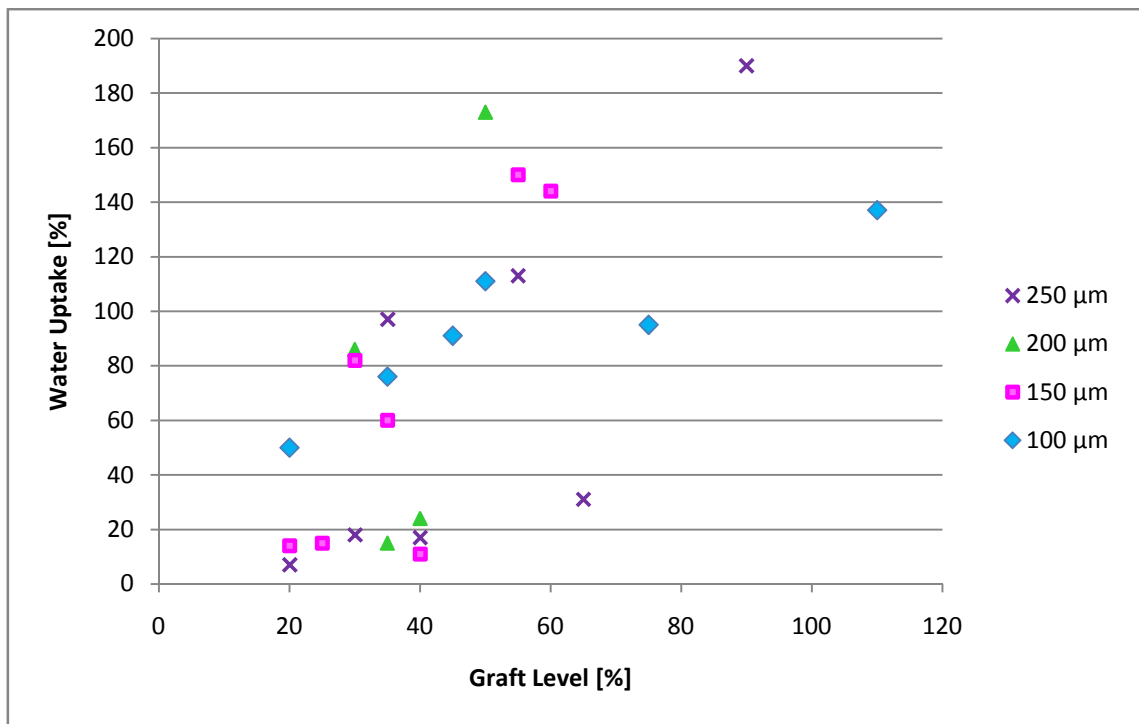


Figure 42. Water Uptake *versus* Graft Level values

The 100μm thick ETFE films showed the most linear increase in water uptake (vs. graft level) values among all thicknesses. This may indicate that the 100μm ETFE films were grafted in the most homogenous form across the thickness. The thicker films might be suffered more by the homopolymerization effects as described previously. Homopolymerizations on surface may lead to water uptakes that are more than 100%

water content (Figure 42). Moreover, difficulty in monomer diffusion and polymer chain growth and also radical recombination may lead to lower water uptake values at relatively high graft levels. Because, it is stated that the sulfonation of phenyl groups in fluoropolymer matrix is 100% efficient [43].

On the other hand, the variations in the water uptake data may be arising from experimental errors. The membranes are tended to float over the water, partially; therefore membranes could not uptake the water sufficiently. Likewise, there may be some errors during weighing of especially the wet membranes.

3.3 Ionic Conductivity

The conductivity of Nafion[®] was measured as 80 mS/cm. The graft levels lower than approximately 75% yield ionic conductivities below 50 mS/cm, generally. Ionic conductivity of 250 μ m membranes did not exceed 50 mS/cm even at 150% graft levels. This might be attributed to inhomogeneous grafting structure, either and also all grafting fronts may have not met completely.

The increasing graft levels resulted in increase in ionic conductivity, slightly (Figure 43). The number of sulfonic acid groups is expected to increase as graft level increases. It is known that the sulfonic acid groups are the responsible for ion conduction in ETFE-g-PSSA membranes [3]. Sulfonic acid groups act as hydrophilic end groups and hold water; thus hold the protons in the hydrophobic ETFE film.

This approach may evoke an expectation of a linear behavior between the ionic conductivity and graft levels. However, a certain linear relation between ionic conductivity and graft level was not observed; and also the relation does not necessarily impose linearity but increasing graft level gives higher conductivity [41]. Nevertheless, one of the reasons for non-linear results is arising from the inhomogeneous grafting structure.

The inhomogeneous structural distribution of the grafted polystyrene chains is basically observable from the physical appearance of the grafted films. (The color gradients depict the inhomogeneity in the structure. The gradient difference was seen even on the very high quality films (Figure 38)). In addition to these, all the aforementioned factors that affect the achieved graft level with respect to time, can be effective in ionic conduction or proton transport.

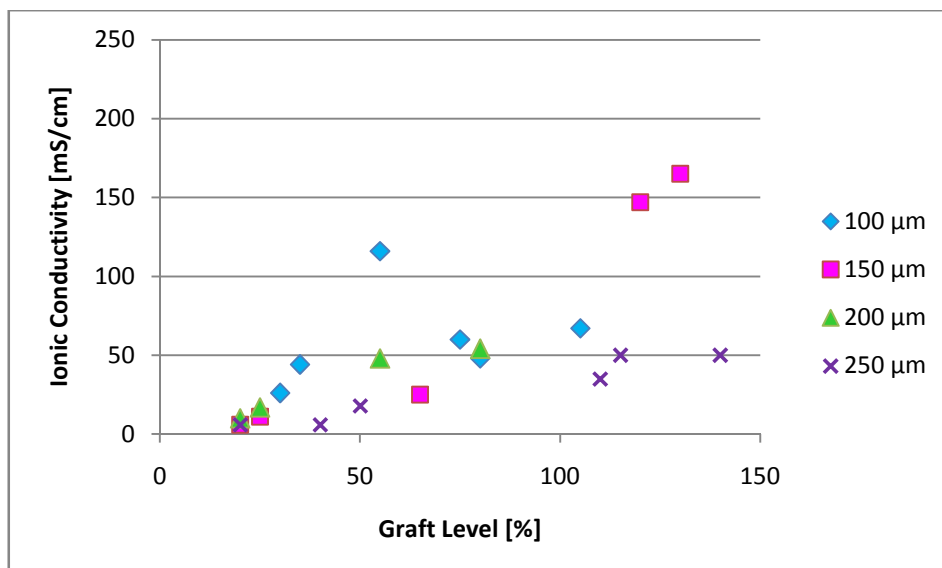


Figure 43. ‘Ionic Conductivity *versus* Graft Level’ results.

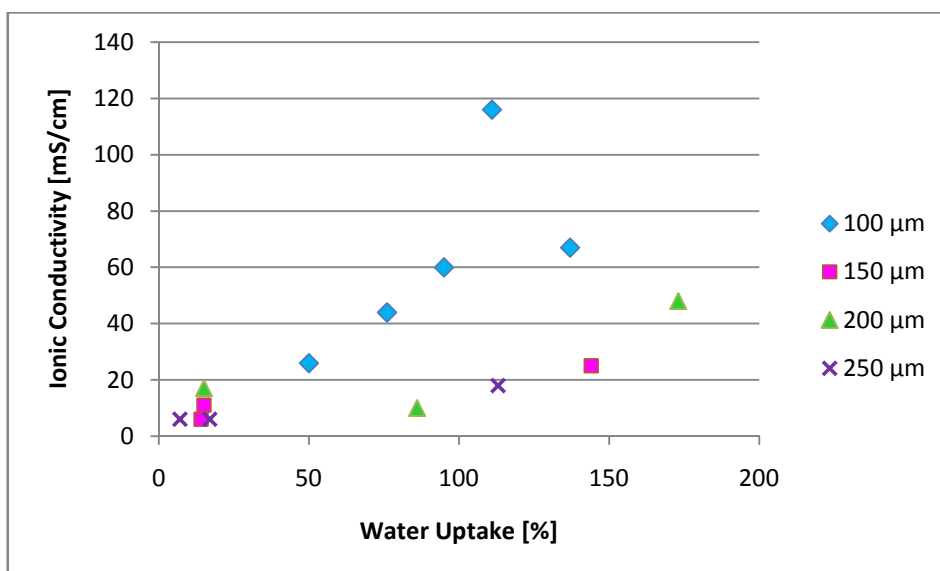


Figure 44. ‘Ionic Conductivity *versus* Water Uptake’ results.

Secondly, water uptake is another important factor in ionic conduction [46]. Figure 44 shows the behavior of conductivity change with respect to the change in water uptake. An increase in ionic conductivity was observed with the increase in water uptake. This supports the fact that water is an effective parameter in ionic conduction in the ETFE-g-PSSA membranes. But, the ionic conductivity cannot be directly related to the amount of uptaken water, as it is also seen in Figure 45 [46]. The types of water have an importance, too (The “bound water” that is bound to the ionic species in the membrane and the “free” water which is not bound by the ion solvation) [46] since the

difference between the water uptake values and conductivity values widens by increasing graft levels, mostly. However, it has been studied that the water content and the water types are not good indicators of membrane conductivity within the series and between the series. That is to say, water is effective in ionic conduction; but it is not a distinctive indicator of the conduction.

The other reason must be revealing in the nature of the conduction mechanism, itself, which strongly depends on the structural morphology of the membrane as mentioned in the 1.3.1 Nafion[®] Section. Essentially, in order to understand the ionic conductivity of ETFE-g-PSSA membranes, one should investigate the structural morphology of the membrane [46; 70] as also mentioned in 1.3.1 Nafion[®] Section. There is not available literature on ETFE-g-PSSA's structural morphology, yet [3]. Furthermore, in the sulfonic acid containing ETFE membranes very fast morphological changes were observed by Atomic Force Microscopy when water droplets introduced [106]. Therefore, application of an electric field may also induce further changes in the membrane structure in order to adapt the membrane to these new conditions. In addition to these, the distinction between the ion transport, *i.e.* the hydronium transport, and the ionic conduction should be made [46]; in this way the effect of water content (the water uptake) can be realized.

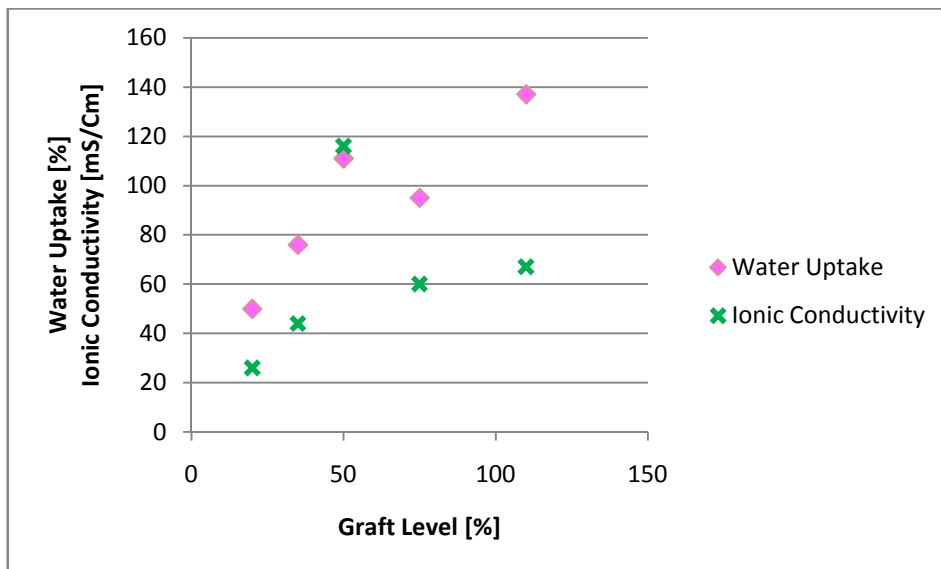


Figure 45. Changes in Water Uptake and Ionic Conductivity with respect to Graft Level in 100 μm wet membranes.

3.4 Mechanical Testing

ETFE-g-PSSA membranes were tested in wet state in UTM (Universal Testing Machine). The membranes showed sweating during the tension test. Since the membranes were in wet state, rending and slipping from the UTM grips have been observed. Rending and slipping might be caused of the fact that the specimen size could not fit into ASTM International Standards. ASTM International (Standards require a specimen that has at least 10 [cm] grip to grip separation for 100 μ m to 250 μ m thick thin films; however size of the films that are used in this study were already in 8 [cm] x 8 [cm]).

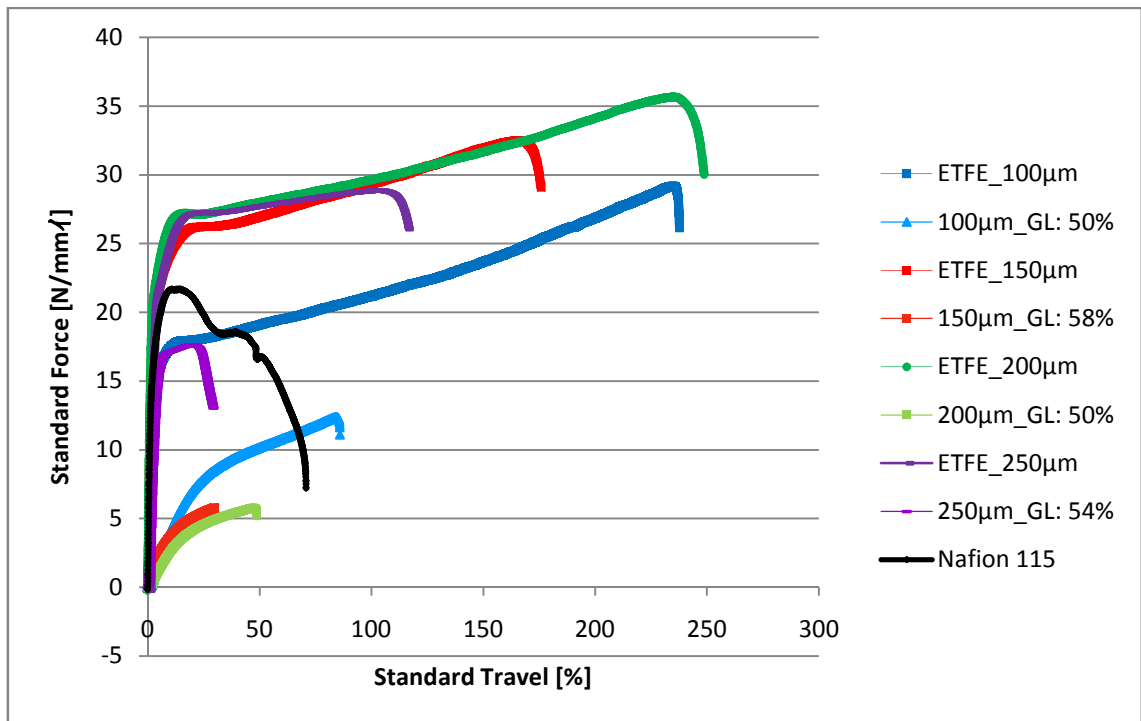


Figure 46. UTM results of different thicknesses of raw ETFE films and wet ETFE membranes. Nafion[®] 115 is in pristine state (non-activated).

Nafion[®] 115 showed a similar modulus of elasticity with the pristine ETFE (Figure 46, 48 and Table 1). A decrease in elastic modulus as well as in tensile strength was observed in all thicknesses with introduction of grafted polystyrene chains (Figure 46). The decrease in these mechanical properties is attributed to the penetration of the polystyrene chains into the ETFE matrix.

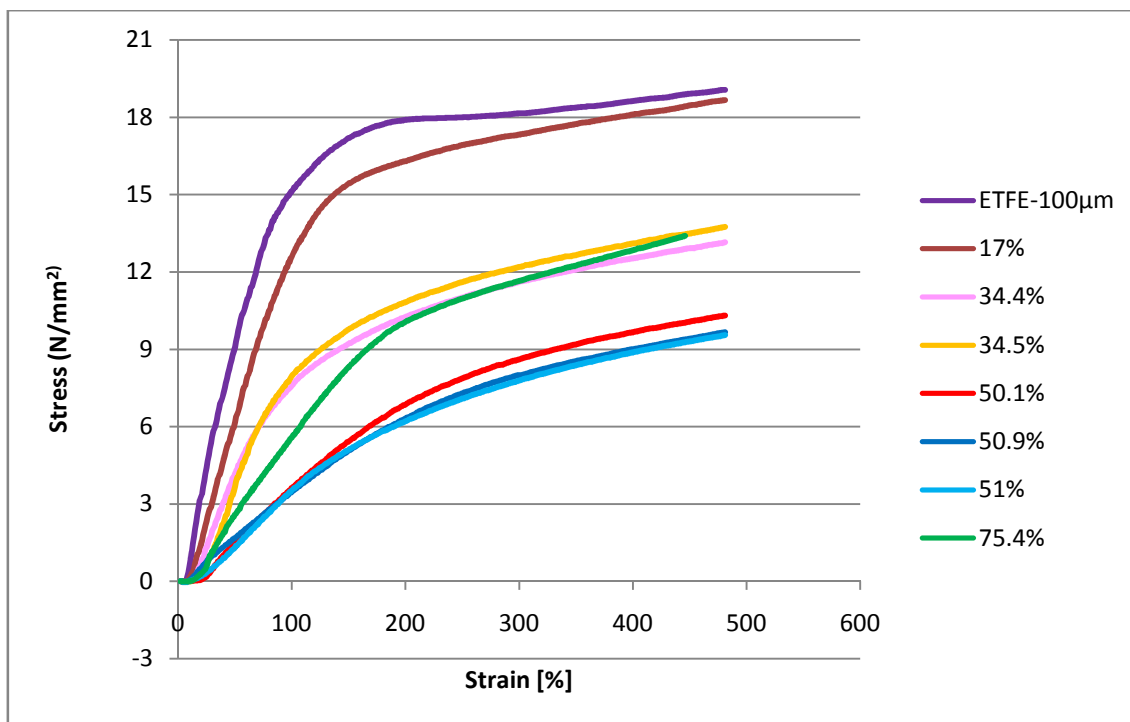


Figure 47. UTM results for 100 μm raw ETFE and grafted 100 μm ETFE films, under tension.

A decrease in yield strength by increase in graft levels was observed in 100 μm wet ETFE-g-PSSA membranes (Figure 47) except the GL: 75.4 %.

The modulus of elasticity was decreased by increasing graft levels, either (Figure 47, 48 and Table 1). That is the increasing graft level decreases the stiffness.

| Graft Level [%] | Modulus of Elasticity [MPa] |
|-------------------------|-----------------------------|
| Nafion [®] 115 | 12 |
| Raw-ETFE | 9 |
| 17 | 4 |
| 34.4 | 2 |
| 34.5 | 2 |
| 50.1 | 0.45 |
| 50.9 | 0.35 |
| 75 | 0.7 |

Table 1. Modulus of Elasticity of 100 μm wet ETFE-g-PSSA membranes.

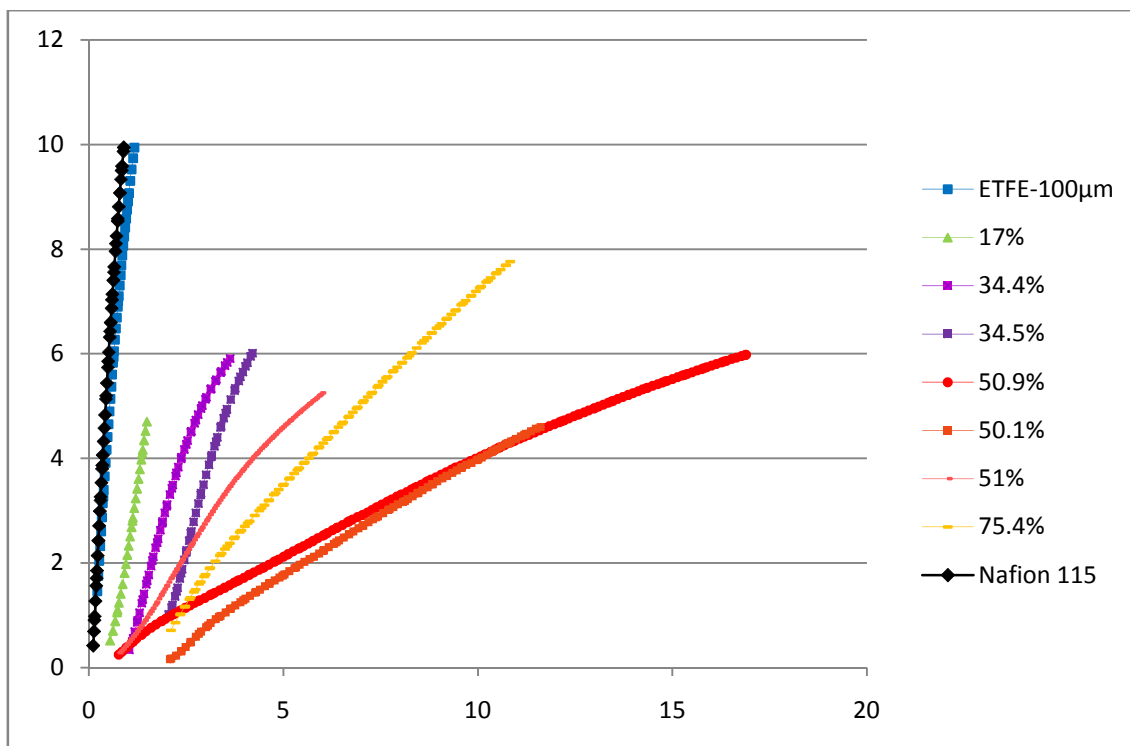


Figure 48. The linear elastic part of Nafion[®] 115 and the 100µm wet ETFE-g-PSSA membranes.

Ultimate strength, elongation at break and rupture analysis was not done since most of the membranes rent and slipped from the grips during characterization,

3.5 Platinum (Pt) Deposition

The deposition of platinum on ETFE-g-PSSA membranes was successfully achieved as depicted in Figure 49-51. Figure 49 shows the difference in surface morphology of Pt deposited and non-deposited ETFE films by SEM images. Figure 50 depicts cross-section of non-displaced 100µm_{GL}: 80% ETFE based IPMC. The deposited Pt layer can be seen at the edges. Additionally, Figure 51 shows Pt deposition with elemental analysis characterized by EDX.

The Figure 52 depicts that the deposited electrode layer is in between 10µm to 20µm. Since the Pt plating has two steps: reduction and growth, the outermost 10µm to 20µm layer (the brightest) may be attributed to the growth and the subsequent 10µm to 20µm layer (less bright) may be attributed to the reduction step (See Section 2.5).

Cracks and very small holes (the diameter is less than 500 nm) (Figure 53) were observed on the Pt deposited membranes that were subjected to electromechanical tests

which resulted in large bending type displacements. The existence of these cracks is attributed to the bending type loading.

Application of 5V and above electrical potential breaks off the Pt plates from the surface (Figure 54). This might be arising from the extremely fast and high displacement of the IPMC, mostly.

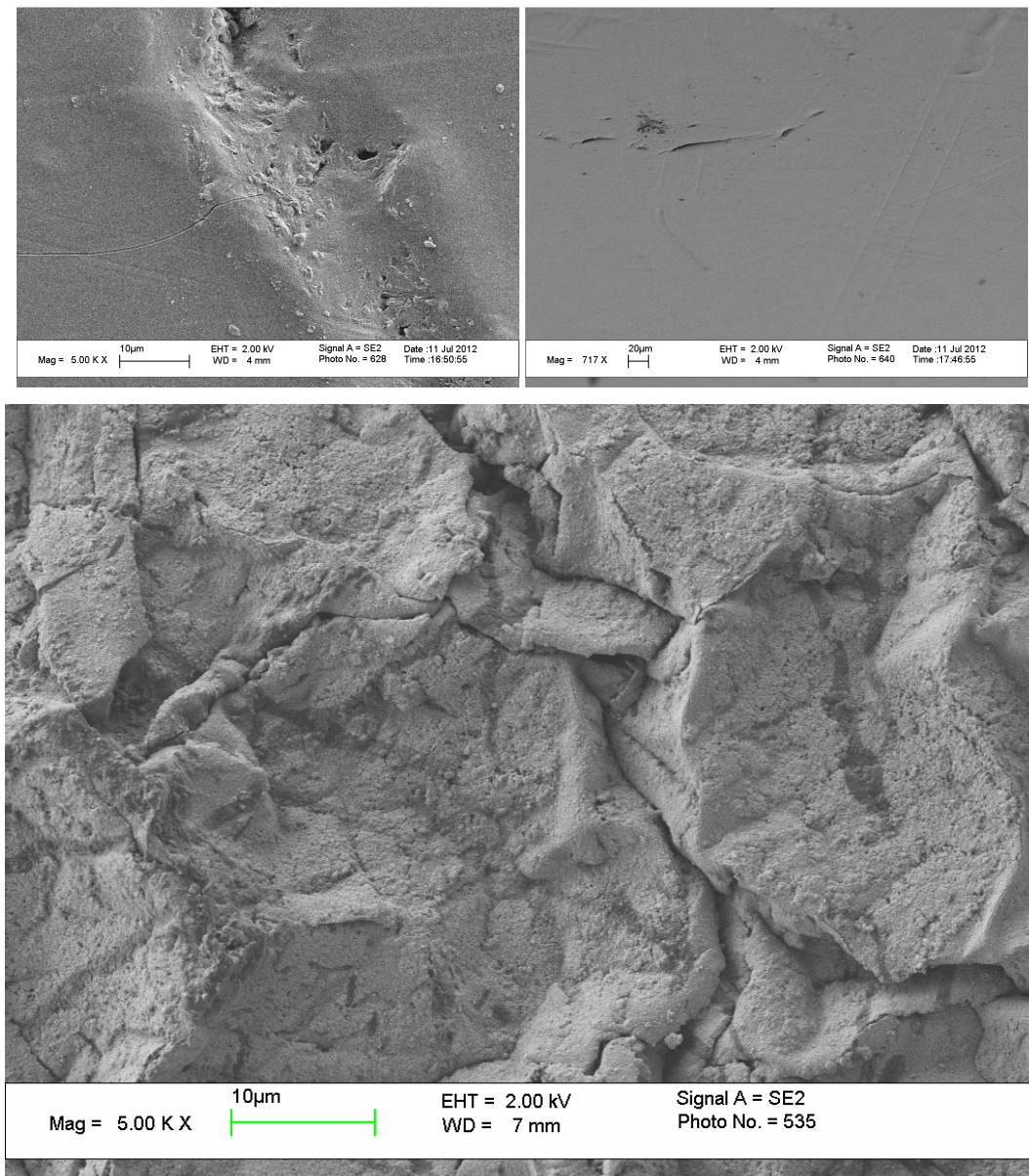


Figure 49. Non- displaced 100µm_GL: 80% ETFE-g-PSSA/IPMC surface (bottom). Surface of pristine, non-Pt deposited ETFE film, 250µm; scale bar: 10µm (top, left). Surface of 17% grafted, non-Pt deposited 100µm_ETFE film; scale bar is 20µm (top, right). For larger non-Pt deposited images, please see Appendix C.

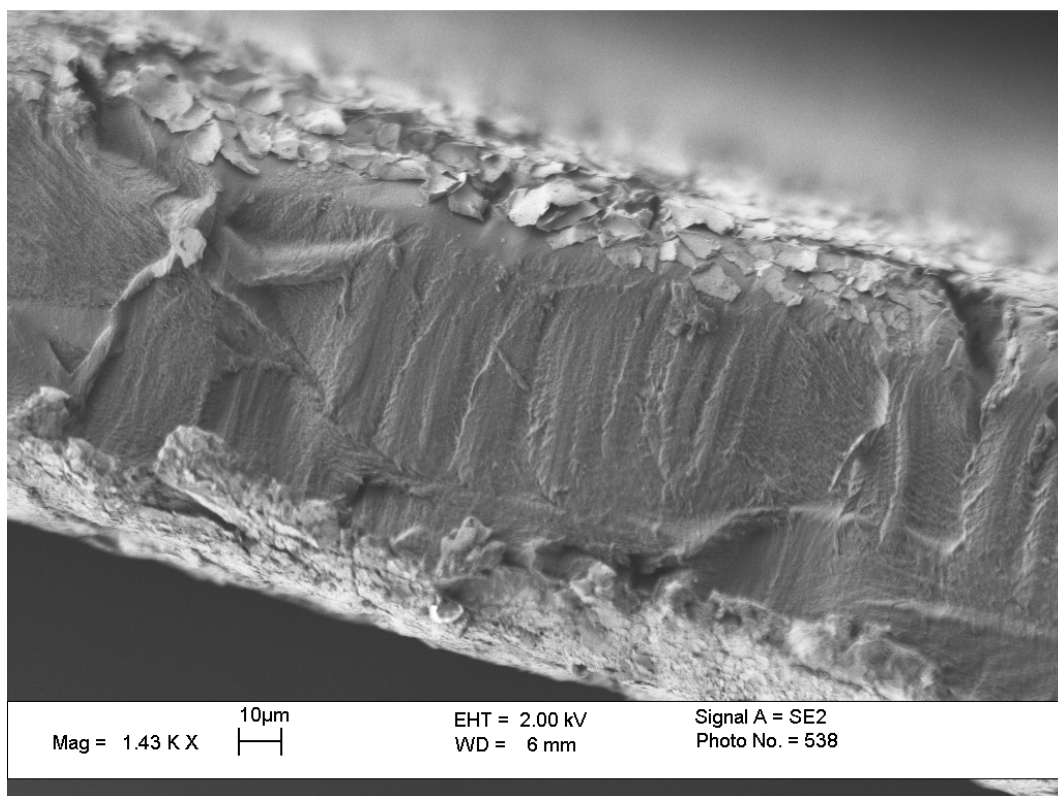


Figure 50. Cross-section of non-displaced 100µm_GL: 80% ETFE based IPMC.

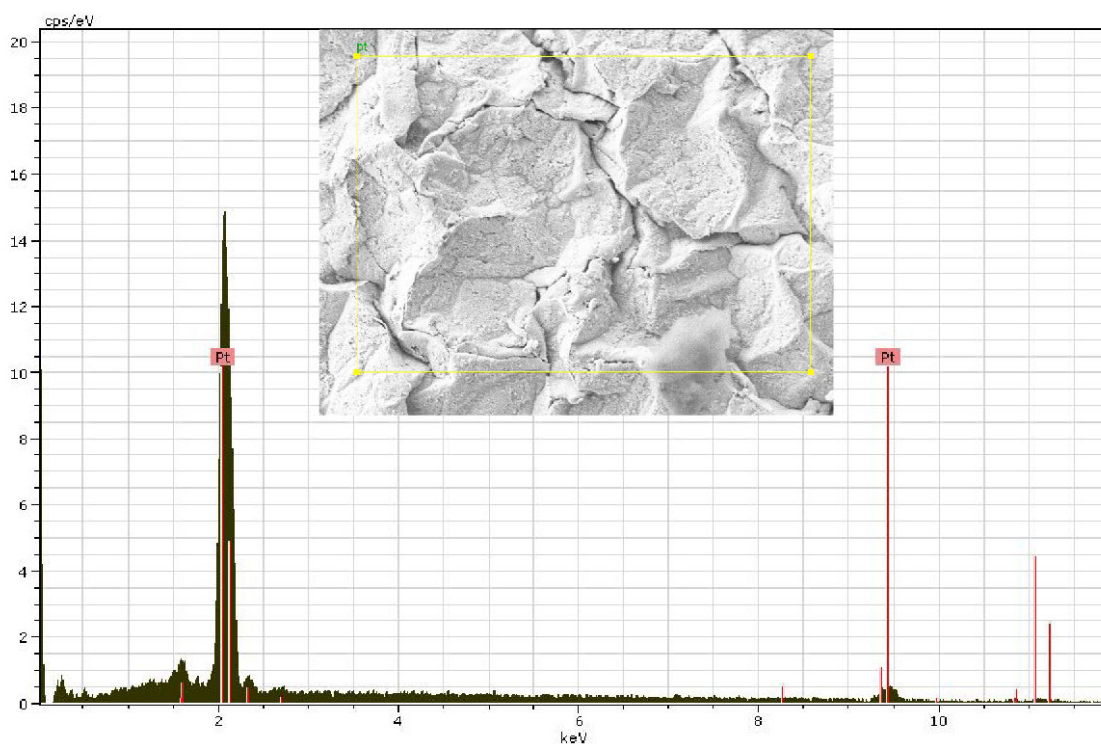


Figure 51. The EDX surface spectrum of the non-displaced 100µm_GL: 80% ETFE-g-PSSA based IPMC surface.

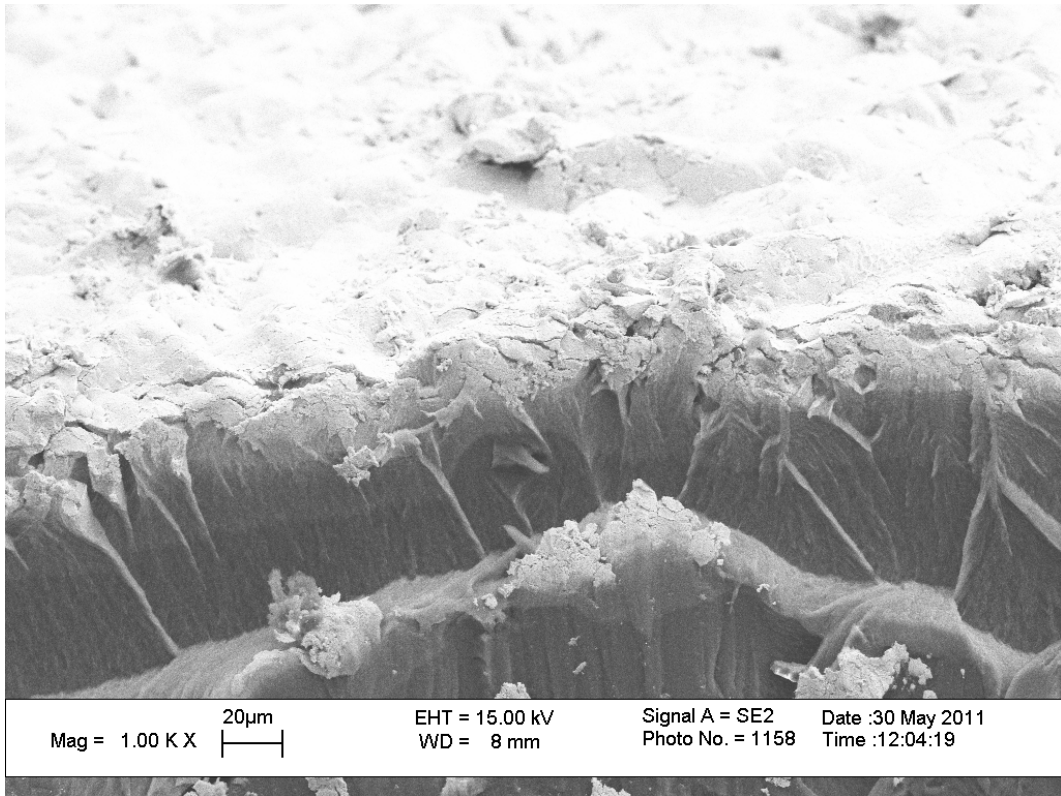


Figure 52. Cross-section of 200µm_GL: 55% ETFE based IPMC.

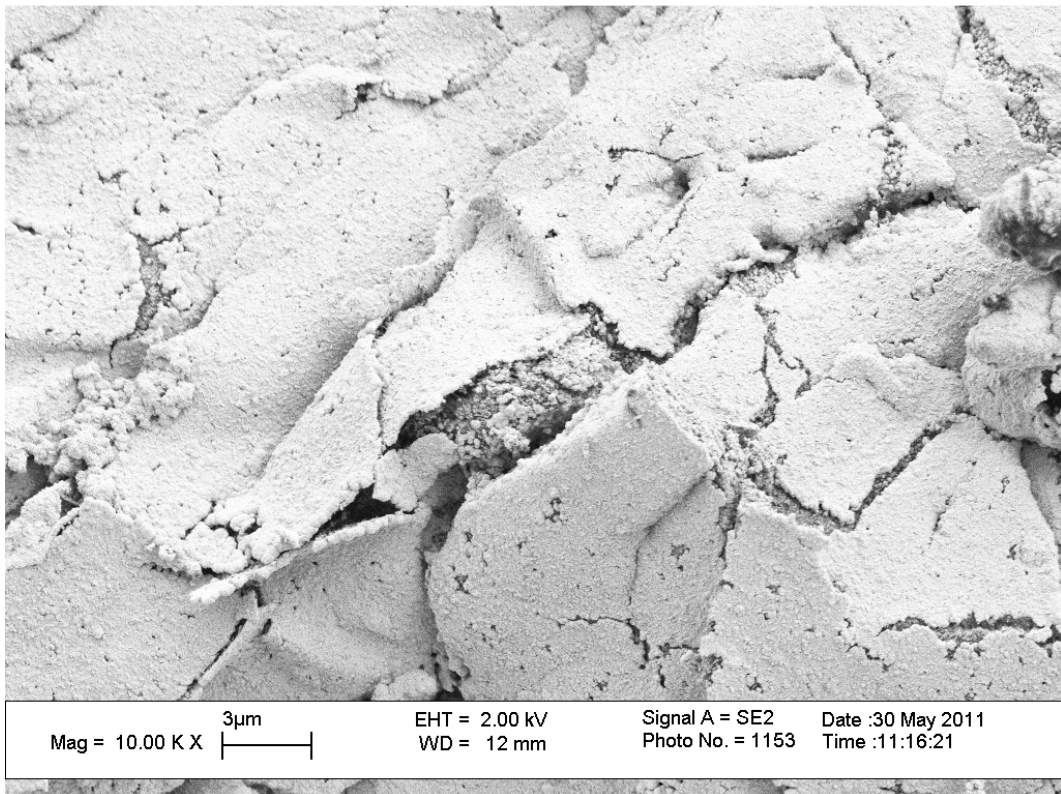


Figure 53. Surface of displaced 200µm_GL: 55% ETFE based IPMC. Applied maximum voltage is 3V; both in DC and in AC form.

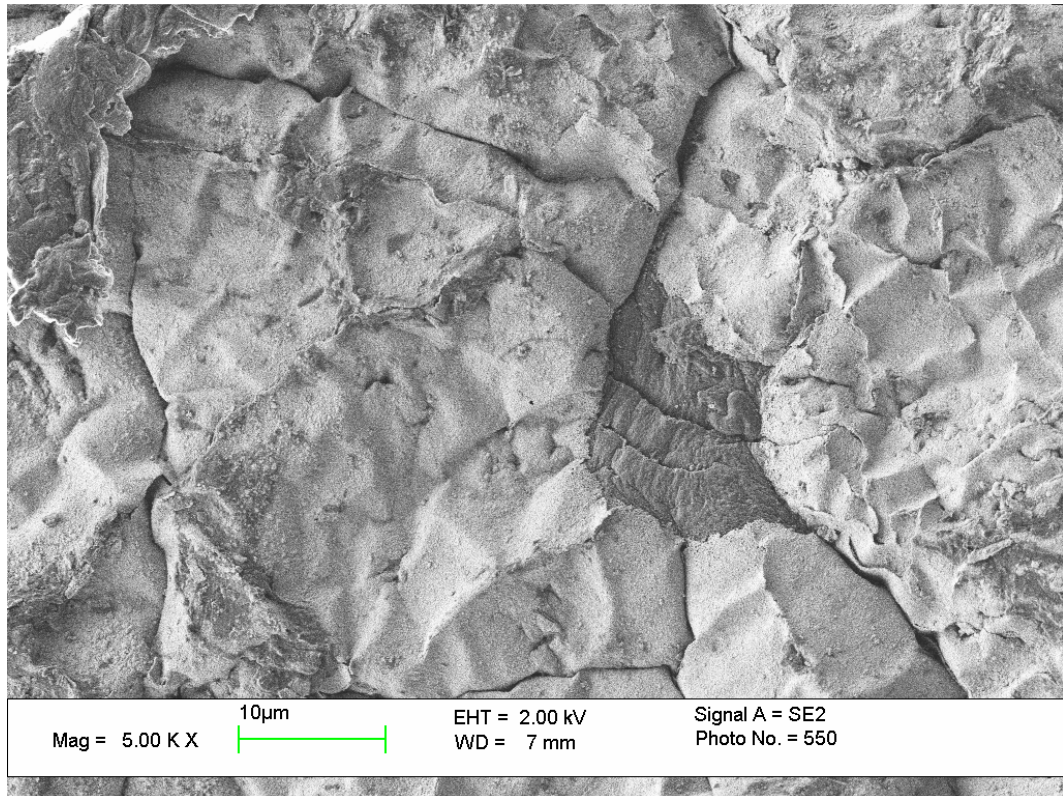


Figure 54. Surface of displaced 100µm_GL: 80% ETFE based IPMC both under AC and DC. The applied maximum voltage is 5V to 10 V in DC.

In addition to these, the details of cracked surface may give an idea about the Pt formation, its state and properties; however these have not been an elaborative subject of this thesis. The details of the cracked surface can be seen in Appendix C.

The cross-section at the tip of the specimen -100µm_GL: 80% ETFE-g-PSSA based IPMC, which was subjected to repeated displacement experiments- is shown in Figure 55, 56. The tip of the IPMC, at the free end, is the part moving the most. The changes in morphology is noticeable when it is compared with the same specimen before ever tested for electroactivity (Figure 50). The spherical convex structures appeared after repeated displacement experiments. This change in the surface morphology might be attributed to the change in the membrane morphology. On the other hand, the change might be arising from the Pt and Cu diffusion to inner sides of the tip part (Figure 57). If the metal diffusion or accumulation was the reason, the IPMC could not bend due to the lack of electric field through-the-thickness; in other words due to the electricity conduction. However, IPMC bends; therefore change in the cross section morphology is attributed to the changes in the membrane morphology.

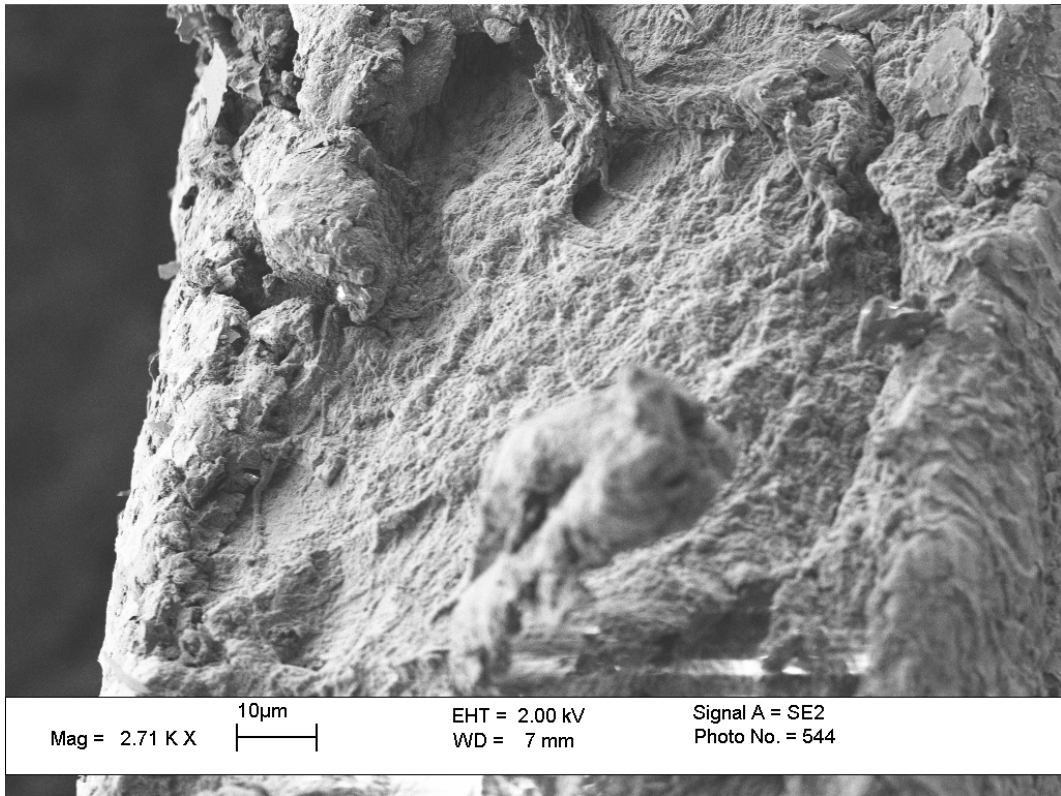


Figure 55. Tip of repeatedly displaced 100µm_GL: 80% ETFE based IPMC (cross-section).

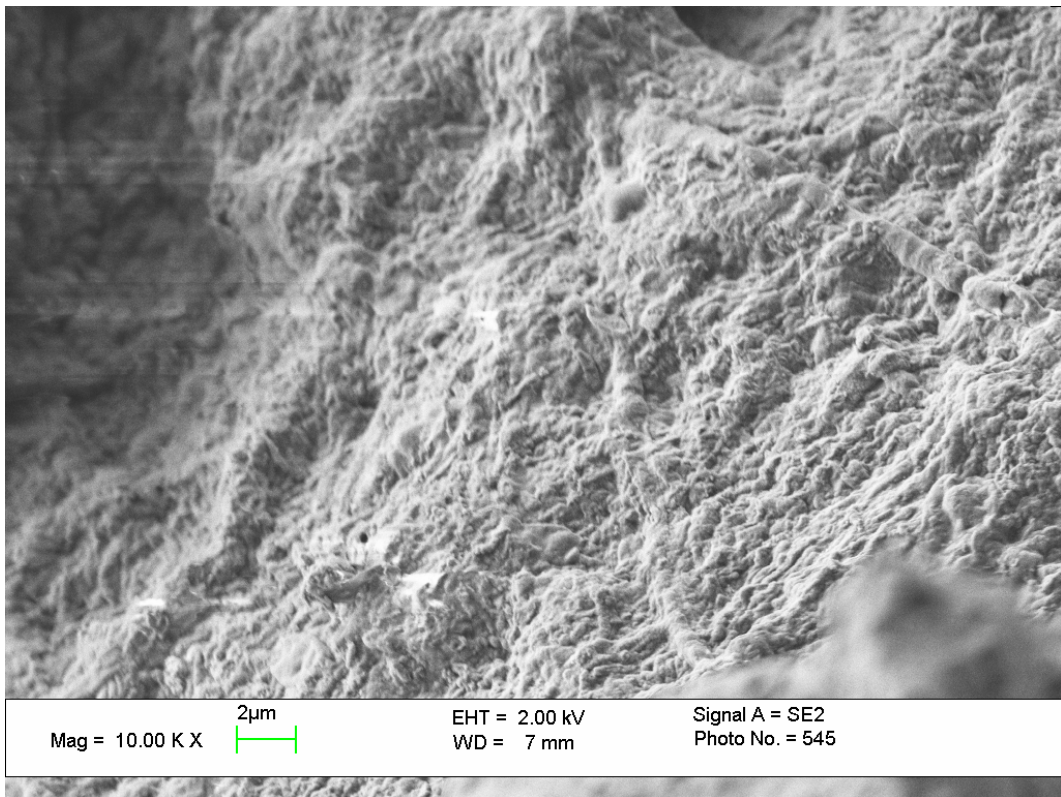


Figure 56. Tip of the repeatedly displaced 100µm_GL: 80% ETFE based IPMC (Cross-section).

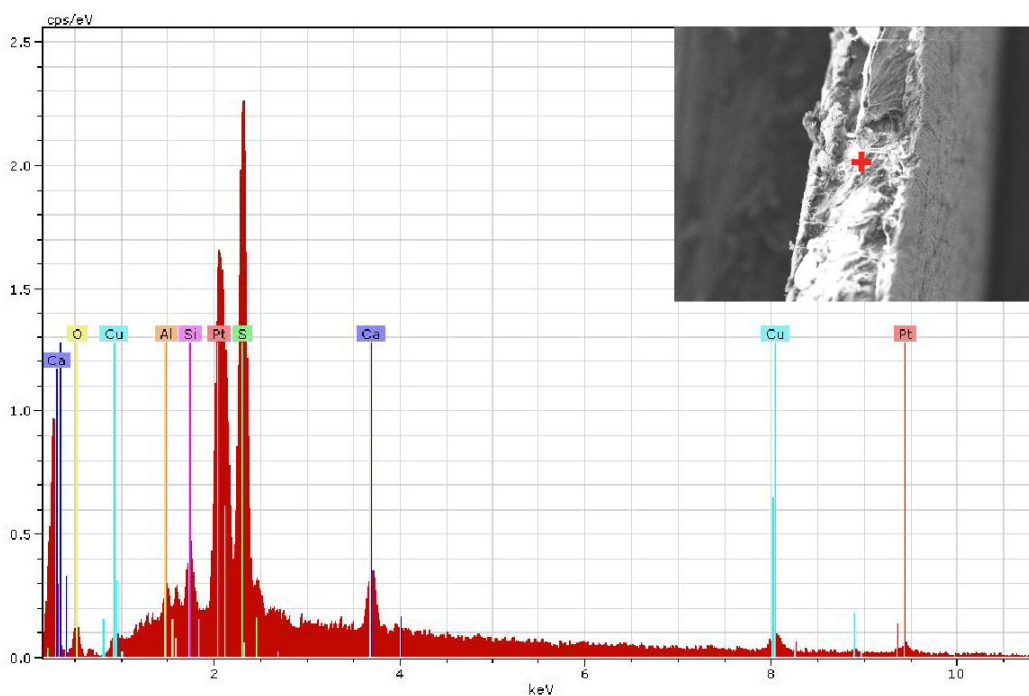


Figure 57. EDX spectrum of the repetitively displaced tip, 100 μm _GL: 80% ETFE based IPMC (cross-section). Point analysis (red cross) was made at the center.

Cu-tape has been used to contact the Pt electrodes with the power source on the holder. A striking observation is that, the Cu-tape was in contact with the fixed end; but existence of Cu was detected at the free end (at the tip) (Figure 57). O and S elemental peaks are arising from the sulfonate groups. Ca might be contaminated from the water, even though de-ionized water has been used in the experiments; however the existence of Al and Si could not be explained (Figure 57) with the available data.

In addition to these, Pt element was found in the interior of the membrane that is distant from the tip (Figure 58); where the intensity of S from the sulfonate groups dominates the other elemental peaks. The O peak also belongs to the sulfonate groups and F peak belongs to the ETFE backbone. Ca might be a contamination from water and existence of Al is unknown (Figure 58). While tracing towards the edge of the cross-section, the intensity of Pt dominates; whereas the F and Ca decreases (Figure 60). The S peak shows slight increase in intensity at a step forward (Figure 59) and then diminishes (Figure 60), finally finishes completely (Figure 61). This may indicate that the regions closer to the surface are more sulfonated than the most inner side. The Ca peak follows the same route with S. The O peak diminishes towards the edge; however still exist at the edge (Figure 61). Therefore Pt layer might have been oxidized. At the edge, Pt dominates as expected; the C peak becomes visible (either belongs to the membrane or coming from the C-coating prior to the SEM/EDX characterization).

Intensity of Al increases; therefore, even though a point analysis has been done in EDX, the data might be collected from the sample holder or Al definitely exists on the surface while it is hidden under the dominating intensity of Pt in the regional EDX analysis in Figure 51. Nevertheless, the existence of Pt in the interior of the membrane has been reported also elsewhere [48; 30; 68; 33; 97].

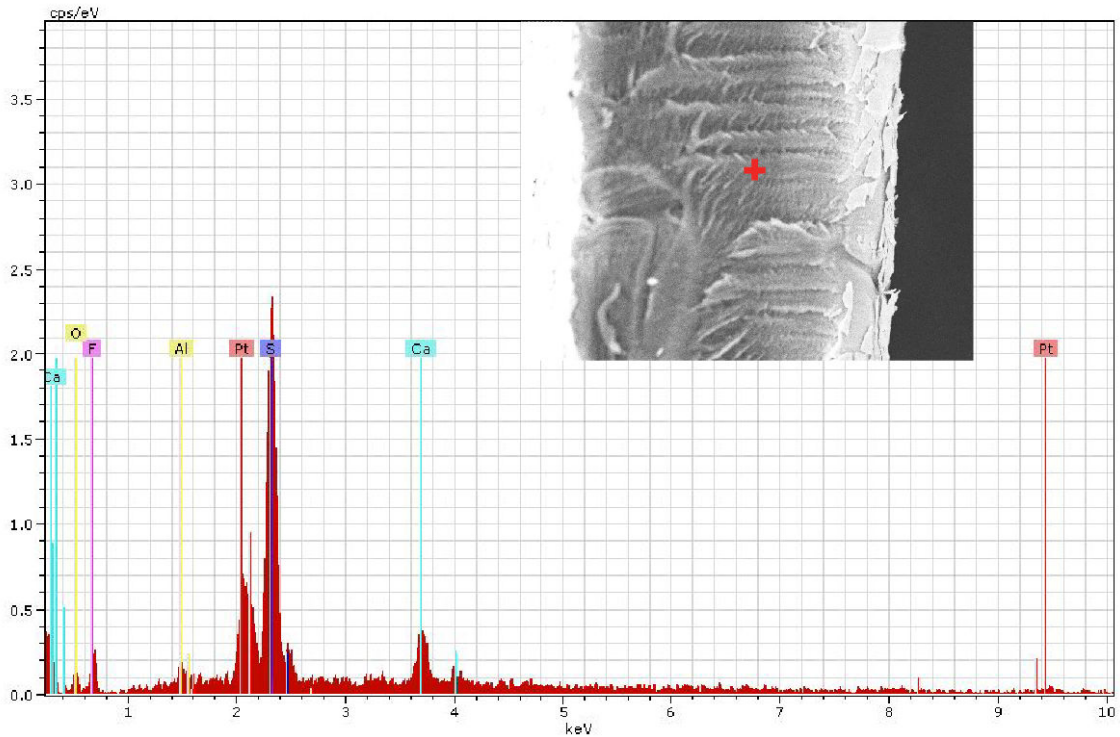


Figure 58. EDX spectrum of the non-displaced 100 μ m_GL: 80% ETFE based IPMC (cross-section). Point analysis (red cross) was made at the center.

The cross-sectional EDX spectrum of the 100 μ m_GL: 80% ETFE-g-PSSA based IPMC which has been used many times in electroactivity tests showed in Figure 62-66. Cu peak is seen in these EDX spectrums, also (Figure 62, 63) in addition to all other elemental peaks that are observed in the same, but non-displaced part of 100 μ m_GL: 80% ETFE-g-PSSA. All elemental peaks diminish while tracing towards edge except from Pt peak, like in the non-displaced sample. However, at the edge (Figure 64), Cu peaks disappear; which tells that Cu diffuses through the membrane. The point analysis on the surface also correlates that Cu appears in the membrane; but not on the Pt electrode (Figure 65, 66). This is an indication of Cu diffusion through the membrane, either. On the other hand, C, O, F and S peaks are still observable at the edge of the cross-section in Figure 64; whereas in the non-displaced IPMC, F and S peaks does not appear at the edge and intensity of O is very low (Figure 61). This may be an indication of the morphology change in the membrane, as well.

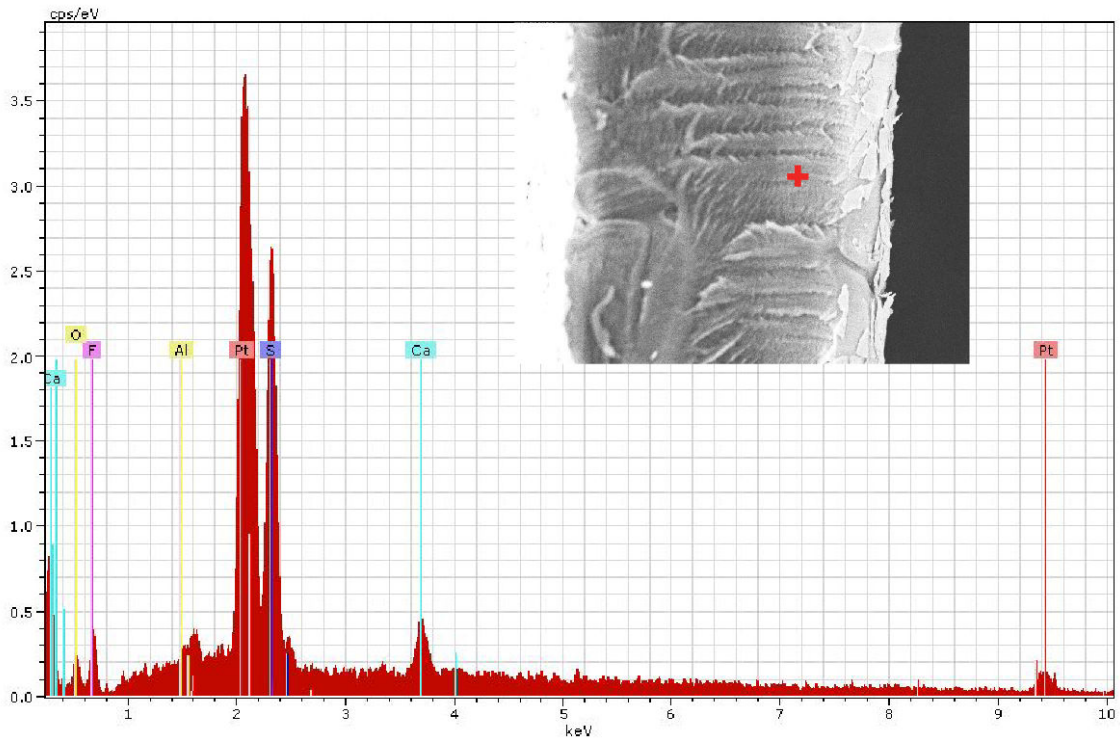


Figure 59. The non-displaced 100µm_GL: 80% ETFE based IPMC (cross-section). Red cross indicates that point analysis was made between the center and the edge

e

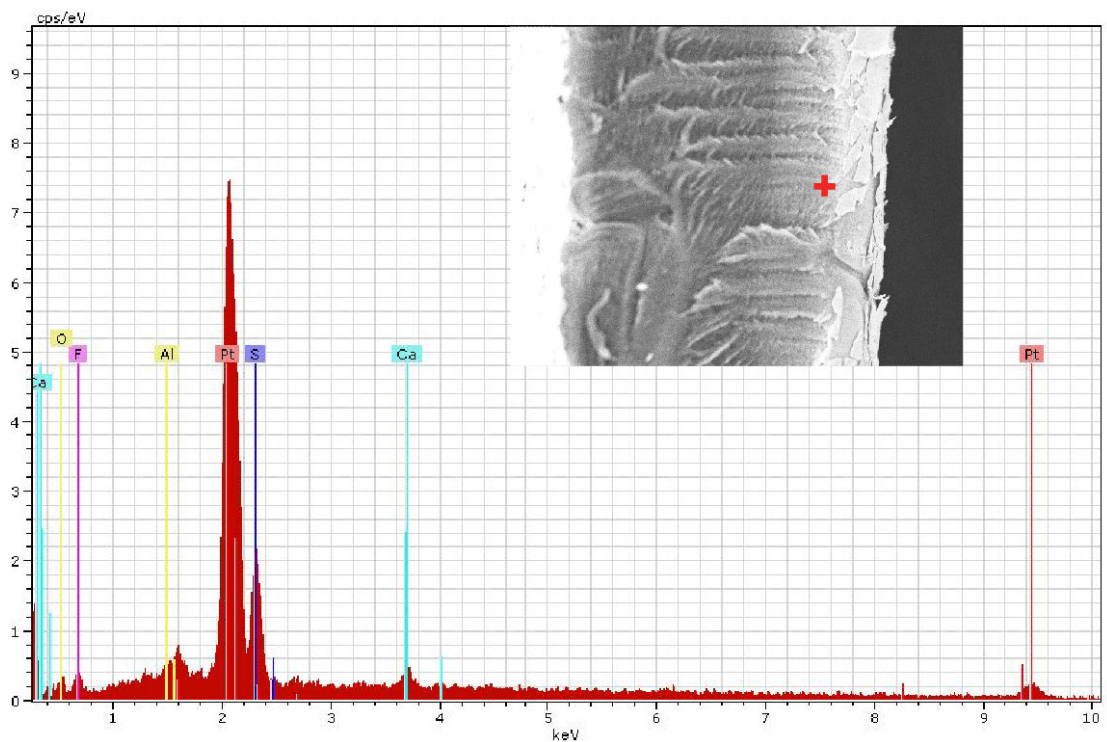


Figure 60. The non-displaced 100µm_GL: 80% ETFE based IPMC (cross-section). Red cross indicates that point analysis was made close to the edge.

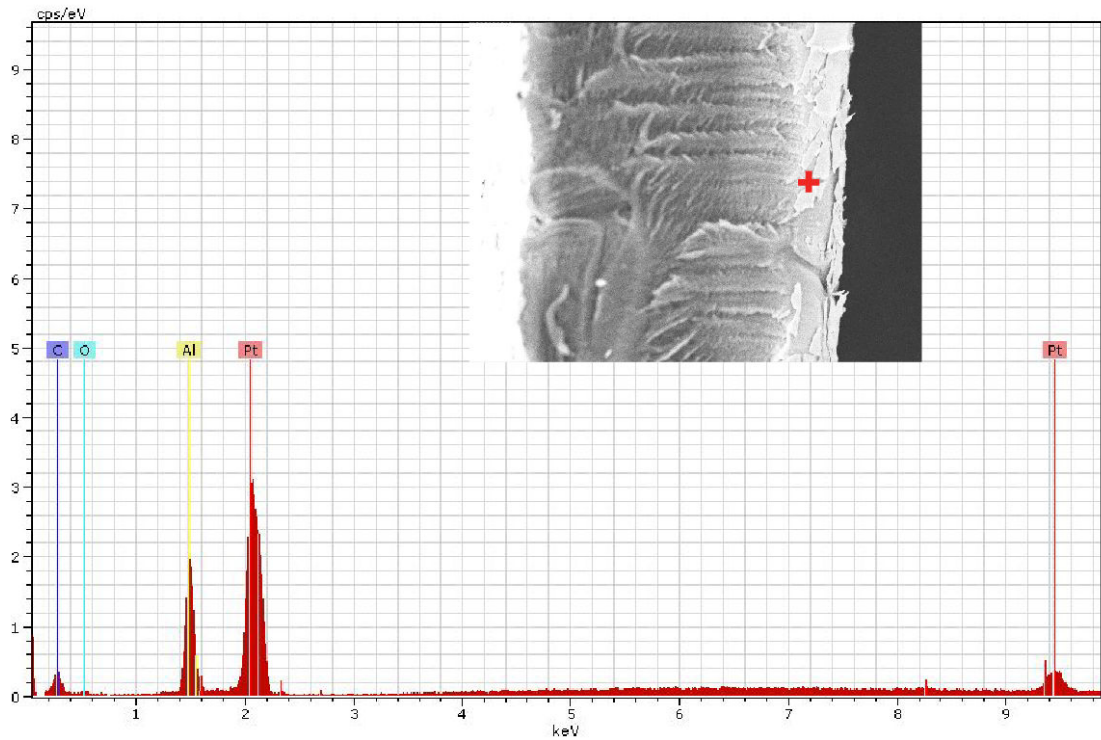


Figure 61. The non-displaced 100µm_GL: 80% ETFE based IPMC (cross-section). Red cross indicates that point analysis was made at the edge.

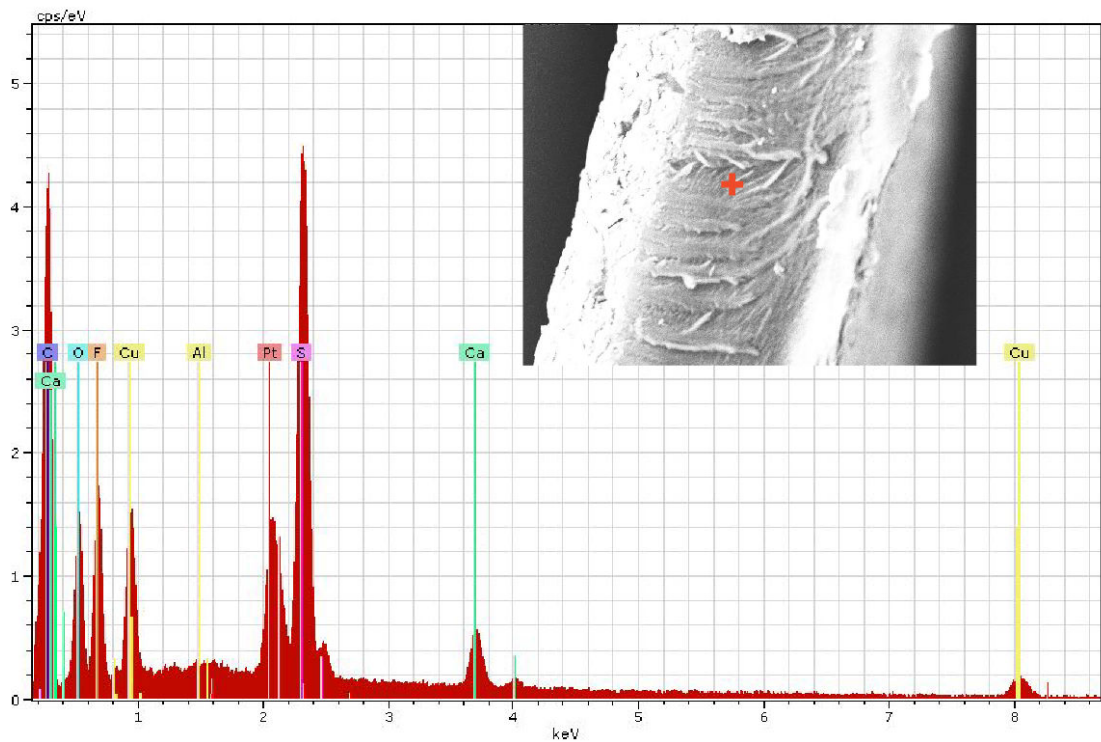


Figure 62. The repetitively-displaced 100µm_GL: 80% ETFE based IPMC (cross-section). Red cross indicates that point analysis was made at the center.

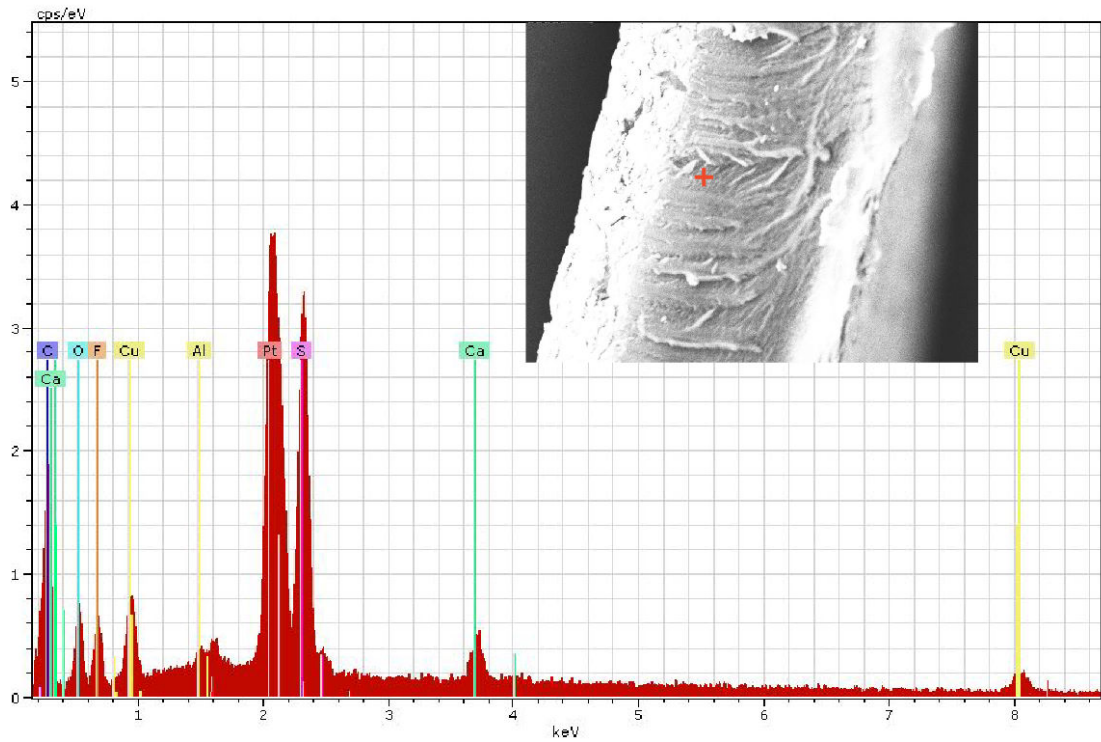


Figure 63 The repetitively-displaced 100μm_GL: 80% ETFE based IPMC (cross-section). Red cross indicates that point analysis was made between the center and edge.

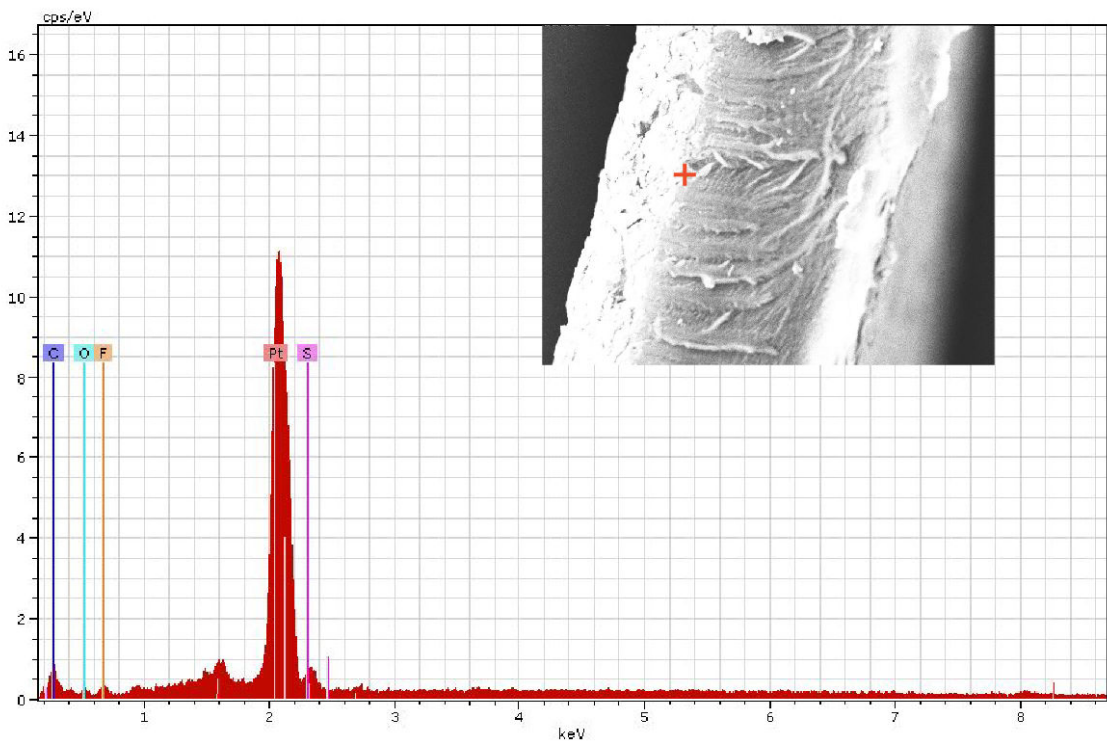


Figure 64. The repetitively-displaced 100μm_GL: 80% ETFE based IPMC (cross-section). Red cross indicates that point analysis was made at the edge.

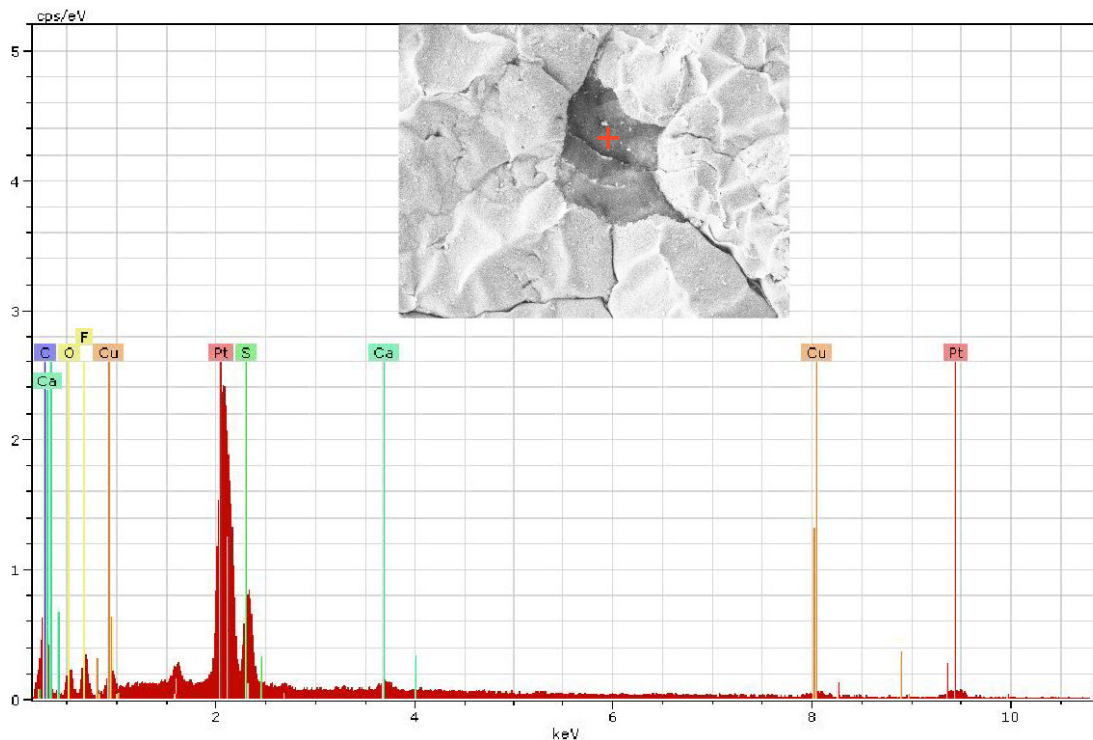


Figure 65. The EDX surface spectrum of the displaced 100µm_GL: 80% ETFE-g-PSSA based IPMC. Point analysis made on the membrane, where a part of Pt plate was broke off.

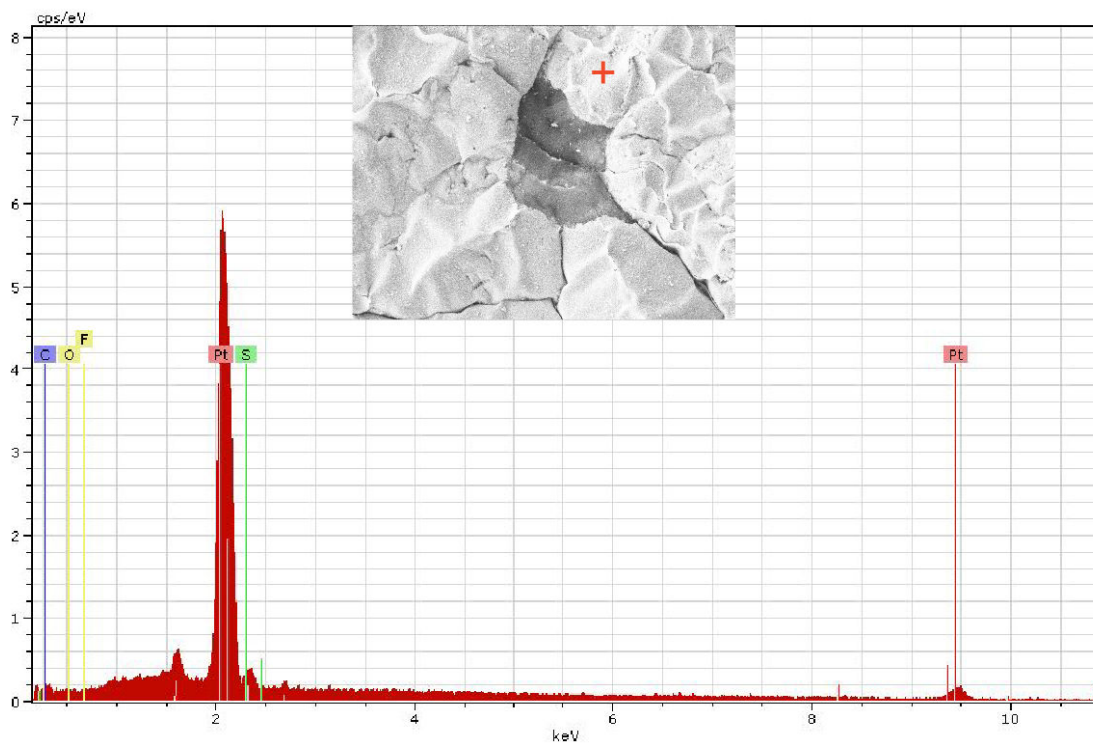


Figure 66. The EDX surface spectrum of the displaced 100µm_GL: 80% ETFE-g-PSSA based IPMC. Point analysis made on the Pt surface.

3.6 Actuation and Displacement

ETFE-g-PSSA membranes were turned into IPMC successfully (Figure 67). The ETFE-g-PSSA based IPMCs with high graft levels resulted in larger tip displacement capability than Nafion[®] based IPMCs (Figure 69, See Appendix C).

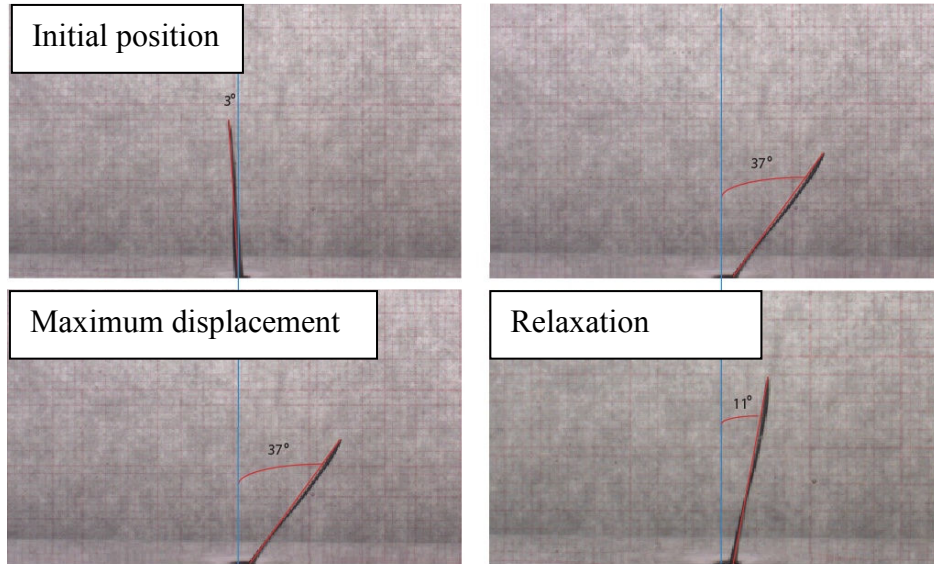


Figure 67. Bending of 150 μm _GL: 77% under 3V DC (left). Relaxation appeared when electric field was removed (right). Back-relaxation was not observed.

3.6.1 Effect of Graft Level

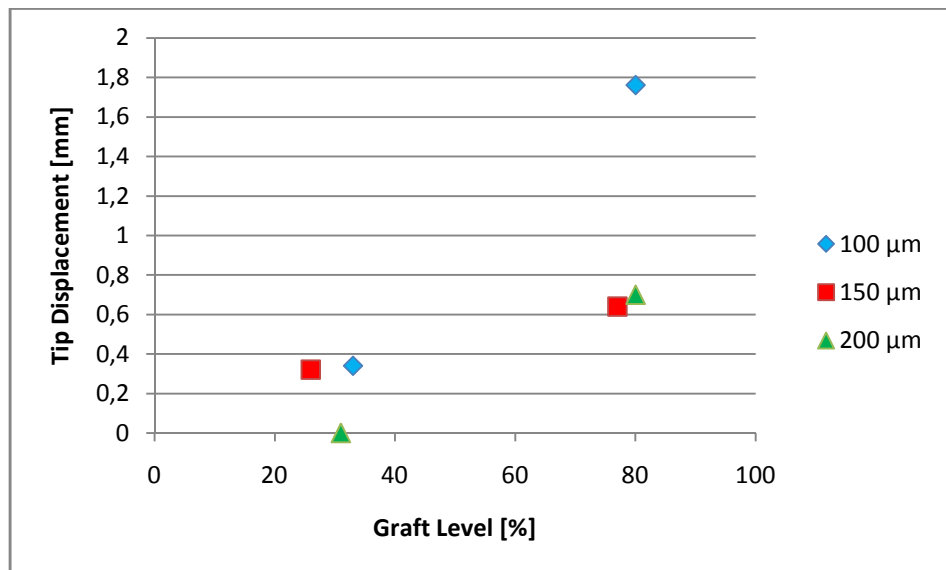


Figure 68. Tip Displacement *versus* Graft Level in different thicknesses under 1V and 0,5 Hz.

The bending behavior of IPMC has been mostly attributed to the ionic movements (Section 1.2.1), as such the higher the graft levels and associated increasing ionic conductivity (Figure 43) facilitated the larger the tip displacements (Figure 68).

The ETFE-g-PSSA based IPMCs with lower graft levels (~GL: 30 %) have not showed distinct tip displacement differences with respect to the applied voltage and frequency; and also their tiny tip movements created difficulty to record the tip displacement with the available set-up. Therefore, the higher graft levels, such as ~GL: 80%, were mainly presented in this study.

3.6.2 Effect of Thickness

Figure 69 shows varying displacement character with respect to thickness. However, a comparison between different thicknesses may not reveal the truth. Because, it was noticed that ETFE-g-PSSA membranes requires an adaptation period for actuation response. Some of the membranes which had not showed any bending at the beginning, such as 200 μm _ GL: 80%, showed very high displacement responses after a period of potential load and unload. Since, this behavior was discovered by coincidence; repetitive experiments could not be done. Nevertheless, the same behavior is observed in PEM fuel cells, called as “the conditioning time” [122].

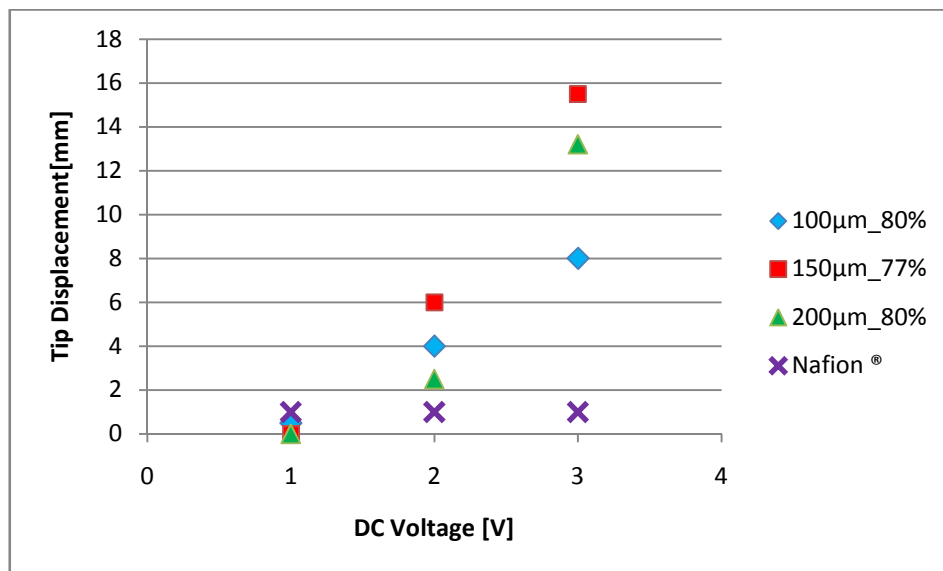


Figure 69. ‘Tip displacement *versus* DC Voltage’ with ETFE-g-PSSA in different thicknesses and similar graft levels

Therefore, Nafion[®] based IPMCs or 250 μ m thick ETFE-g-PSSA based IPMCs may have been requiring more conditioning time since the former showed a weak actuation compared to the 100 μ m, 150 μ m and 200 μ m ETFE-g-PSSA based IPMCs; and the latter in low grafting levels (250 μ m_GL: 30% and 250 μ m_GL: 60%) has not shown any displacement in the first five trial cycles.

On the other hand, 250 μ m_GL: 110% showed a standard displacement; while the lower graft levels of 250 μ m_ETFE-g-PSSA based IPMCs have not shown any bending behavior. Therefore, the 250 μ m thick IPMCs may also require higher grafting levels in order to be able to create a pressure difference across the membrane with its mobile species in addition to the its adaptation period.

3.6.3 Effect of Voltage

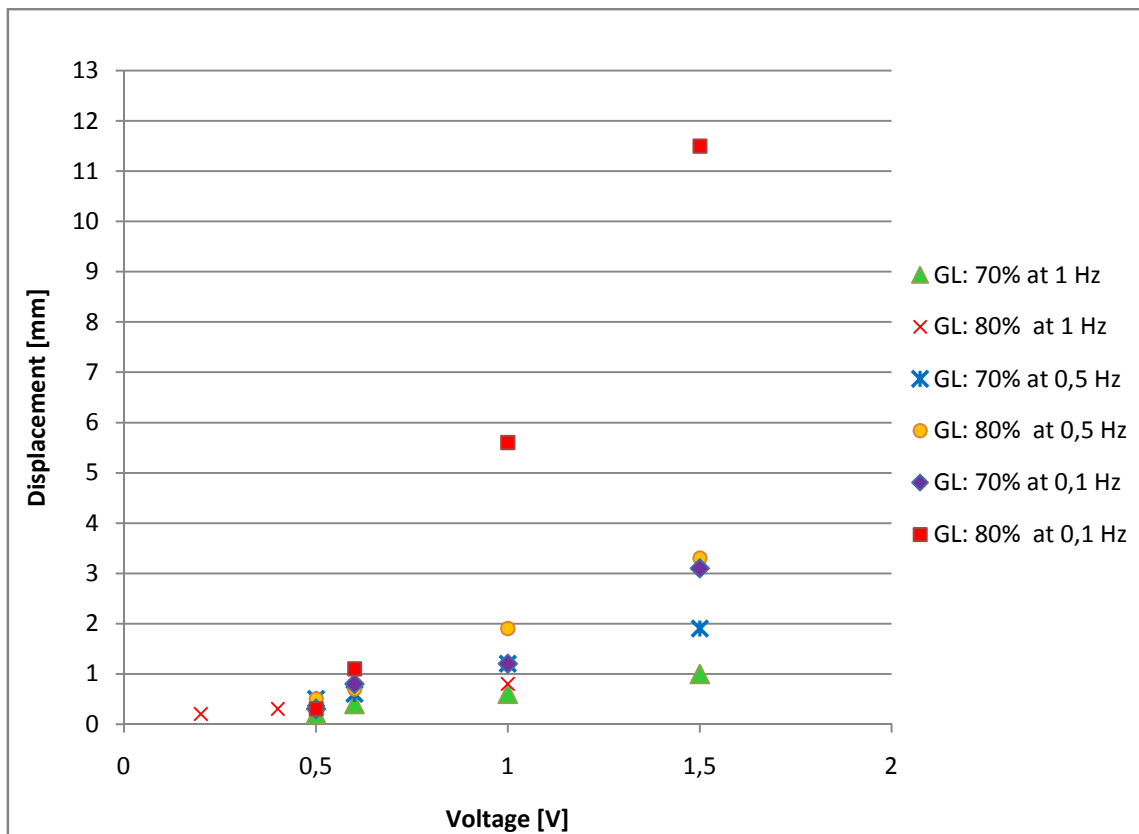


Figure 70. ‘Tip Displacement *versus* Voltage under AC Potential’ for 100 μ m_GL: 70% and GL: 80% ETFE-g-PSSA based IPMC at various frequencies.

The increasing voltage led to larger displacement as expected in ETFE-g-PSSA based IPMCs both under DC (direct current) (Figure 69) and AC (alternating current) (Figure 70) potential fields. Since the applied voltage is the stimulant of the bending

behavior, the higher voltages must be leading to the activation of the more species that creates bending. As described in Section 1.2.1, these species have been addressed as cations, hydrated cations or the solvent (water) (However, it must be noted that the actual working mechanism has not been discovered yet).

3.6.4 Effect of Frequency

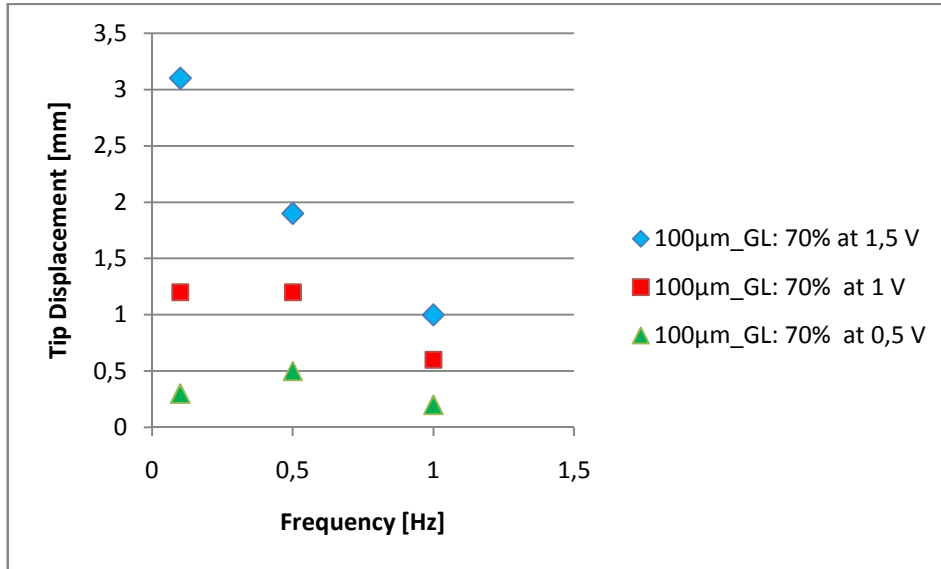


Figure 71. ‘Tip Displacement *versus* Frequency’ for 100 μm_GL: 70% ETFE-g-PSSA based IPMC

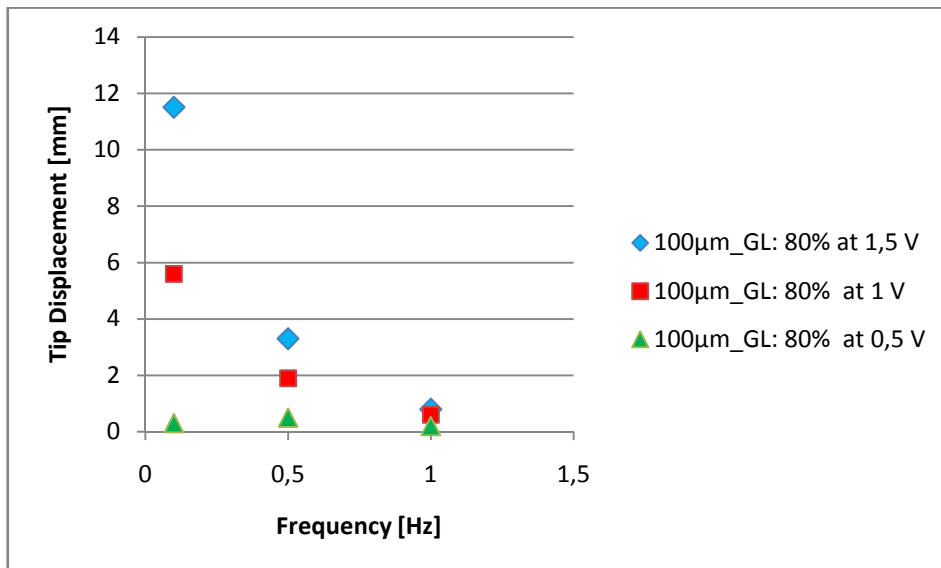


Figure 72. ‘Tip Displacement *versus* Frequency’ for 100 μm_GL: 80% ETFE-g-PSSA based IPMC

The lower the frequency was the higher the displacement (Figure 71, 72) [52]. The decrease in frequency resulted in larger differences in tip displacement. The tip displacement of 100 μm _GL: 80% ETFE-g-PSSA IPMC went up to 11,5 [mm] (Figure 72). That is to say, at the higher frequency range, the mobile species cannot keep up with the field. However, at the lower frequencies (such as 0,1 Hz) IPMC can behave as under DC potential and shows higher tip displacement.

3.6.5 Effect of Ionic Conductivity and Water Uptake

The bending behavior of IPMC has been mostly attributed to the ionic movements (Section 1.2.1), as such the higher the graft levels and associated increasing ionic conductivity (Figure 43) facilitated the larger the tip displacements (Figure 73, 74). On the other hand, a study based on NMR (Nuclear Magnetic Resonance) has been stated that deformation property of IPMC depends strongly on the water content and the different types of waters (The “bound water” that is bound to the ionic species in the membrane and the “free” water which is not bound by the ion salvation [46; 125]. In addition to these, different types of water were also observed in wet ETFE-g-PSSA membranes (See Appendix E).

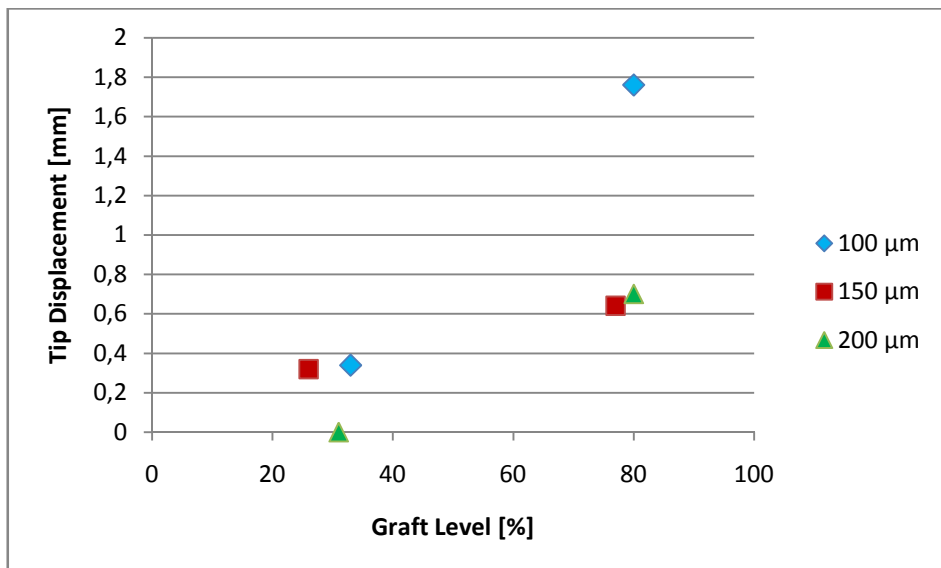


Figure 73. Tip Displacement *versus* Graft Level under 1 V and 0,5 Hz.

Tip displacement versus water uptake in Figure 75 shows that water uptake disposes an effect on bending behavior. The increasing water uptake increases the

displacement very roughly. However, the trends in tip displacement versus (Figure 73) graft level and tip displacement versus ionic conductivity (Figure 75) approaches to each other more than the water uptake trend. Therefore, ionic conductivity is more indicative than the water uptake in term of determining the bending behavior. That is to say, the cation migration based approaches –if the ionic conductivity in perflourinated membranes are supplied by the cation diffusion- are more descriptive than the solvent transport centered approaches.

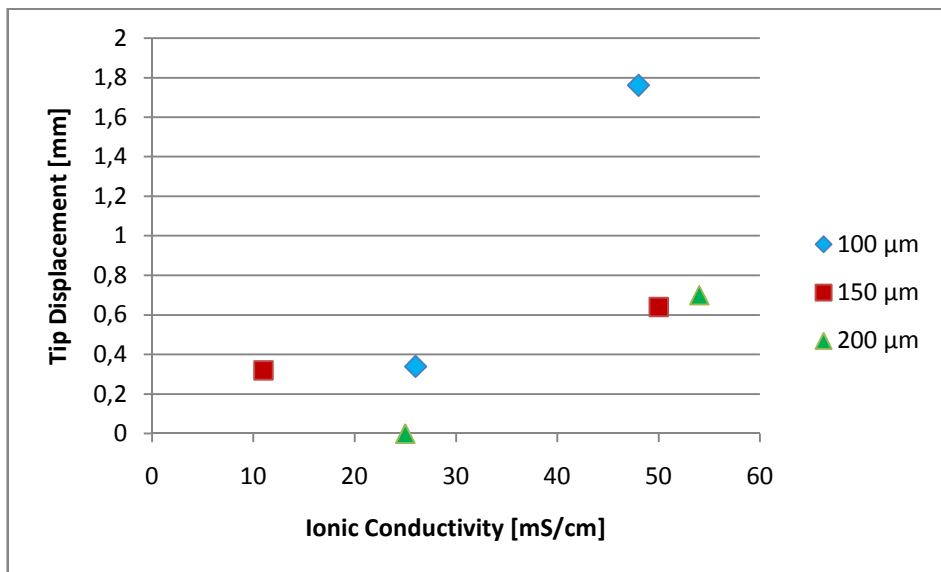


Figure 74. Tip Displacement *versus* ionic conductivity under 1 V and 0,5 Hz.

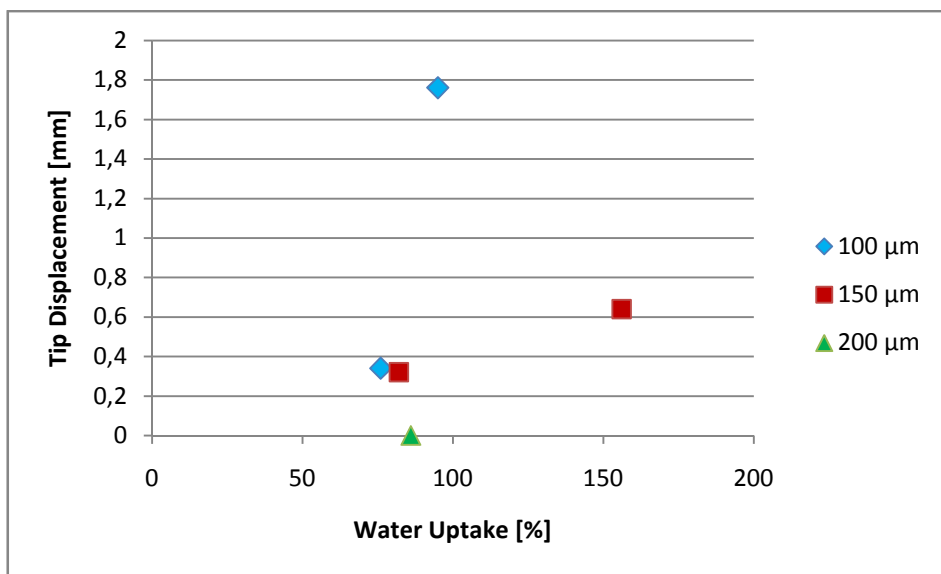


Figure 75. Tip Displacement *versus* Water Uptake under 1 V and 0,5 Hz.

3.6.6 Notes on Characteristics of ETFE-g-PSSA

Some of the observed characteristics of the ETFE-g-PSSA based IPMCs revealed different behavior than the Nafion[®] based IPMCs which have not been reported in the current literature:

As stated before, most of the ETFE-g-PSSA based IPMCs, did not show an immediate actuation response immediately after the synthesis; however the same ETFE-g-PSSA based IPMC samples showed an actuation performance after being subjected to some periods of potential load. Moreover, the actuation performance of the ETFE-g-PSSA based IPMCs has been increased by being subjected to more periods of the load (The more and more displacements have been observed in the samples which have been repetitively used for the displacement experiments). Although an analogy has been built with the conditioning of proton exchange membranes (PEM); the reason which causes to this delay-behavior has not been explained for PEMs as well. On the other hand, ETFE-g-PSSA based IPMC samples have been kept their conditions for 3 years without any change with their actuation capabilities (The samples which had been displacing, they displaces 3 years later as well; and the samples which had not been displacing, requires either a prior load-potential period to displace or they have not displaced 3 years later, either.)

In the literature, the highest applied voltage is 3V, in general. In ETFE-g-PSSA based IPMCs, it has been observed that the IPMC have been continued to bend towards anode up to applied 3V (both in DC and AC form). When 5V DC potential was applied, an extremely fast actuation was observed towards anode and also generation of a smoke was observed. When the same sample was undergone 5V (DC) again, a leakage of 2V of the potential was observed while the 3V were used to bent the IPMC (with a lower tip-displacement). Furthermore, the IPMC showed an actuation displacement towards cathode and then sometimes a large back-relaxation towards anode side. This behavior is opposite of the usual behavior. This abnormal behavior might be resulted from the Pt and Cu diffusion into the IPMC membrane (Figure 62); or some additional chemical reactions might be appearing during the application of 5V.

Nevertheless, in order to be able to interpret the displacement results, the actual mechanism of actuation must be known. However, the discovery of Pt and Cu diffusion into the membrane and the observations of different behaviors would add value into the exploration of the complete mechanism.

4 CONCLUSION

In this study, ionic polymer metal composites were synthesized successfully from poly(ethylene-*alt*-tetrafluoroethylene)-*g*-polystyrenesulfonic acid (ETFE-*g*-PSSA) membranes. Moreover, grafting properties and the effect of grafting on the ion conductive membranes and on the IPMC performance were investigated. The different characteristics of ETFE-*g*-PSSA than Nafion[®] based IPMCs have revealed. In addition to these, the importance of the morphological studies on the ETFE-*g*-PSSA membrane structure was emphasized.

Radiation grafting is a diffusion induced process. Graft levels increase by the increase in grafting time. Furthermore, it is found that the thicker films require more time to reach to the same graft levels as thinner films have.

On the other hand, some deviations in graft levels were observed. These deviations may arise from the radical decomposition in the film, homopolymer formation during grafting, insufficient and improper nitrogen purging and difficulties because of the reactor geometries. We tried to reduce these deviations. For instance, in order to reduce the effect of reactor geometry, new reactors were produced.

Water uptake of ETFE-*g*-PSSA membranes increases with the increase of graft levels. However, it was determined that the increase is not linear. The reasons of non-linear increase were attributed to the non-homogeneous grafting in the membranes, structural morphology and also to the experimental errors during the measurement of water uptake. The smoothest increase was observed on 100 μ m ETFE-*g*-PSSA membranes.

Ionic conductivity increases while graft level increases. A linear relation was not observed as in the water uptake results. The reason was attributed to the inhomogeneous grafting as well.

An increase in ionic conductivity was observed with increase in water uptake. However, it is noted that water uptake is not a distinctive indicator of the ionic conduction. Essentially, in order to understand ionic conductivity behavior micro- or nano- structural analysis of ETFE-*g*-PSSA, and also of the other ionic conducting polymeric mediums, must be taken into consideration.

In mechanical properties of wet ETFE-*g*-PSSA membranes, elastic modulus and tensile strength decrease with introduction of grafted polystyrene chains for all

thickness values. Yield strength also decreases by increase in graft levels in 100 μ m wet ETFE-g-PSSA membranes. Increase in graft levels decreases the stiffness, as well.

SEM and EDX images showed that Pt was deposited onto Nafion[®] and onto ETFE-g-PSSA membranes. Surface and cross-sectional analysis made by SEM and EDX showed that bending results in cracks. Furthermore, Pt and Cu can diffuse from electrodes into the membrane. In addition to these, applied electric field might be inducing morphological changes in membrane structure.

Higher graft levels led to the larger the tip displacements in ETFE-g-PSSA based IPMCs. An increase in tip displacement was observed with increasing voltage both under AC and DC potential fields. On the other hand, the lower the frequency was the higher the displacement.

In the manner of description of the bending mechanism, it was observed that ionic conduction has a dominative effect than the water uptake capability.

In addition to these, several different characteristics of the ETFE-g-PSSA based IPMCs than the conventional Nafion[®] based IPMCs, which have not been reported in the current literature, were determined. An adaptation period to the applied electric field was observed such as the conditioning time in PEM (proton exchange membrane) fuel cells. 5V and above applied potentials are effecting the displacement character widely. After application of 5V, in the next electromechanical tests, a reverse actuation character (actuation towards cathode and back-relaxation towards anode) was observed. The application of higher voltages, 5V and above, might be even deteriorating the actuation mechanism. The applied higher voltages damage the ETFE-g-PSSA based IPMCs' surface.

Lastly, it was observed that ETFE-g-PSSA based IPMC can keep their state at least 3 years long.

5 FUTURE WORKS

In this thesis, aim was to reach to some specific graft levels. However, approaching to the kinetical conditions in grafting with very precise purging system would be very descriptive in terms of interpreting the ionic conductivity and water uptake properties of the grafted membranes in the future works. Additionally, grafting of ETFE films with

polystyrene at high thicknesses as above 100 μ m has not been studied in the literature widely. Therefore, this approach would add value to the radiation grafting literature.

Grafting of the ETFE films should be carried in the new grafting reactor in order to increase the grafted film quality and also in order to being able to use the same film in various characterization systems (See Section 3.1.1). In this way, the water uptake measurements can be done in the size of IPMC strips; rather than using small pieces of the grafted membranes. Hence, the effect of the water uptake in displacement can be seen more obviously. In addition to these, NMR analysis should be cooperated into the study in order to observe the effect of the water content and water types to the bending behavior [125]. AFM characterizations should be conducted into the investigation, either, owing to see the effect of water uptake in ETFE-*g*-PSSA membranes' morphology change during the water diffusion [106]. Because, morphology change is a possible adaptation behavior to the new wet environment. This response, if exists in the ETFE-*g*-PSSA membranes, may help to understand the bending mechanism of the ETFE-*g*-PSSA based IPMCs as well as the Pt and Cu diffusibility through the membrane. Furthermore, morphology change by introduction of water may induce ionic aggregates in the membrane (See Section 1.3.1). SAXS analysis should be expositive in the case of ionic aggregates' existence (See Section 1.3.1). Therefore, ion conducting character can be investigated by being parallel with the water uptake behavior; hence the relation presented in Section 3.6.5 in a primitive form can be understood clearly.

In terms of ionic conduction, an approach which aims distinguishing difference between ion transport, *i.e.* the hydronium transport, and the electronically stimulated conduction (such as relation between the electrode layers and the polymeric membrane interface) would be taken into account [46]. In this way nature of the conduction through the IPMC might be understood. Furthermore, in order to understand the stimulating character of applied electrical potential in the ion conducting fluoropolymer membranes in general, an approach that Maier [70] offers should be taken into account: The size of the tiny water channels in Nafion[®] (as stated in the 1.3.1. Nafion[®] Section) are very small; thus the electronic properties in the interface between the water channels and the polymer membrane can be studied like in a crystal matrix. When the similarity of ETFE-*g*-PSSA membranes to Nafion[®] is taken into consideration, this approach also holds for the ETFE-*g*-PSSA. Owing to materialize these approaches, electron or ion beam lithography can be used to irradiate the pristine ETFE films (Section 1.4.1). The lithography creates patterned active sites on the film. Therefore, grafting may also be

achieved in patterned forms. Creating an ordered arrangement in the ion conductive membrane can help the observations of electronic properties that Maier suggested [70].

The Pt and Cu diffusions through the ETFE-g-PSSA membranes are an interesting fact of this thesis. In order to understand the diffusion mechanism, oxidation states of the diffused Pt and Cu can be analyzed by EELS (Electron Energy Loss Spectroscopy) and also their crystal structure can be exposed by the diffraction patterns via TEM (Transmission Electron Microscopy) if the diffused metals aggregated.

Mechanical tests of grafted ETFE films and dry sulfonated ETFE membranes should be made in order to observe the effect of mechanical properties on the displacement character.

The adaptation periods of ETFE-g-PSSA based IPMCs towards actuation should be observed by precise voltage loads with respect to time in an automated photonic sensor displacement system. Lastly, the effect of graft level, water uptake, ionic conductivity and the mechanical properties on the actuation and displacement character should be interpreted by aforementioned future work investigations.

APPENDIX A/1 RADIATION GRAFTING RESULTS

8 x 8 [cm²] films:

| Film Name (100 μm grafted films) | GL [%] | Graft Time [Hours] |
|---|-------------------|-------------------------------|
| 12.06.06_100μm_1.1 | 14.41 | 01:00 |
| 12.06.06_100μm_1.2 | 18.54 | 01:00 |
| 12.04.12_100μm_1.1 | 17.45 | 01:00 |
| 12.04.12_100μm_1.2 | 9.54 | 01:00 |
| 12.04.30_100μm_1.1 | 34.28 | 01:30 |
| 12.04.30_100μm_1.2 | 34.50 | 01:30 |
| 12.04.16_100μm_1.1 | 34.42 | 01:30 |
| 12.04.16_100μm_1.2 | 24.10 | 01:30 |
| 12.05.07_100μm_1.3 | 50.10 | 02:00 |
| 12.05.07_100μm_1.4 | 50.90 | 02:00 |
| 12.04.16_100μm_1.3 | 51.18 | 02:00 |
| 12.04.16_100μm_1.4 | 45.01 | 02:00 |
| 12.06.04_100μm_1.3 | 49.15 | 02:15 |
| 12.06.04_100μm_1.4 | 40.85 | 02:15 |
| 12.04.06_100μm_1.1 | 75.40 | 02:40 |
| 12.04.06_100μm_1.2 | 36.53 | 02:40 |
| 12.04.06_100μm_1.3 | 81.72 | 02:40 |
| 12.05.31_100μm_1.1 | 54.23 | 02:40 |
| 12.05.31_100μm_1.2 | 78.51 | 02:40 |
| 12.05.03_100μm_1.1 | 56.72 | 03:00 |
| 12.05.03_100μm_1.2 | 68.27 | 03:00 |
| 12.06.04_100μm_1.1 | 73.31 | 03:30 |
| 12.06.04_100μm_1.2 | 86.60 | 03:30 |
| 12.05.31_100μm_1.3 | 110.7 | 04:00 |
| 12.05.31_100μm_1.4 | 109.4 | 04:00 |
| 12.06.06_100μm_1.3 | 113.1 | 05:00 |
| 12.06.06_100μm_1.4 | 108 | 05:00 |

| Film Name (150 μm grafted films) | GL [%] | Graft Time [Hours] |
|---|-------------------|-------------------------------|
| 12.06.04_150 μm _1.1 | 28.19 | 02:30 |
| 12.06.04_150 μm _1.2 | 19.63 | 02:30 |
| 12.04.12_150 μm _1.1 | 24.50 | 02:30 |
| 12.04.12_150 μm _1.2 | 20.98 | 02:30 |
| 12.06.04_150 μm _1.3 | 38.89 | 03:00 |
| 12.06.04_150 μm _1.4 | 27.74 | 03:00 |
| 12.05.03_150 μm _1.1 | 40.15 | 03:15 |
| 12.05.03_150 μm _1.2 | 35.08 | 03:15 |
| 12.04.20_150 μm _1.1 | 56.63 | 04:00 |
| 12.04.20_150 μm _1.2 | 58.70 | 04:00 |
| 12.06.06_150 μm _1.5 | 61.33 | 06:00 |
| 12.06.06_150 μm _1.6 | 68.75 | 06:00 |
| 12.06.06_150 μm _1.7 | 141.57 | 07:00 |
| 12.06.06_150 μm _1.8 | 91.53 | 07:00 |
| 12.05.07_150 μm _1.3 | 107.5868 | 08:00 |
| 12.05.07_150 μm _1.4 | 120.9653 | 08:00 |
| 12.04.30_150 μm _1.1 | 136.3064 | 09:00 |
| 12.04.30_150 μm _1.2 | 120,8548 | 09:00 |

| Film Name (200 μm grafted films) | GL [%] | Graft Time [Hours] |
|---|-------------------|-------------------------------|
| 12.04.12_200 μm _1.1 | 29.08 | 04:30 |
| 12.04.12_200 μm _1.2 | 31.14 | 04:30 |
| 12.04.20_200 μm _1.1 | 38.69 | 04:30 |
| 12.04.20_200 μm _1.2 | 34.95 | 04:30 |
| 12.04.11_200 μm _1.1 | 49.70 | 06:30 |
| 12.04.11_200 μm _1.2 | 49.02 | 06:30 |
| 12.05.03_200 μm _1.1 | 82.85 | 08:30 |
| 12.05.03_200 μm _1.2 | 106.8 | 08:30 |
| 12.06.06_200 μm _1.1 | 74.14 | 08:30 |
| 12.06.06_200 μm _1.2 | 52.21 | 08:30 |
| 12.05.31_200 μm _1.1 | 84.25 | 10:30 |
| 12.05.31_200 μm _1.2 | 115.6 | 10:30 |
| 12.05.04_200 μm _1.1 | 87.63 | 12:30 |
| 12.05.04_200 μm _1.2 | 130.1 | 12:30 |
| 12.04.30_200 μm _1.1 | 73.20 | 14:30 |
| 12.04.30_200 μm _1.2 | 107.6 | 14:30 |

| Film Name (250 μm grafted films) | GL [%] | Graft Time [Hours] |
|---|-------------------|-------------------------------|
| 12.05.31_250 μm _1.1 | 19.74 | 04:00 |
| 12.05.31_250 μm _1.2 | 19.12 | 04:00 |
| 12.04.12_250 μm _1.1 | 37.87 | 06:00 |
| 12.04.12_250 μm _1.2 | 27.65 | 06:00 |
| 12.04.11_250 μm -2.3 | 38.37 | 09:00 |
| 12.04.11_250 μm -2.4 | 32.41 | 09:00 |
| 12.05.31_250 μm _1.3 | 49.55 | 10:00 |
| 12.05.31_250 μm _1.4 | 54.10 | 10:00 |
| 12.05.04_250 μm _1.3 | 65.27 | 12:00 |
| 12.05.04_250 μm _1.4 | 73.36 | 12:00 |
| 12.04.30_250 μm _1.3 | 65.85 | 15:15 |
| 12.04.30_250 μm _1.4 | 63.048 | 15:15 |
| 12.05.31_250 μm _1.5 | 88.74 | 17:00 |
| 12.05.31_250 μm _1.6 | 74.43 | 17:00 |
| 12.05.04_250 μm _1.1 | 90.93 | 18:00 |
| 12.05.04_250 μm _1.2 | 94.27 | 18:00 |
| 12.04.16_250 μm _1.1 | 78.54 | 18:00 |
| 12.04.16_250 μm _1.2 | 17.46 | 18:00 |
| 12.04.30_250 μm _1.1 | 20.52 | 21:45 |
| 12.04.30_250 μm _1.2 | 98.32931 | 21:45 |

All the ETFE films were in 8 x 8 [cm²] dimensions and irradiated under 50 kGy, grafted at 60°C. All the grafted films were washed with toluene and dried at 70°C. The graft levels were calculated gravimetrically. The grafting scheme was not intended towards a kinetic study.

APPENDIX A/2 RADIATION GRAFTING RESULTS

8 x 1 [cm²] films:

| Film Name (100 μm grafted films) | Graft Level [%] | Grafting Time [hours] |
|---|----------------------------|----------------------------------|
| 12.04.12_100μm_2.1 | 4 | 1 |
| 12.04.20_100μm_1.1 | 30 | 01:30 |
| 12.04.20_100μm_2.2 | 31 | 01:30 |
| 12.04.20_100μm_2.3 | 35 | 02:00 |
| 12.04.20_100μm_2.4 | 5 | 02:00 |
| 12.04.06_100μm_2.1 | 63 | 02:00 |
| 12.04.06_100μm_2.2 | 34 | 02:20 |
| 12.05.03_100μm_2.1 | 24 | 03:00 |
| 12.05.03_100μm_2.2 | 55 | 03:00 |

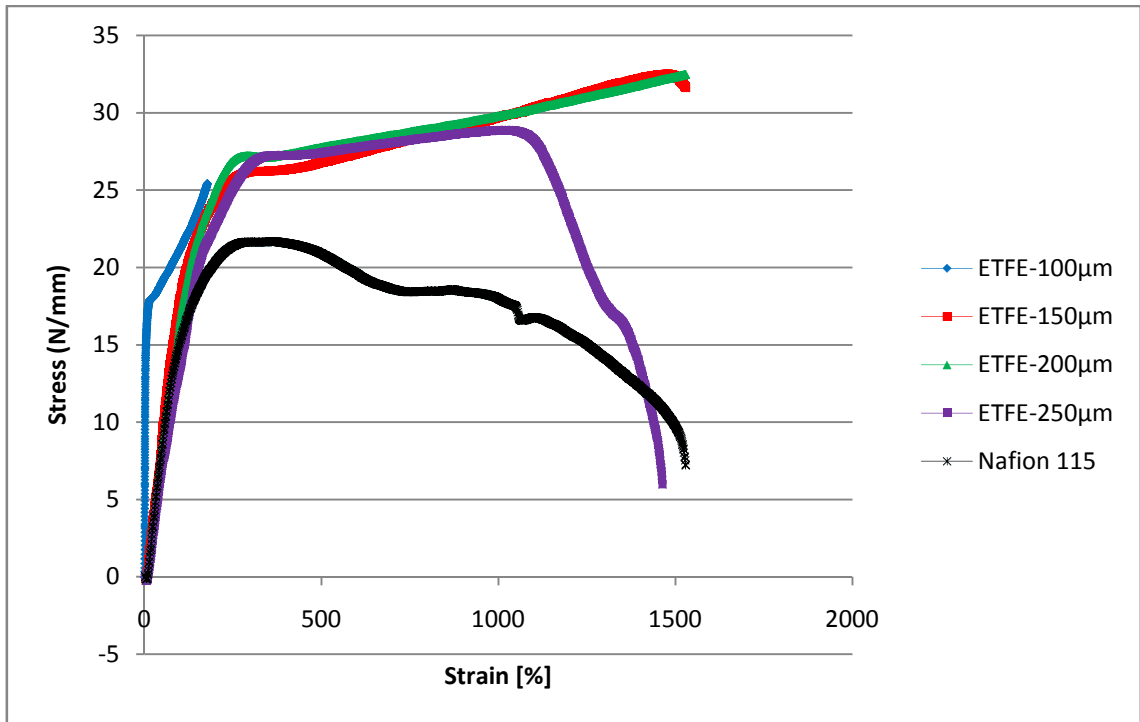
| Film Name (150 μm grafted films) | Graft Level [%] | Grafting Time [hours] |
|---|----------------------------|----------------------------------|
| 12.04.12_150μm_2.1 | 28 | 02:30 |
| 12.04.12_150μm_2.2 | 8 | 02:30 |
| 12.04.20_150μm_2.1 | 13 | 02:30 |
| 12.04.20_150μm_2.1 | 11 | 02:30 |
| 12.05.03_150μm_2.1 | 83 | 03:15 |
| 12.05.03_150μm_2.2 | 26 | 03:15 |
| 12.04.20_150μm_2.1 | 94 | 04:00 |
| 12.04.20_150μm_2.2 | 32 | 04:00 |
| 12.05.07_150μm_2.3 | 84 | 08:00 |
| 12.05.07_150μm_2.4 | 96 | 08:00 |
| 12.04.30_150μm_2.1 | 82 | 09:00 |
| 12.04.30_150μm_2.2 | 171 | 23:15 |

| Film Name (200 µm grafted films) | Graft Level [%] | Grafting Time [hours] |
|---|----------------------------|----------------------------------|
| 12.04.12_200µm_2.1 | 16 | 03:00 |
| 12.04.12_200µm_2.2 | 43 | 03:00 |
| 12.04.11_200µm_2.1 | 99 | 06:30 |
| 12.04.11_200µm_2.2 | 130 | 06:30 |
| 12.05.03_200µm_2.1 | 112 | 08:00 |
| 12.05.03_200µm_2.2 | 104 | 08:00 |
| 12.05.04_200µm_2.1 | 150 | 12:30 |
| 12.05.04_200µm_2.1 | 165 | 12:30 |

| Film Name (250 µm grafted films) | Graft Level [%] | Grafting Time [hours] |
|---|----------------------------|----------------------------------|
| 12.04.12_250µm_2.3 | 13 | 05:10 |
| 12.04.12_250µm_2.4 | 14 | 05:20 |
| 12.04.12_250µm_2.1 | 21 | 06:00 |
| 12.04.12_250µm_2.2 | 37 | 06:00 |
| 12.04.11_250µm-2.1 | 20 | 09:00 |
| 12.04.11_250µm-2.2 | 110 | 09:00 |
| 12.05.04_250µm_2.3 | 122 | 12:00 |
| 12.05.04_250µm_2.4 | 62 | 12:00 |
| 12.04.30_250µm_2.3 | 6 | 15:10 |
| 12.04.30_250µm_2.4 | 185 | 14:30 |
| 12.05.04_250µm_2.1 | 54 | 18:00 |
| 12.05.04_250µm_2.2 | 172 | 18:00 |
| 12.04.16_250µm_2.1 | 139 | 18:00 |
| 12.04.16_250µm_2.2 | 6 | 18:00 |
| 12.04.30_250µm_2.1 | 185 | 21:45 |
| 12.04.30_250µm_2.2 | 161 | 21:55 |

All the ETFE films were in 8 x 1 [cm²] dimensions and irradiated under 50 kGy, grafted at 60°C. All the grafted films were washed with toluene and dried at 70°C. The graft levels were calculated gravimetrically. The grafting scheme was not intended towards a kinetic study.

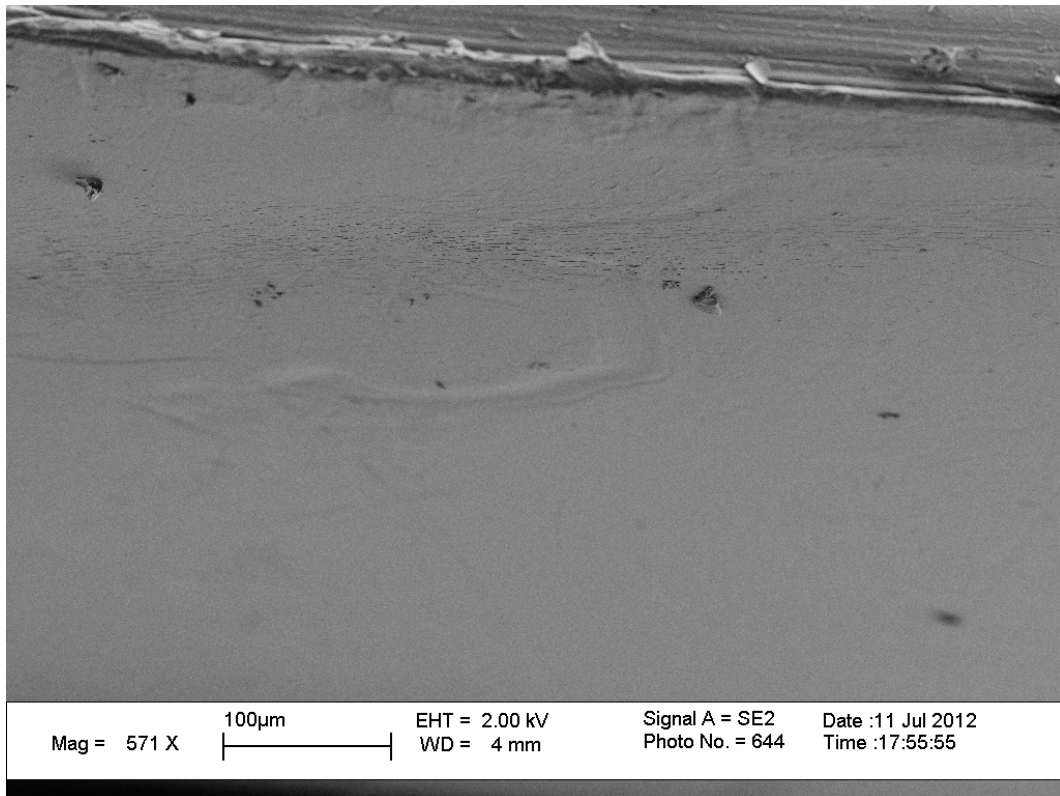
APPENDIX B UTM RESULTS



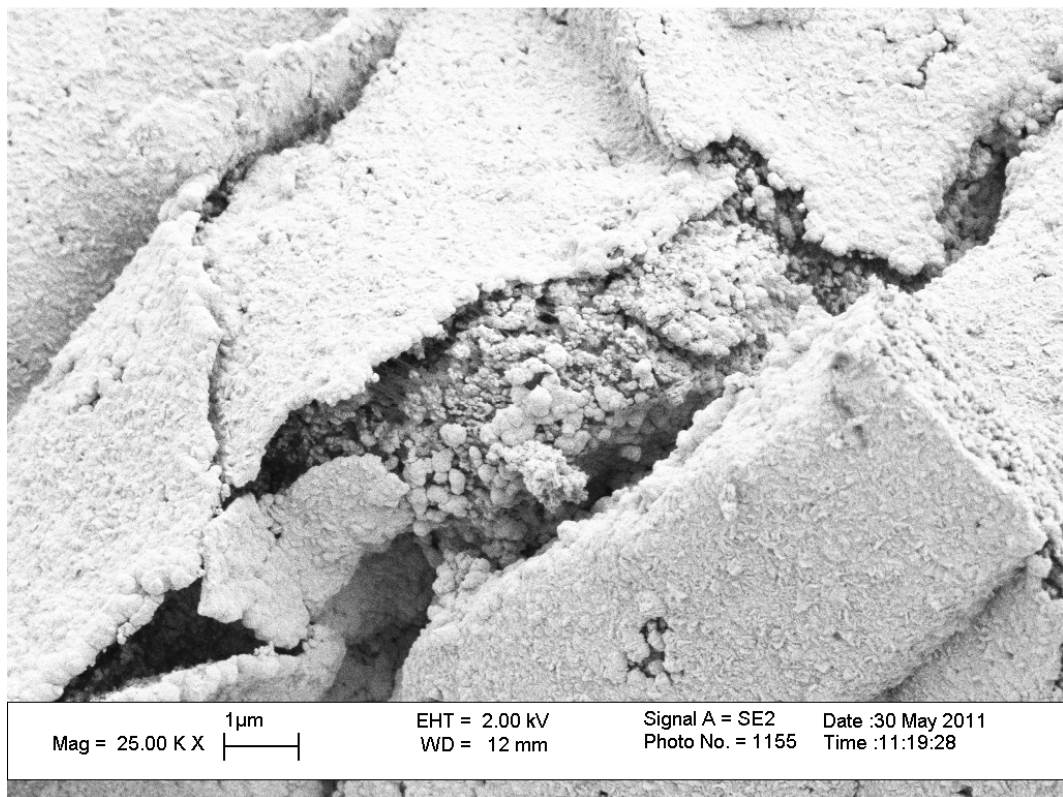
Pristine ETFE films and Nafion[®] 115

| | Elastic Modulus [MPa] |
|-------------------------|-----------------------|
| ETFE_100 µm | 9 |
| ETFE_150 µm | 14 |
| ETFE_200 µm | 15 |
| ETFE_250 µm | 12 |
| Nafion [®] 115 | 12 |

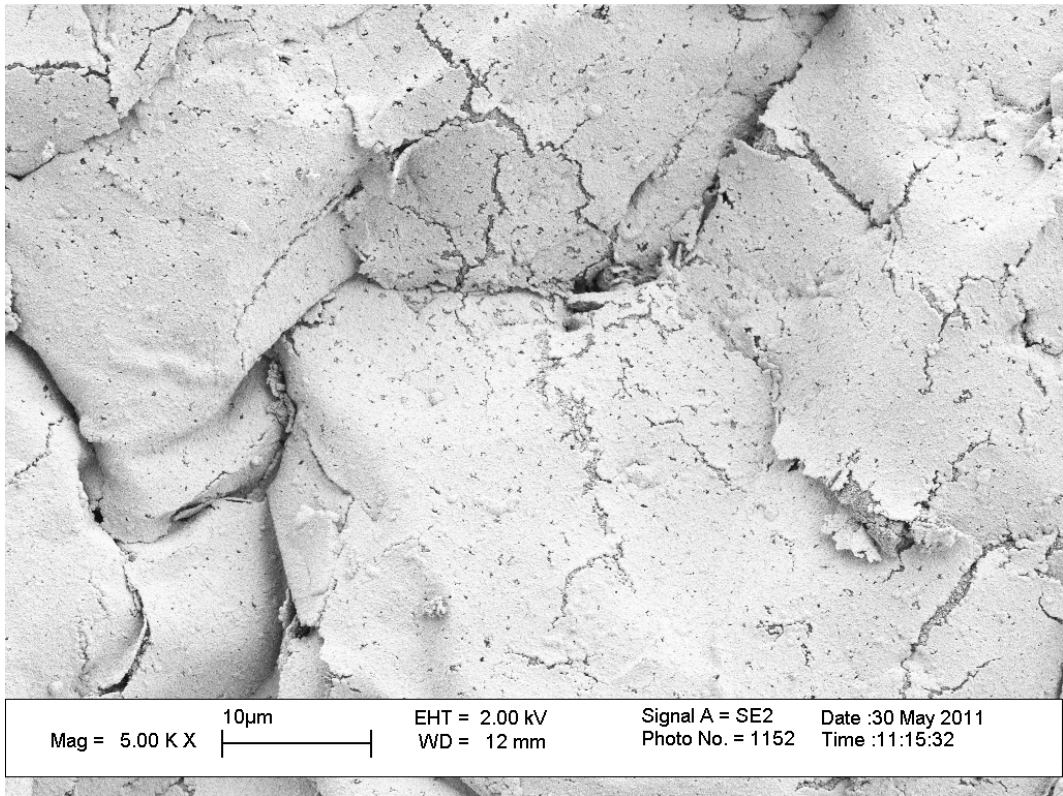
APPENDIX C SEM RESULTS



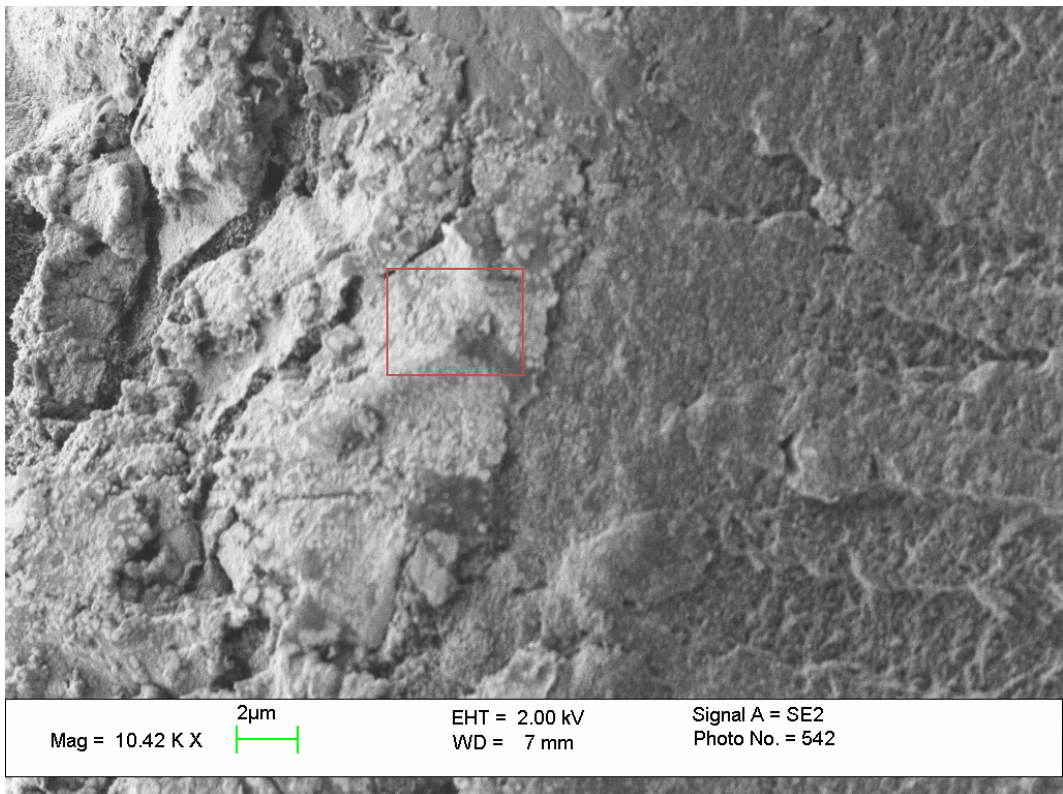
The cross-section of 17% grafted 100µm ETFE film



Details of the cracked surface of 200µm GL:55% ETFE-g-PSSA based membrane.



Cracked surface of 200µm_GL:55% ETFE-g-PSSA based membrane.



Cross-section of displaced 100µm_GL:80% ETFE-g-PSSA based membrane, cut in the horizontal direction.

APPENDIX D DISPLACEMENT RESULTS

Displacement angle and back-relaxations of ETFE-g-PSSA based IPMCs with different thickness and similar graft levels under applied 2V, 3V

| | Applied Potential (DC) | δ (degrees) | Γ (degrees)-still applied potential | Γ (degree)-removed potential |
|---------------------|------------------------|--------------------|--|-------------------------------------|
| Nafion [®] | 2V | 0 * | * | * |
| Nafion [®] | 3V | 0 * | * | * |
| 100 μ m_80% | 2V | 11 | 0 | 6 |
| 100 μ m_80% | 3V | 21 | 24 ** | - |
| 150 μ m_77% | 2V | 13 | 3 | 5 |
| 150 μ m_77% | 3V | 40 | 0 | 26 |
| 200 μ m_80% | 2V | 7 | 0 | 2 |
| 200 μ m_80% | 3V | 38 | 12 | 23 |

* Small oscillations has been observed

** The IPMC strip oscillated harmonically

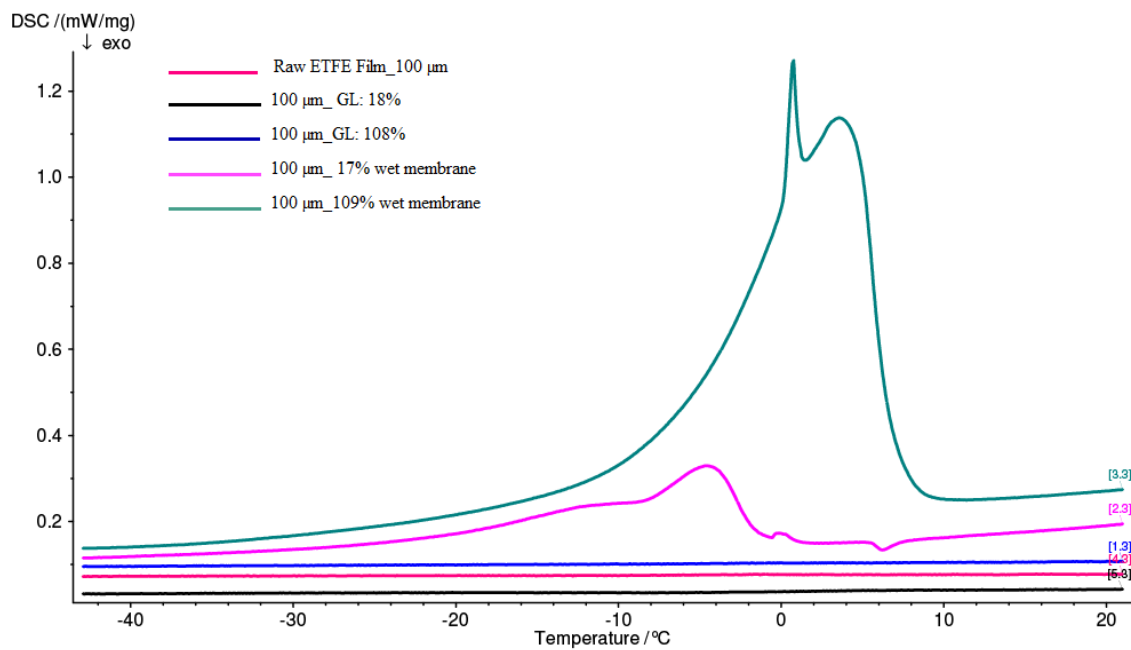
Tip displacement and back-relaxations of ETFE-g-PSSA based IPMCs with different thickness and similar graft levels, and corresponding durations

| | DC potential | δ (max)-[mm] | Response to field at sec] | δ (max)-duration [sec] | Γ^* [mm] | Γ^* duration [sec] |
|------------------------|--------------|---------------------|---------------------------|-------------------------------|-----------------|---------------------------|
| 100 μ m_80% | 1V- | 0.5 | 0 . | 1-2 | oscillations | - |
| 100 μ m_80% | 2V | 4 | 1. | 12 | - 0.25 | 13 |
| 100 μ m_80% | 3V | 8.0 | 1. | 15 | -9.89 | 44 |
| | | | | | | |
| 150 μ m_77% | 1 V | 0 | - | - | - | - |
| 150 μ m_77% | 2 V | 6 | 0 | 10 | -1 | 45 |
| 150 μ m_77% | 3 V | 15.5 | 3. | 36 | - | - |
| | | | | | | |
| 200 μ m_80% | 1 V | 0 | - | - | - | - |
| 200 μ m_80% | 2 V | 2.5 | 1. | 11 | 0 | - |
| 200 μ m_80% | 3 V | 13.2 | 1. | 32 | +6.95 | 03:50 |
| | | | | | | |
| Nafion [®] | 1 V | 1 | 9 . | - | oscillations | - |
| Nafion [®] | 2 V | ~1 | 6 . | - | oscillations | - |
| Nafion [®] | 3 V | - | 12 . | - | oscillations | - |
| | | | | | | |
| Nafion [®] -2 | 1 V | ~1 | - | - | oscillations | - |
| Nafion [®] -2 | 2 V | ~1 | - | - | oscillations | - |
| Nafion [®] -2 | 3 V | ~1 | - | - | oscillations | - |

δ (max)- Maximum displacement. The maximum displacement was calculated by the addition of δ (x) and δ (y) vectors.

Γ^* - back relaxation under still applied potential

APPENDIX E DIFFERENTIAL SCANNING CALORIMETRY (DSC) RESULT



The samples were analyzed in N_2 environment and heated with $5^\circ\text{C}/\text{min}$.

REFERENCES

- [1] Abdelnour, K., Mancia, E., Peterson, S. D., & Porifiri, M. (2011). Fluid flow in the vicinity of vibrating ionic polymer metal composites. Part-1: Numerical Study. Brooklyn, Newyork.
- [2] Agmon, N. (1995). The Grotthuss mechanism. *Chemical Physics Letter* , 244, 456-462.
- [3] Alkan Gürsel, S., Gubler, L., Gupta, B., & Scherer, G. G. (2008). Radiation Grafted Membranes. *Advanced Polymer Science* , 215, 157–217.
- [4] Aureli, M., Lin, W., & Porfiri, M. (2009). On the capacitance-boost of ionic polymer metal composites due to electroless plating: Theory and experiments. *Journals of Applied Physics* , 105, 104911.
- [5] Balkus Jr., K. J. (2012). Nafion-sulfonated dendrimer composite membranes for fuel cell applications. *Journal of Membrane Science* , 392-393, 175–180.
- [6] Bandopadhyaya, D., & Njuguna, J. (2009). Estimation of bending resistance of Ionic Polymer Metal Composite (IPMC) actuator following variable parameters pseudo-rigid body model. *Materials Letter* , 63, 745-747.
- [7] Bandopadhyaya, D., Bhattacharya, B., & Dutta, A. (2007). Active Vibration Control Strategy for a Single-Link Flexible Manipulator Using Ionic Polymer Metal. *Journal of Intelligent Material Systems and Structures* , 19, 487-496.
- [8] Bandopadhyaya, D., Bhattacharya, B., & Dutta, A. (2009). Pseudo-rigid Body Modeling of IPMC for a Partially Compliant Four-bar Mechanism for Work Volume Generation. *Journal of Intelligent Material Systems and Structures* , 20.
- [9] Bar-Cohen, Y. (2006). *Biomimetics: Biologically Inspired Technologies*. New York: Taylor & Francis.
- [10] Bar-Cohen, Y. (2006). *Biomimetics: Biologically Inspired Technologies*. New York: Taylor & Francis.
- [11] Bar-Cohen, Y. (2001). *Electroactive Polymer (EAP) Actuators as Artificial Muscles- Reality, Potential and Challenges*. Bellingham: SPIE.
- [12] Bar-Cohen, Y. (2005). *Worldwide-Electroactive Polymers (Artificial Muscles) Newsletter*.
- [13] Bar-Cohen, Y., & Breazeal, C. (2003). *Biologically Inspired Intelligent Robots*. Washington: SPE Press.
- [14] Ben youcef, H., Alkan Gürlse, S., Buisson, A., Gubler, L., Wokaun, A., & Scherer, G. (2010). Influence of radiation- induced grafting process on mechanical properties of ETFE-based membrabes for fuel cells. *Fuel Cells* , 10 (3), 401-410.
- [15] Bennett, M. D., Leo, D. J., Wilkes, G. L., Beyer, F. L., & Pechar, T. W. (2006). A model of charge transport and electromechanical transduction in ionic liquid swollen Nafion membranes. *Polymer* , 47, 6782-6796.
- [16] Bhat, N., & Kim, W.-j. (2003). Precision control of force produced by ionic polymer metal composites., (pp. 15-21).
- [17] Brack, H.-P., Bühner, H. G., Bonorand, L., & Scherer, G. G. (2000). Grafting of pre-irradiated poly(ethylene-alt-tetrafluoroethylene) films with styrene: influence of base polymer film properties and processing parameters. *Journals of Material Chemistry* , 10, 1795-1803.
- [18] Brack, H.-P., Ruegg, D., Bühner, H. G., Slaski, M., Alkan Gürsel, S., & Scherer, G. G. (2004). Differential Scanning Calorimetry and Thermogravimetric Analysis Investigation of Thermal Properties and Degredation of Some Radiation-Grafted Films and Membranes. *Journal of Polymer Science, Part B: Polymer Physics* , 42, 2612-2624.

- [19] Chapiro, A. (1962). *Radiation chemistry of polymeric systems*. London: Interscience.
- [20] Cho, B. e. (2008). Preparation and properties of nanofibrous Nafion mats for ionic polymer metal composites. *Composites Science and Technology*, 68, 2960-2964.
- [21] Cho, S., & Lee, D. (2008). A biomimetic micro-collector based on an ionic polymer metal composite. *Microelectronic Engineering*.
- [22] Chung, C. K. (2006). A novel fabrication of ionic polymer-metal composites (IPMC) actuator with silver nano-powders. *Sensors and Actuators B*, 117, 367-375.
- [23] Chung, C., Fung, P. K., Hong, Y. Z., Ju, M. S., Lin, C. C., & Wu, T. C. (2006). A novel fabrication of ionic polymer-metal composites (IPMC) actuator with silver nano-powders. *Sensors and Actuators B*, 117, 367-375.
- [24] Cilingir Dogan, H., & Alkan Gürsel, S. (2011). Preparation and Characterisation of Novel Compositated Based on a Radiation Grafted Membrane for Fuel Cells. *Fuel Cells*, 11 (3), 361-371.
- [25] Costa Branco, P., & Dente, J. (2006). Derivation of a continuum model and its electric equivalent-circuit representation for ionic polymer-metal composite (IPMC) electromechanics. *SmartMater.Struct.*, 15, 378-392.
- [26] da Silva, C. M., Silva, A. L., Percira, R., & Rocco, A. M. (2009). Conductivity of Thermal Behaviour of Sulfonated ABS Membranes for Fuel Cell Applications. *ECS Transactions*, 25 (1), 881-889.
- [27] Dai, C.-A. e. (2008). Fabrication of novel proton exchange membranes for DMFC via UV curing. *Journal of Power Sources*, 177, 262-272.
- [28] Dai, C.-A. e. (2009). Polymer actuator based on PVA/PAMPS ionic membrane: Optimization of ion transport properties. *Sensors and Actuators A*, 155, 152-162.
- [29] Dargaville, T. R., George, G. R., Hill, D. J., & Whittaker, A. K. (2003). High energy radiation grafting of fluoropolymers. *Progress in Polymer Science*, 28, 1355-1376.
- [30] Darling, R. M., & Meyers, J. P. (2003). Kinetic model of dissolution in PEMFCs. *The Journal of the Electrochemical Society*, 150 (11), A1523-A1527.
- [31] Del Bufalo, G., Placidi, L., & Porfiri, M. (2008). *Smart Mat. Struct.*, 17.
- [32] Deole, U., Lumia, R., Shahinpoor, M., & Bermudez, M. (2008). Design and test of IPMC artificial muscle microgripper. *J. Micro- Nano Mech.*, 4, 95-102.
- [33] Diloyan, G., Sobel, M., Das, K., & Hutapea, P. (2012). Effect of mechanical vibration on platinum particle agglomeration and growth in Polymer Electrolyte Membrane Fuel Cell catalyst layers. *Journal of Power Sources*, 214, 59-67.
- [34] Elliott, J. A., & Paddison, S. J. (2007). Modelling of morphology and proton transport in PFSA membranes. *Phys. Chem. Chem. Phys.*, 9, 2602-2618.
- [35] Fang, B.-K., Ju, M.-S., & Lin, C.-C. K. (2007). A new approach to develop ionic polymer-metal composites (IPMC) actuator: Fabrication and control for active catheter systems. *Sensor and Actuators A*, 321-329.
- [36] Fang, B.-K., Ju, M.-S., & Lin, C.-C. K. (2010). Development of sensing/actuating ionic polymer-metal composite (IPMC) for active guide wire system. *Sensors and Act. A*, 158, 1-9.
- [37] Feng, G.-H. (2010). Numerical study on dynamic characteristics of micro machined ionic polymer metal composite devices based on molecular-sclae modeling. *Computational Materials Science*, 50, 158-166.
- [38] Flatau, A. B., & Chong, K. (2002). Dynamic smart material and structural systems. *Engineering Structures*, 24, 261-270.

- [39] *Fuel Cell Testing Products and Services*. (n.d.). Retrieved 06 01, 2012, from <http://www.bekktech.com/>
- [40] Gao, F., & Weiland, L. M. (2011). Streaming Potential Hypothesis for Ionic Polymer Transducers in Sensing: Roles of Ionomer State and Morphology. *Journal of Intelligent Material Systems and Structures*, 22, 1623-1630.
- [41] Gubler, L., Prost, N., S, G. A., & G., S. (2005). Proton exchange membranes prepared by radiation grafting of styrene/divinylbenzene onto poly(ethylene-alt-tetrafluoroethylene) for low temperature fuel cells. *Solid State Ionics*, 176, 2849-2860.
- [42] Gubler, L., S, G. A., & G., S. (2005). Radiation Grafted Membranes for Polymer Electrolyte Fuel Cells. *Fuel Cells*, 5 (3), 317-335.
- [43] Guilmeau, I., Esnouf, S., Betz, N., & Le Mod, A. (1997). Kinetics and characterization of radiation-induced grafting of styrene on fluoropolymers. *Nuclear Instruments and Methods in Physics Research B*, 131, 270-275.
- [44] Guo, S., Sugimoto, K., Hata, S., Su, J., & Oguro, K. (2000). A new type of underwater fish-like microrobot. *Proceedings of the 2000 IEEE/RSJ International Conference on Intelligent Robotics and Systems*, 2, pp. 867-872.
- [45] Hase, K., Nakano, T., & Koiwai, A. (2007). Performance of high density acid electrolyte and analysis of proton conduction mechanism. *ECS transactions*, 11 (1), 159-164.
- [46] Holdcroft, S. e. (2001). Ionic conductivity of proton exchange membranes. *Journal of Electroanalytical Chemistry*, 503, 45-56.
- [47] Jain, R. K., Datta, S., Majumder, S., & Dutta, A. (2011). Two IPMC fingers based on micro gripper for handling. *International Journal of Advanced Robotic Systems*, 8 (1).
- [48] Jeong, H. M., Kim, H., Lee, S. J., & Mun, M. (2005). Characteristics of ionic polymer metal composites prepared with fluorinated acrylic copolymer contained sulfonate anion. *Journal of Macromolecular Science: Part B*, 44, 225-235.
- [49] Jeong, H. Y., & Kim, B. K. (2006). Electrochemical behavior of a new type of perfluorinated carboxylate membrane/platinum complexes. *Journal of Applied Polymer Science*, 99, 2687-2693.
- [50] Jho, J. Y., & al., e. (2012). Performance enhancement of polymer electrolyte membrane fuel cell by employing line-patterned Nafion membrane. *Journal of Industrial and Engineering Chemistry*, 18, 876-879.
- [51] Jung, J.-H., Vadahanambi, S., & Oh, I.-K. (2010). Electro-active nano-composite actuator based on fullerene-reinforced Nafion. *Composites Science and Technology*, 70, 584-592.
- [52] Jung, K., Nam, J., & Choi, H. (2003). Investigations on actuation characteristics of IPMC artificial muscle actuator. *Sensors and Actuators A*, 107, 183-192.
- [53] Kallio, T. e. (2002). Electrochemical characterization of radiation-grafted ion-exchange membranes based on different matrix polymers. 32, 11-18.
- [54] Kikuchi, K., Tsuchitani, S., Mawa, M., & Asaka, K. (2008). Formation of patterned electrode in ionic polymer-metal composite using dry film photoresist. *Transactions on electrical and electronic engineering*, 3, 452-454.
- [55] Kim, K. J., & Kim, D. (2006). Experimental investigation on electrochemical properties of ionic polymer metal composites. *Journal of Intelligent Material Systems and Structures*, 17, 449-454.
- [56] Kim, K. J., & Shahinpoor, M. (2003). Ionic polymer-metal composites: II. Manufacturing techniques. *Smart Mater. Struct.*, 12, 65-79.

- [57] Kim, K. J., Yim, W., Paquette, J. W., & Kim, D. (2007). Ionic Polymer-metal Composites for Underwater Operation. *Journal of Intelligent Material Systems and Structures*, *18*, 123-131.
- [58] Kim, S.-M., Tiwari, R., & Kim, K. J. (2011). A novel ionic polymer metal ZnO composite. *Sensors*, *11*, 4674-4687.
- [59] Kreuer, K. D. (2001). On the development of proton conducting polymer membranes for hydrogen and methanol fuel cells. *185* (1), 29-39.
- [60] Krishen, K. (2009). Space applications for ionic polymer metal composite sensors, actuator, and artificial muscles. *Acta Astronautica*, *64*, 1160-1166.
- [61] Lee, J.-W., Kim, J.-H., Goo, N. S., Lee, J. Y., & Yoo, Y.-T. (2010). Ion-conductive poly(vinyl-alcohol) based IPMCs. *Journal of Bionic Engineering*, *7*, 19-28.
- [62] Lee, M. J., Jung, S. H., Kim, G. S., Moon, I., & Mun, S. L. (2007). Actuation of the Artificial Muscle Based on Ionic Polymer Metal Composite by Electromyography (EMG) Signals. *JOURNAL OF INTELLIGENT MATERIAL SYSTEMS AND STRUCTURES*, *18*, 165-170.
- [63] Lee, S. J. (2006). A new fabrication method for IPMC actuators and application to artificial fingers. *Smart Mater. Struct.*, *15* (5), 1217-1224.
- [64] Lee, S., Park, H. C., & Kim, K. J. (2005). Equivalent modeling for ionic polymer-metal composite actuators based on beam theories. *Smart Mater. Struct.*, *14*, 1363-1368.
- [65] Lee, S., Park, H. C., & Kim, K. J. (2005). Equivalent modeling for ionic polymer-metal composite actuators based on beam theories. *Smart Mater. Struct.*, *14*, 1363-1368.
- [66] Li, L., Deng, B., Ji, Y., Yu, Y., Xie, L., & Li, J. (2010). A novel approach to prepare proton exchange membranes from fluoropolymer by powder irradiation induced graft polymerization. *Journal of membrane science*, *346*, 113-120.
- [67] Li, L., Su, L., & Zhang, Y. (2012). Enhanced performance of supercritical CO₂ treated Nafion 212 membranes for direct methanol fuel cells. *International Journal of Hydrogen Energy*, *37*, 4439-4447.
- [68] Lin, R., Li, B., Hou, Y. P., & Ma, J. (2009). Investigation of dynamic driving cycle effect on performance degradation micro-structure change of PEM fuel cell. *International Journal of Hydrogen Energy*, *34*, 2369-2376.
- [69] Ludueña, G. A., Kühne, T. D., & Sebastiani, D. (2011). Mixed Grotthuss and Vehicle Transport Mechanism in Proton Conducting Polymers from Ab initio Molecular Dynamics Simulations. *Chem. Mater.*, *23* (6), 1424-1429.
- [70] Maier, J. (2005). Nanoionics: ion transport and electrochemical storage in confined systems. *Nature Materials*, *4*, 805-815.
- [71] Makuuchi, K., & Cheng, S. (2012). *Radiation Processing of Polymer Materials and Its Industrial Applications*. John Wiley and Sons, Inc.
- [72] Mauritz, K. A., & Moore, R. B. (2004). State of Understanding of Nafion. *Chemical Reviews*, *104* (10).
- [73] Nah, C., & Ch, B. H. (2008). Preparation and properties of nanofibrous Nafion mats for ionic polymer metal composites. *Composites Science and Technology*, *68*, 2960-2964.
- [74] Nasef, M. M., & H. E.-S. (2004). Preparation and applications of ion exchange membranes. *Prog. Poly. Sci.*, *29*, 499-561.
- [75] Nasef, M. M., Saidi, H., & Dahlan, K. Z. (2003). Electron beam irradiation effects on ethylene-tetrafluoroethylene copolymer films. *Radiation Physics and Chemistry*, *63*, 875-883.

- [76] Nemat-Nasser, S., & Li, J. Y. (2000). Electromechanical response of ionic polymer-metal composites. *Journal of Applied Physics*, 87 (7).
- [77] Nemat-Nasser, S., & Wu, Y. (2003). Comparative experimental study of ionic polymer-metal composites with different backbone ionomers and in various cation forms. *Journal of Applied Physics*, 93 (9), 5255-5267.
- [78] Nemat-Nasser, S., & Zamani, S. (2006). Modeling of electrochemomechanical response of ionic polymer-metal composites with various solvents. *Journal of Applied Physics*, 100, 064310.
- [79] Nemat-Nasser, S., Zamani, S., & Tor, Y. (2006). Effect of solvents on the chemical and physical properties of ionic polymer metal composites. *Journal of Applied Physics*, 99, 104902.
- [80] Nguyen, V. K., & Yoo, Y. (2007). A novel design and fabrication of multilayered ionic polymer-metal composite actuators based on Nafion/layered silicate and Nafion/silica nanocomposites. *Sensors and Actuators B: Chemical*, 123 (1), 183-190.
- [81] Nguyen, V. K., Lee, J. W., & Yoo, Y. (2007). Characteristics and performance of ionic polymer-metal composite actuators based on Nafion/layered silicate and Nafion/silica nanocomposites. *Sensors and Actuators B*, 120 (2), 529-537.
- [82] Nicholson, J. W. (2012). Autoacceleration. In J. W. Nicholson, *The Chemistry of Polymers*. Cambridge: RSC Publishing.
- [83] Nishida, G., Takagi, K., Maschke, B., & Osada, T. (2011). Multi-scale distributed parameter modeling of ionic polymer-metal composite soft actuator. *Control Engineering Practice*, 19, 321-334.
- [84] Odian, G., Henry, R., Koenig, R., Mangaraj, D., Trung, D., Chao, B., et al. (1975). *Journal of Polymer Science: Chemistry*, 13 (3), 623-643.
- [85] Oguro, K., & Asaka, K. (2000). Bending of polyelectrolyte membrane platinum composites by electric stimuli Part II. Response kinetics. *Journal of Electroanalytical Chemistry*, 480, 186-198.
- [86] Oguro, K., Kawami, Y., & Takenaka, H. (1992). Bending of an ionconducting polymer film-electrode composite by an electric stimulus at low voltage. *Trans. Journal of Micromachine Society*, 5, 27-30.
- [87] Okamoto, S., Kuwabara, K., & Otsuka, K. (2006). Electrical stimuli-induced deformation and material properties of electro active polymer Nafion 117. *Sensors and Actuators A*, 125, 376-381.
- [88] Panda, B., & Dutta, A. (2010). Design of a partially compliant crank rocker mechanism using Ionic Polymer Metal Composite for path generation. *Materials and Design*, 31, 2471-2477.
- [89] Park, I.-S., Jung, K., Kim, D., Kim, S.-M., & Kim J., K. (2008). Physical principles of ionic polymer metal composites as electroactive sensors and actuators. *MRS Bulletin*, 33.
- [90] Park, I.-S., Kim, S.-M., Puga, D., Huang, L., .suk-Wah, T.-C., & Kim, K. J. (2010). Visualization of the cation migration in ionic polymer-metal composite. *Applied Physics Letters*, 96.
- [91] Peterson, S. D., Porifiri, M., & Rovardi, A. (2009). Fluid flow in the vicinity of vibrating ionic polymer metal composites. Part-1: Experimental Study. Hollywood, California.
- [92] Pivovar, B. S. An overview of electro-osmosis in fuel cell polymerelectrolytes. *Polymer*, 47 (11), 4194-4202.
- [93] Poggio, T., & Kapeliouchko, V. (2003). Multimodal fluoropolymer dispersions. *Progress in Organic Coatings*, 48, 310-315.

- [94] Porfiri, M. (2009). An electromechanical model for sensing and actuation of ionic polymer metal composites. *Smart Material Structures* , 18 (1).
- [95] Porfiri, M. (2008). Charge dynamics in ionic polymer metal composites. *Journal of Applied Physics* , 104.
- [96] Postnote. (2008). *Smart Materials and Systems*. London: Parliament Office of Science and Technology.
- [97] Pugal, D., Kim, K. J., & Aabloo, A. (2011). An explicit physics-based model of ionic polymer-metal composite actuators. *Journal of Applied Physics* , 110, 084904.
- [98] Pugal, D., Kim, K. J., Punning, A., Kasemägi, H., & Kruusmaa, M. e. (2008). A self-oscillating ionic polymer-metal composite bending actuator. *Journal of Applied Physics* , 103, 084908-1.
- [99] Punning, A., Kruusmaa, M., & Aabloo, A. (2007). A self-sensing ion conducting polymer metal composite (IPMC) actuator. *Sensors and Actuators A* , 136, 656-664.
- [100] Punning, A., Kruusmaa, M., & Aabloo, A. (2007). Surface resistance experiments with IPMC sensors and actuators. *Sensors and Actuators A* , 133, 200-209.
- [101] Qiao, J., Hamaya, T., & Okada, T. (2005). Chemically modified Poly(vinyl-alcohol)-Poly(2-acrylamido-2-methyl-1-propanesulfonic acid) as anovel proton-conducting fuel cell membrane. *Chem. Mater.* , 17 (9), 2413-2421.
- [102] Rabenau, A., Kreuer, K.-D., & Weppner, W. (1982). Vehicle Mechanism, A new model for the interpretation of conductivity of fast proton conductors. *Angew. Chem.* , 21 (3).
- [103] Rager, T. (2004). Parameter Study for the Pre-Irradiation Grafting of Styrene/Divinylbenzene onto Poly(tetrafluoroethylene-co-hexafluoropropylene) from Isopropanol Solution. *Helvetica Chimica Acta* , 87.
- [104] Rager, T. (2003). Pre-Irradiation Grafting of Styrene Divinylbenzene onto Poly(tetrafluoroethylene-co-hexafluoropropylene) from non-solvents. *Helvetica Chimica Acta* , 86, 1966-1981.
- [105] Rouillya, M., Kötza, E., Haasa, O. S., & Chapiro, A. (1993). Proton exchange membranes prepared by simultaneous radiation grafting of styrene onto Teflon-FEP films. Synthesis and characterization. *Jornal of Membrane Science* , 81 (1-2), 89-95.
- [106] Saarinen, V., Karesoja, M., Kallio, T., Paronen, M., & Kontturi, K. (2006). Characterization of the novel ETFE-based membrane. *Journal of Membrane Science* , 280, 20-28.
- [107] Sadeghipour, K., Salomon, R., & Neogi, S. (1992). Development of A Novel Electrochemically Active Membrane and ‘Smart’ Material Based Vibration Sensor/Damper. *Smart Materials and Structures* , 1, 172-179.
- [108] Saher, S., Moon, S., Kim, S. J., Kim, H. J., & Kim, Y. H. (2010). O₂ plasma treatment for ionic polymer metal nano composite (IPMCN) actuator. *Sensors and Actuators B* , 147, 170-179.
- [109] Santos, J., Lopes, B., & Costa Branco, P. J. (2010). Ionic polymer–metal composite material as a diaphragm for micropump devices. *Sensors and Actuators A* , 161, 225–233.
- [110] Sasaki, M., Onouchi, Y., Ozeki, T., Tamagawa, H., & Ito, S. (2010). Feedforward control of an ionic polymer metal actuators. *International Journal of Applied Electromagnetics and Mechanics* , 33, 875-881.
- [111] Shahinpoor, M. (2005). Smart ionic polymer conductor composite materials as multifuntional distributed nanosensors, nanoactuators and artificial muscles. *Proceedings of IMECE2005*.

- [112] Shahinpoor, M., & Kim, K. (2001). Design, development and testing of a multi-fingered heart compression/assist device equipped with IPMC artificial muscles. *Proc. SPIE. Smart Structures and Materials*, 4329, pp. 411-420.
- [113] Shahinpoor, M., & Kim, K. J. (2001). Ionic polymer-metal composites: I. Fundamentals. *Smart Mater. Struct.*, 10, 819-833.
- [114] Shahinpoor, M., & Kim, K. J. (2001). Ionic polymer-metal composites— I. Fundamentals. 10, 819-833.
- [115] Shahinpoor, M., & Kim, K. J. (2002). Mass transfer induced hydraulic actuation in ionic polymer-metal composites. *Journal of Intelligent Material Systems and Structures*, 13, 369-376.
- [116] Shena, M., Roya, S., Kuhlmann, J., Scott, K., Lovell, K., & Horsfall, J. (2005). Grafted polymer electrolyte membranes for direct methanol fuel cells. 251, 121-130.
- [117] Stoimenov, B. L., Rossiter, J. M., & Mukai, T. Anisotropic surface roughness enhances bending response of ionic polymer-metal composite (IPMC) artificial muscles. *Proc. SPIE*.
- [118] Trommsdorff, E., Kohle, & Lagally, P. (1948). Polymerization of methyl methacrylates. *Makromol. Chem.*, 1.
- [119] Wallmersperger, T., Akle, B. J., Leo, D., & Kröplin, B. (2008). Electrochemical response in ionic polymer transducers: An experimental and theoretical study. *Composites Science and Technology*, 68, 1173-1180.
- [120] Wallmersperger, T., Horstmann, A., Kröplin, B., & Leo, D. J. (2009). Thermodynamical modeling of the electromechanical behavior of ionic polymer metal composites. *Journal of Intelligent Material Systems and Structures*, 20, 741-750.
- [121] Wang, Q., Yang, S., Xia, Q., Zhu, L., Xue, J., & Chen, Q.-m. (2011). Research on the icephobic properties of fluoropolymer-based materials. *Applied Surface Science*, 257, 4956-4962.
- [122] Yuan, X.-Z., Sun, J. C., Wang, H., & Li, H. (2012). Accelerated conditioning for a proton exchange membrane fuel cell. *Journal of Power Sources*, 205, 340-344.
- [123] Zen, H., Ribeiro, G., Geraldes, A., & Souza, C. (2012). Effect of radiation induced crosslinking and degradation of ETFE films. *Journal of Radiation Physics and Chemistry*.
- [124] Zhang, H., Huang, H., & Shen, P. K. (2012). Methanol-blocking Nafion composite membranes fabricated by layer-by-layer self-assembly for direct methanol fuel cells. *International Journal of Hydrogen Energy*, 37, 6875-6879.
- [125] Zhu, Z. e. (2011). NMR study on mechanisms of ionic polymer-metal composites deformation with water content. *EPL Journal*, 96.
- [126] Zou, Z., Liu, J., & al., e. (2012). Experimental study of proton exchange membrane fuel cells using Nafion 212 and Nafion 211 for portable application at ambient pressure and temperature conditions. *International Journal of Hydrogen Energy*, 37, 4673-4677.